

Development of a Boron Neutron Capture Enhanced Fast Neutron Therapy Beam

A Thesis
Presented to
The Academic Faculty

by

Jeremy Ed Sweezy

In Partial Fulfillment
of the Requirements for the Degree
Doctor of Philosophy in Nuclear and Radiological Engineering
G.W. Woodruff School of Mechanical Engineering

Georgia Institute of Technology
March 2002

Copyright © 2002 by Jeremy Ed Sweezy

Development of a Boron Neutron Capture Enhanced Fast Neutron Therapy Beam

Approved:

Dr. Nolan E. Hertel, Committee Chair

Dr. C.-K. Chris Wang

Dr. Rodney D. Ice

Dr. Eva K. Lee

Dr. Arlene J. Lennox

Dr. Mark B. Chadwick

Date Approved _____

DEDICATION

In the memory of my grandfather,

Samuel A. Jenkins, Sr.

ACKNOWLEDGEMENTS

I would like to acknowledge those who have made contributions to this work, both directly and indirectly. First, I would express my gratitude to my advisor Dr. Nolan Hertel for provided me the opportunity to work on so many interesting projects. He has been a guiding force not only in this work, but in so many other endeavors over the last seven years. I would like to thank Dr. C.-K. Chris Wang for his assistance and his advice. I would also like to acknowledge Dr. Rodney Ice for his help in providing an environment where graduate students can perform radiation research.

I thank Dr. Arlene Lennox who has provided the vision for this project. She has been involved in every aspect of this project. I am indebted to her for support and assistance.

I would like to thank Dr. Eva Lee and Dr. Mark Chadwick for giving their time to serve on my reading committee and for providing advise on this research.

Thanks to Dr. Tom Kroc for all his help. He supervised the construction of the filter and collimator. Most importantly, he made sure that it fit. Thanks to Gordon Holmblad for all of his help in performing the experiments and making things work. Thanks also to Vernon Cupps for reading my activation foils promptly.

I have to say a big thanks to Dr. Michele Sutton Ferenci for helping me with my experiments. Without her help there would be quite a few data points missing. Thanks for your help, your advice, and your friendship.

I would like to thank some of my fellow graduate students. Thanks to Dr. Heather Gepford for helping to find this project. Thanks to Gena Poe for just being around to have

someone with whom to talk. Thanks to my friend Dr. Ken Veinot for making those late nights fun with a games of “Skihof”.

To my wife Pari, she is the inspiration and the motivation of this endeavor. Without her I could not have completed this project. Thanks for believing in me and believing that I could fly. Thank you for letting me follow my dreams. I love you. Thanks to Abby and Maggie for making sure I took a walk every day and for always welcoming me home.

To my parents, Cornelia and Gerald, for their love and support. Mom, thanks for making education a priority. Dad, thanks for giving me the desire to create and to be an engineer. Thanks to Noel, Karen, and Ellie for their love. Thanks, to Dick Crosby for believing I could do this before I even wanted to.

TABLE OF CONTENTS

DEDICATION		iii
ACKNOWLEDGEMENTS		iv
LIST OF TABLES		ix
LIST OF FIGURES		xiii
SUMMARY		xx
I INTRODUCTION		1
1.1 Objective		2
1.2 Organization		2
II BACKGROUND		4
2.1 Fast Neutron Therapy		4
2.2 Boron Neutron Capture Therapy		6
2.3 Boron Neutron Capture Enhanced Fast Neutron Therapy		7
2.4 Fermilab Neutron Therapy Facility		10
III METHODS AND EQUIPMENT		13
3.1 Tissue Equivalent Ion Chambers		13
3.1.1 Ion Chamber Design and Composition		13
3.1.2 Absorbed Dose Measurement		16

3.2	Borated Ion Chamber Thermal Neutron Response	20
3.3	Dose Enhancement	22
3.4	Ionization Chamber Calibration	23
IV	DESIGN OF A NEUTRON BEAM FOR BNCEFNT	30
4.1	Benchmarking MCNPX for BNCEFNT.	30
4.1.0.1	20 × 20 cm ² Beam Measurements	31
4.1.0.2	10 × 10 cm ² Beam Measurements	31
4.1.0.3	55.3-cm Diameter Beam Measurements	36
4.1.1	MCNPX Comparison to Measurements	36
4.2	Filter and Collimation Design	43
4.2.1	Material Selection	45
4.2.2	Design Implementation: Second Iteration	47
4.3	Final Design of the BNCEFNT Beam	52
V	MEASUREMENTS OF THE BNCEFNT BEAM	58
5.1	Corrections and Uncertainties	58
5.2	Measurements of the BNCEFNT beam	59
5.2.1	18.3-cm thick iron filter - 20 cm diameter iron collimator	62
5.2.2	10-cm diameter iron collimator	72
5.3	MCNPX Comparison to Measurements of the BNCEFNT Beam	75
VI	CONCEPTUAL DESIGN: PROGRESSION TO A CLINICAL REAL- ITY	82
VII	CONCLUSIONS AND RECOMMENDATIONS	89
7.1	Conclusions	89
7.2	Recommendations	90
APPENDIX A	— LIST OF ABBREVIATIONS	92

APPENDIX B — TABULATED DEPTH-DOSE RESULTS	94
APPENDIX C — RAW MEASUREMENT DATA	101
APPENDIX D — MCNPX INPUT FILES	113
REFERENCES	134

LIST OF TABLES

1	Composition of various tissue equivalent materials (weight percent).	15
2	AAPM recommend values and uncertainties of the constants for Equation 7. Alternate values are also listed.	18
3	Gamma calibration results of the ^{60}Co and the ^{137}Cs calibrations.	24
4	Coefficients used to determine the saturated activity due to thermal neutron activation of gold foil from ASTM E 262-97.	28
5	Experiment-to-calculated ratios (E/C) of the (n+ γ) dose and percent dose enhancement (PDE) at 5-cm deep in a water phantom.	39
6	Results of selected material for the first iteration of the filter material testing. The “(n+ γ) dose ratio” is the ratio of the intensity of the (n+ γ) dose rate without any filter over the (n+ γ) dose rate of the filter under investigation. The PDE listed is the maximum PDE.	47
7	Results of the collimator material optimization for selected materials. The results shown here are materials with a PDE greater than 13% and an (n+ γ)dose rate less than that of the iron collimator. The “(n+ γ) dose ratio” is the ratio of the (n+ γ) dose rate of the beam without any filter over the (n+ γ) dose rate of the system under investigation. The PDE listed is the maximum.	49

8 PDE and (n+ γ) dose ratio for selected filter materials in the final geometry. The “(n+ γ) dose ratio” is the ratio of the (n+ γ) dose rate of the beam without any filter over the (n+ γ) dose rate of the filter under investigation. The PDE listed is the maximum PDE. 51

9 Dimensions of the filter and collimator components. All units are in inches. 57

10 Coefficients resulting from a least squares fit of Equation 30. These coefficients describe the loss in dose rate as a function of filter thickness. WSSR/ndf is also known as the reduced chi-square. WSSR is the weighted sum of squared residuals and ndf is the number of degrees of freedom. . . . 63

11 Experiment-to-calculated ratios (E/C) of the (n+ γ) dose at 3-cm in the water phantom and the PDE at 5-cm deep in the water phantom for the BNCEFNT beam. 77

12 Constants for the mathematical head phantom. 83

13 PDE as a function of tungsten filter thickness and a 5.64-cm diameter tungsten collimator placed near the head. The head is surrounded by a moderator of varying amounts of graphite. Using the 20 \times 20 cm² standard treatment beam incident on the tungsten filter and collimator. 85

14 The depth-dose measurements of the 20 \times 20 cm² standard therapy beam using the borated and non-borated chambers. The borated chamber response and the percent dose enhancement have been normalized to 100-ppm ¹⁰B. . 94

15 The depth-dose measurements of the 10 \times 10 cm² standard therapy beam using the borated and non-borated chambers. The borated chamber response and the percent dose enhancement have been normalized to 100-ppm ¹⁰B. . 95

16 The depth-dose measurements of the 55.3-cm diameter standard therapy beam using the borated and non-borated chambers. The borated chamber response and the percent dose enhancement have been normalized to 100-ppm ¹⁰B. 95

17 Measurements used to optimize iron filter thickness for the 20-cm diameter BNCEFNT beam. All data given here is for 5-cm deep in the water phantom. The measurements have been normalized to 100-ppm ¹⁰B. 96

18 The depth-dose measurements of the BNCEFNT beam filtered with 18.3-cm of iron and collimated with iron to a diameter of 20 cm at the isocenter using the borated and non-borated chambers. The results have been normalized to 100-ppm ¹⁰B. 96

19 The depth-dose measurements of the BNCEFNT beam filtered with 18.3-cm of iron and collimated with iron to a diameter of 10 cm at the isocenter using the borated and non-borated chambers. The results have been normalized to 100-ppm ¹⁰B. 97

20 MCNPX depth-dose calculation of the 20 × 20 cm² standard treatment beam. The borated chamber response and the percent dose enhancement were normalized to 100-ppm ¹⁰B. 98

21 MCNPX depth-dose calculation of the 10 × 10 cm² standard treatment beam. The borated chamber response and the percent dose enhancement were normalized to 100-ppm ¹⁰B. 99

22 MCNPX depth-dose calculation of the 55.3-cm diameter standard treatment beam. The borated chamber response and the percent dose enhancement were normalized to 100-ppm ¹⁰B. 99

23 MCNPX depth-dose calculation of the 20-cm BNCEFNT beam. The borated chamber response and the percent dose enhancement were normalized to 100-ppm ¹⁰B. 100

24 MCNPX depth-dose calculation of the 10-cm BNCEFNT beam. The borated chamber response and the percent dose enhancement were normalized to 100-ppm ¹⁰B. 100

25	Borated detector measurement data of the $20 \times 20 \text{ cm}^2$ standard therapy beam. Measurements made Jan. 2001.	102
26	Borated detector measurement data of the $20 \times 20 \text{ cm}^2$ standard therapy beam. Measurements made Dec. 2001.	103
27	Non-borated detector measurement data of the $20 \times 20 \text{ cm}^2$ standard therapy beam. Measurements made Jan. 2001.	103
28	Non-borated detector measurement data of the $20 \times 20 \text{ cm}^2$ standard therapy beam. Measurements made Dec. 2001.	104
29	Borated detector measurement data of the $10 \times 10 \text{ cm}^2$ standard therapy beam. Measurements made Jan. 2001.	105
30	Non-borated detector measurement data of the $10 \times 10 \text{ cm}^2$ standard therapy beam. Measurements made Jan. 2001.	106
31	Borated detector measurement data of the 55.3-cm diameter standard therapy beam. Measurements made Jan. 2001.	107
32	Non-borated detector measurement data of the 55.3-cm diameter standard therapy beam. Measurements made Jan. 2001.	108
33	Borated detector measurement data of the 20-cm diameter iron collimated and iron filtered BNCEFNT beam.	109
34	Non-borated detector measurement data of the 20-cm diameter iron collimated and iron filtered BNCEFNT beam.	110
35	Borated detector measurement data of the 10-cm diameter iron collimated and iron filtered BNCEFNT beam.	111
36	Non-borated detector measurement data of the 10-cm diameter iron collimated and iron filtered BNCEFNT beam.	112

LIST OF FIGURES

1	Plot of the tumor control probability. The plot is shown only to illustrate the shape of the tumor control probability function not to indicate actual safe treatment doses.	8
2	Diagram of the Fermilab Neutron Therapy Facility beryllium target, primary collimator, and transmission chamber.	11
3	Diagram of the Fermilab Neutron Therapy Facility target and collimator.	11
4	Exradin Model T2 tissue-equivalent ion chamber.	14
5	^{137}Cs calibration source located in the Fermilab Neutron Therapy Facility treatment room. The source was used for checking the proper operation of the ionization chambers before use.	25
6	Thermal neutron calibration of the TE ionization chambers at the Oregon State University Research Reactor. Here a detector has been placed on a plastic holder and inserted into the thermal column of the reactor.	26
7	Depth-dose measurement of the $20 \times 20 \text{ cm}^2$ standard therapy beam as measured with the borated and non-borated TE ionization chambers. The borated detector measurements have been normalized to 100-ppm ^{10}B . The errors shown do not include the 9% error associated with the coefficients of the Bragg-Gray equation.	32

8	PDE of the $20 \times 20 \text{ cm}^2$ standard therapy beam as measured with the borated and non-borated TE ionization chambers. The PDE has been normalized to 100-ppm ^{10}B . The error shown is the total experimental and systematic error.	33
9	Depth-dose measurement of the $10 \times 10 \text{ cm}^2$ standard therapy beam as measured with the borated and non-borated TE ionization chambers. The borated detector measurements have been normalized to 100-ppm ^{10}B . The experimental errors are shown.	34
10	PDE of the $10 \times 10 \text{ cm}^2$ standard therapy beam as measured with the borated and non-borated TE ionization chambers. The PDE has been normalized to 100-ppm ^{10}B . The total experimental and systematic errors are shown.	35
11	Depth-dose measurement of the 55.3-cm diameter beam as measured with the borated and non-borated TE ionization chambers. The borated detector measurements have been normalized to 100-ppm ^{10}B . Only the experimental errors are shown.	37
12	PDE of the 55.3-cm diameter beam as measured with the borated and non-borated TE ionization chambers. The PDE has been normalized to 100-ppm ^{10}B . The total experimental and systematic errors are shown.	38
13	Depth-dose measurement and MCNPX calculation of the Fermilab Neutron Therapy Facility standard treatment beam ($20 \times 20 \text{ cm}^2$ field). The non-borated detector represents fast neutron and gamma dose. The borated detector represents fast neutron, gamma, and boron capture dose for 100-ppm ^{10}B . The MCNPX calculation has been normalized to the non-borated detector measurement at 3-cm deep, resulting in a 2.69 normalization factor.	40

14 Depth-dose measurement and MCNPX calculation of the Fermilab Neutron Therapy Facility standard treatment beam ($10 \times 10 \text{ cm}^2$ field). The non-borated detector represents fast neutron and gamma dose. The borated detector represents fast neutron, gamma, and boron capture dose for 100 ppm ^{10}B . The MCNPX calculation has been normalized to the non-borated detector measurement at 3-cm deep, resulting in a 2.96 normalization factor. 41

15 Depth-dose measurement and MCNPX calculation of the Fermilab Neutron Therapy Facility standard treatment beam (55.3-cm dia. field). The non-borated detector represents fast neutron and gamma dose. The borated detector represents fast neutron, gamma, and boron capture dose for 100-ppm ^{10}B . The MCNPX calculation has been normalized to the non-borated detector measurement at 3-cm deep, resulting in a 2.73 normalization factor. 42

16 Measurements and MCNPX calculations of the Percent Dose Enhancement (PDE) for three fields: $10 \times 10 \text{ cm}^2$, $20 \times 20 \text{ cm}^2$, and 55.3-cm diameter. The results have been normalized to 100-ppm ^{10}B . The MCNPX calculations are performed using the Bertini INC model. 44

17 MCNPX model geometry for the first iteration of the filter material testing. The filter was tested for 6 thicknesses of 83 materials. The thicknesses tested were 5, 10, 15, 20, 25, and 30 cm. 46

18 MCNPX calculated values for the PDE and the $(n+\gamma)$ dose ratio. The $(n+\gamma)$ dose ratio is the ratio of the $(n+\gamma)$ dose rate of the beam without any filter over the $(n+\gamma)$ dose rate of the filter under investigation. The plotted PDE is the PDE at 7-cm in depth. 48

19 Diagram of the iron filter and filter holder, along with the 20-cm-diameter-field steel collimator. The field size is the projected size of the collimated field at the isocenter. The diagram in the upper left depicts the collimator inserted in the Fermilab facility. 50

20	PDE and intensity vs the iron filter thickness for the proposed design. . . .	52
21	Diagram of the base section of the BNCEFNT filter and collimator. The base section provides an interface to the Fermilab FNT facility collimator geometry. This base section is inserted in place of the small Benelex liner. .	53
22	Diagram of the filter holder. All dimensions are in inches.	54
23	Diagram of the iron filter. All dimensions are in inches.	54
24	Diagram of the BNCEFNT 20-cm diameter collimator. The insert in the upper right shows the 20-cm diameter collimator (hatched) inserted into the base section.	55
25	Diagram of the BNCEFNT 10-cm diameter collimator. The boxed insert in the upper right shows the 10-cm diameter collimator (hatched) inserted into the BNCEFNT 20-cm collimator.	56
26	Photograph of the BNCEFNT filter and collimator.	56
27	Photograph of the 20-cm diameter collimator inserted into the Fermilab Neutron Therapy Facility.	57
28	Measurements of the PDE as a function of depth in the water phantom for five iron filter thickness. The beam was collimated with the 20-cm diameter iron collimator. The PDE is normalized to 100-ppm ^{10}B . The errors shown do not include errors in the PDE correction factor. Only the experimental errors are shown.	60
29	Measurements of the PDE at 5-cm deep and measurements of the dose rate ratios as a function of iron filter thickness. The beam was collimated with the 20-cm diameter iron collimator.	61
30	Depth-dose measurement of the 20-cm diameter BNCEFNT beam filtered with 18.3-cm of low carbon steel. The borated detector measurements have been normalized to 100-ppm ^{10}B	65

31	Central axis relative depth-dose measurement of the 20-cm diameter BNCEFNT beam filtered with 18.3-cm of low carbon steel and the $20 \times 20 \text{ cm}^2$ standard treatment beam. The measurements have been normalized at 2.0-cm deep in the water phantom.	66
32	PDE measurements of the 20-cm diameter BNCEFNT beam filtered with 18.3-cm of low carbon steel.	67
33	Off-axis measurements taken perpendicular to the beam direction at a depth of 4-cm in the water phantom for the 20-cm diameter BNCEFNT beam filtered with 18.3-cm of low carbon steel. The borated detector measurements have been normalized to 100-ppm ^{10}B	68
34	Off-axis boron capture dose measured perpendicular to the beam direction at a depth of 4-cm in the water phantom for the 20-cm diameter BNCEFNT beam filtered with 18.3-cm of low carbon steel. The boron capture dose has been normalized to 100-ppm ^{10}B	70
35	X-ray film irradiated with the 20-cm diameter iron collimator and the 18.3-cm thick low carbon steel filter. Three of the threaded holes used for inserting and removing the filter pieces can be seen as dark circles. The image has been contrasted to show the effects of the threaded holes. The width of the beam is 20.5 cm and the height of the beam is 20.0 cm	71
36	Depth-dose measurement of the 10-cm diameter BNCEFNT beam filtered with 18.3-cm of low carbon steel. The borated detector measurements have been normalized to 100-ppm ^{10}B	72
37	PDE measurements of the 10-cm diameter BNCEFNT beam filtered with 18.3-cm of low carbon steel.	73

38	Central axis relative depth-dose measurement of the 10-cm diameter BNCEFNT beam filtered with 18.3-cm of low carbon steel and the $10 \times 10 \text{ cm}^2$ standard treatment beam. The measurements were normalized at 2.0-cm deep in the water phantom.	74
39	Off-axis measurements taken perpendicular to the beam direction at a depth of 4-cm in the water phantom for the 10-cm diameter BNCEFNT beam filtered with 18.3-cm of low carbon steel. The borated detector measurements have been normalized to 100-ppm ^{10}B	75
40	Off-axis boron capture dose measured perpendicular to the beam direction at a depth of 4-cm in the water phantom for the 10-cm diameter BNCEFNT beam filtered with 18.3-cm of iron. The boron capture dose has been normalized to 100-ppm ^{10}B	76
41	Depth-dose measurement and MCNPX calculation of the 20-cm diameter BNCEFNT beam. The non-borated detector represents fast neutron and gamma dose. The borated detector represents fast neutron, gamma, and boron capture dose for 100 ppm ^{10}B . The MCNPX calculation has been normalized to the non-borated detector measurement at 3-cm deep, resulting in a 2.88 normalization factor.	78
42	Depth-dose measurement and MCNPX calculation of the 10-cm diameter BNCEFNT beam. The non-borated detector represents fast neutron and gamma dose. The borated detector represents fast neutron, gamma, and boron capture dose for 100 ppm ^{10}B . The MCNPX calculation has been normalized to the non-borated detector measurement at 3-cm deep, resulting in a 2.92 normalization factor.	79
43	MCNPX calculation of the PDE vs. measurements of the 20-cm BNCEFNT beam filtered with 18.3-cm of low carbon steel.	80

44	MCNPX calculation of the PDE vs. measurements of the 10cm BNCEFNT beam filtered with 18.3-cm of low carbon steel.	81
45	Diagram of the mathematical head phantom used in MCNPX to estimate dose enhancement in a head.	83
46	Diagram of the MCNPX model of a tungsten filter, tungsten collimator, full graphite moderator, and mathematical head phantom.	86
47	Diagram of the MCNPX model of the partial graphite moderator, tungsten collimator, and mathematical head phantom.	87
48	Calculated isodose curve of the (n,γ) dose for the partial graphite moderator, 5.64-cm diameter tungsten collimator, 1.5-cm tungsten filter, and mathematical head phantom. The thick elliptical line is the outline of the head phantom.	88

SUMMARY

The combination of fast neutron therapy and boron neutron capture therapy is currently under investigation at several fast neutron therapy centers worldwide. This treatment method, termed boron neutron capture enhanced fast neutron therapy (BNCEFNT) utilizes a boron containing drug to selectively increase the dose to the target tumor. BNCEFNT may be useful in the treatment of some radioresistant brain tumors, such as glioblastoma multiforme.

A neutron therapy beam for boron neutron capture enhanced fast neutron therapy has been developed for the existing Fermilab Neutron Therapy Facility. This beam produces a significant dose enhancement due to the the boron neutron capture reaction. The beam was developed by designing a filter and collimator system using the Monte Carlo radiation transport code, MCNPX. The MCNPX code was benchmarked against depth-dose measurements of the standard treatment beam. The new BNCEFNT beam is filtered with 18.3-cm of low carbon steel and is collimated with steel.

Measurements of the dose enhancement of the new BNCEFNT beam were performed with paired tissue equivalent ion chambers. One of the ion chambers has boron incorporated in the wall of the chamber to measure the dose due to boron neutron capture. The measured boron dose enhancement of the BNCEFNT beam is $(16.3 \pm 2.6)\%$ per 100-ppm ^{10}B for a 20-cm diameter beam and $(10.0 \pm 1.6)\%$ per 100-ppm ^{10}B for a 10-cm diameter beam. The dose rate of the new beam is reduced to 4.4% of the dose rate of the standard treatment beam.

A conceptual design that overcomes the reduced dose rate is also presented. This design uses a tungsten collimator placed near the patient, with a 1.5-cm tungsten filter just upstream of the collimator. Using graphite moderation of neutrons around the patient a percent dose enhancement of 15% can be attained with good collimation, for field sizes as small as $5 \times 5 \text{ cm}^2$, and without a reduction in dose rate.

CHAPTER I

INTRODUCTION

Cancer is the second leading cause of death in the U.S. with approximately 1 in 4 deaths caused by cancer. About one-half of all men and one-third of all women will contract cancer in their lifetimes. Approximately 555,500 people in the U.S. will die from cancer in 2002 [1]. About 8000 will die from an aggressive form of brain cancer, a tumor known as glioblastoma multiforme (GBM). Diagnosis of this tumor type is a virtual death sentence, with a mean length of survival between 8 to 10 months, and a survival rate after 2 years of only 10%.

Glioblastoma multiforme is a primary, grade 4, brain tumor. This type of tumor is radio-resistant and removal of the complete tumor is difficult due to the finger-like extensions that protrude from the main tumor mass. Both photon therapy and fast neutron therapy have failed to provide a cure for GBM. However, the use of postoperative radio-therapy has been shown to increase the median survival rate [2]. Results from studies of fast neutron therapy to control GBM have prompted interest in the use of high-linear energy transfer (LET) radiation in the treatment of GBM. Comparing fast neutron and megavoltage x-rays in the treatment of GBM, Catterall reported a greater anti-tumor effect for patients receiving fast neutron therapy as opposed to photon therapy [3].

There has been much interest in the use of boron neutron capture therapy (BNCT) to treat glioblastoma. In this treatment a boron containing drug is used to localize ^{10}B in the tumor cells. The tumor is then irradiated with a thermal or epithermal neutron beam from a nuclear reactor or other neutron source. The boron capture reaction emits a alpha

particle and a lithium ion, resulting in a large localized dose to the tumor. Attempts to treat GBM patients with BNCT have met with limited success.

In 1978 Waterman proposed the combination of boron neutron capture therapy and fast neutron therapy [4]. This therapy, known as boron neutron capture enhanced fast neutron therapy (BNCEFNT) utilizes boron containing drugs during treatment with a fast neutron beam. Some fast neutrons will thermalize in tissue and undergo neutron capture with ^{10}B , thus providing a localized boost to the tumor. Several investigations into the use of BNCEFNT have occurred at fast neutron therapy facilities worldwide. However, no GBM patients have yet been treated with BNCEFNT.

1.1 Objective

The objective of this work was to design a beam tailored for BNCEFNT at the Fermilab Neutron Therapy Facility. Since neutron therapy is on-going at the Fermilab Neutron Therapy Facility, this design must not interfere with current patient treatment. It is estimated that the dose required to control glioblastoma is approximately 15% greater than the safe dose to healthy tissue. Therefore, the goal of this design is to provide a 15% fractional increase in the absorbed dose for a tumor concentration of 100-ppm ^{10}B and a field size of $20 \times 20 \text{ cm}^2$.

A limitation of the design is that the dose rate must be high enough to perform patient treatments in an acceptable time period. This limitation would be achieved by maintaining a dose rate of $1/15^{\text{th}}$ the dose rate of the standard treatment beam.

1.2 Organization

This work is organized in the following manner. In Chapter 2 a brief review of BNCT, fast neutron therapy, and BNCEFNT is given. A description of the Fermilab Neutron Therapy Facility is also included in Chapter 2. The equipment and methods used to measure the fast neutron dose and the boron neutron capture dose are presented in Chapter 3. The

results of the calibration of the detectors used in this work are also reported in Chapter 3, with an emphasis on the thermal neutron calibration of the detectors. The benchmarking of the radiation transport code used to develop the BNCEFNT beam and the design of the BNCEFNT beam are presented in Chapter 4. Chapter 5 describes the results of measurements performed on the constructed BNCEFNT beam and summarizes how the final measurements compared with calculations. Chapter 6 lists possible methods for further increasing the dose enhancement while minimizing the treatment time. Conclusions and final recommendations for future investigations are presented in Chapter 7.

A list of acronyms is provided in Appendix A. Tabulated results of the measurements and calculations are listed in Appendix B. The raw data from the depth-dose measurements is given in Appendix C. And selected MCNPX input files are listed in Appendix D.

CHAPTER II

BACKGROUND

2.1 Fast Neutron Therapy

The beneficial uses of neutrons in the treatment of cancer was recognized soon after James Chadwick's discovery of the neutron in 1932 [5]. In 1936 John Lawrence and Ernest Lawrence began studying the biological effectiveness of neutrons relative to x-rays. They found that neutrons were about ten times more effective than x-rays in reducing the white blood cell count in rats [6]. Concurrently, Raymond Zirkle and Paul Aebersold found that neutrons were about 20 times more effective in retarding the growth of wheat seedlings [7]. Noting the difference in the biological effectiveness of neutrons relative to x-rays for white blood cells and wheat, Zirkle and Aebersold made a prophetic leap.

"... if the ratio of neutron effectiveness to x-ray effectiveness is not the same for all biological systems, there exists the strong possibility that this ratio may be lower for normal tissue than for tumor tissue, in which case there would be a distinct advantage in using neutrons."

In the same year John Lawrence, Paul Aebersold, and Ernest Lawrence demonstrated that neutrons were more "selectively effective" in killing tumor tissue than healthy tissue compared to x-rays [8]. Only 6 years after the discovery of the neutron Stone and Larkin began studies on patients using fast neutrons [9]. In 1939, they began to treat patients in earnest using a neutron beam produced by 16-MeV deuterons on a beryllium target. Stone reported

that the neutrons produced a beneficial tumor response, but the treatment resulted in unacceptable late skin and subcutaneous radiation changes [10]. Stone's findings discouraged the pursuit of neutron therapy for the next 2 decades.

Interest in fast neutron therapy re-surfed in the 1960's spurred by studies of the reduction in the oxygen enhancement ratio with neutrons as compared to photons [11]. The oxygen enhancement ratio (OER) is the ratio of the dose required to reach a biological end-point when irradiation is performed under oxygenated conditions to the dose required to reach the same end-point under hypoxic (oxygen deficient) conditions. The use of neutrons reduces the oxygen enhancement ratio from about 3 for x-rays to about 1.6. All tumors contain some portion of hypoxic cells, but after irradiation the hypoxic cells of some types of tumors will undergo re-oxygenation. However, some slowly growing tumors do not undergo re-oxygenation. Thus, researchers concluded that the use of neutrons to treat these slowly growing tumors would benefit from the reduction in the oxygen enhancement ratio.

The resurgence in fast neutron therapy was centered at Hammersmith Hospital in London under the direction of Mary Catterall. Investigators at Hammersmith demonstrated that fast neutron therapy could be used to treat tumors that are radio-resistant to conventional treatment [12, 13].

With the promising results of the Hammersmith group, interest in fast neutron therapy soared. Fast neutron centers were built throughout the world. In the U.S. the National Cancer Institute funded the construction of three neutron facilities at medical centers in Houston, Los Angeles, and Seattle. However, enthusiasm in fast neutron therapy soon subsided.

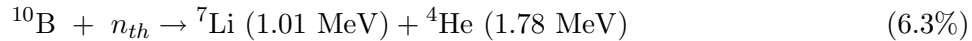
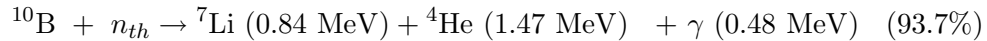
The neutron energy of the early facilities was generally too low. Even using sub-optimal neutron beams several tumors types were identified for which fast neutrons have a substantial advantage over conventional photon therapy. These tumor types include salivary gland tumors, prostatic adenocarcinomas, and advanced tumors of the head and neck area. It is estimated that 10-20% of all oncology patients would benefit from fast neutron therapy [14].

Today only three fast neutron therapy facilities are in operation in the U.S: The University of Washington in Seattle, Harper Hospital in Detroit, and Fermilab Neutron Therapy Facility in Batavia, IL.

2.2 Boron Neutron Capture Therapy

The use of the neutron capture therapy for the treatment of cancer was proposed by Locker [15] in 1936. The advantage of ^{10}B in neutron capture therapy over other isotopes is its large reaction cross section, 3839 barns at 0.0253 eV, its high natural abundance 19.82%, and the short range of the resulting reaction products. ^{10}B is also available enriched to greater than 90%.

The boron capture reaction releases an average of 2.79 MeV per neutron capture. The recoiling alpha particle and lithium ion carry away an average of 2.34 MeV in the following manner:



The lithium ion and alpha particle lose their energy over distances less than $10 \mu\text{m}$, which is in turn less than the diameter of a cell nucleus. The alpha particle (1.5 MeV) has a stopping power of about 150 MeV/mm and the lithium ion (0.85 MeV) has a stopping power of 52 MeV/mm. This is compared to only 0.2 MeV/mm for electrons [16].

William Sweet was the first to apply boron neutron capture therapy (BNCT) to the treatment of brain tumors. Sweet showed that the blood-brain barrier prevents “first generation” borated compounds from reaching normal tissue [17]. Sweet’s work led to the first clinical trials of BNCT in February of 1951 at Brookhaven National Laboratory. Trials continued at Brookhaven and at Massachusetts Institute of Technology (MIT) until they were halted in the early 1960’s. These trials did indicate that BNCT lead to temporary improvement of the patients symptoms. However, there were severe complications from the

treatments. The patients suffered from radiation induced necrosis of the brain, severe skin lesions due to boron neutron capture in the scalp, and recurrent tumor [18].

In 1968 BNCT trials began in Japan under the direction of Hiroshi Hatanaka. Hatanaka reported a 5-year survival rate of 58% for 38 patients who were treated solely with BNCT and had superficially located tumors [19].

These results helped to maintain interest in BNCT worldwide. Clinical trials returned to the United States in 1994 with trials performed at Brookhaven and MIT. These new trials failed to prove that BNCT is a viable treatment modality for GBM. Recently, BNCT research has been conducted using more penetrating epithermal neutron beams. These beams cause the thermal neutron flux peak to be at depth in the tissue rather than on the surface.

2.3 Boron Neutron Capture Enhanced Fast Neutron Therapy

Boron neutron capture enhanced fast neutron therapy (BNCEFNT) was first proposed by Waterman in 1978 [4]. In this treatment, a boron containing drug would conceptually be used to selectively load the tumor cells with boron. Instead of irradiating the tumor with a thermal or epithermal neutron beam, the tumor is irradiated with a fast neutron therapy beam. Since fast neutron beams are designed to minimize the thermal neutron spectral component, very little neutron capture in boron occurs. In order to increase the rate of boron neutron capture, modification of the neutron spectrum to include a thermal neutron component is required. Several fast neutron therapy facilities are currently investigating ways of increasing the boron neutron capture dose, including the Fermilab Neutron Therapy Facility. The objective of this work is to design a beam filtration system for boron neutron capture enhanced fast neutron therapy for the Fermilab Neutron Therapy Facility.

Clinical trials comparing fast neutron therapy with conventional photon therapy in the treatment of glioblastoma multiforme (GBM) showed that neutron therapy produced a temporary improvement for many patients [20]. Autopsies of GBM patients treated

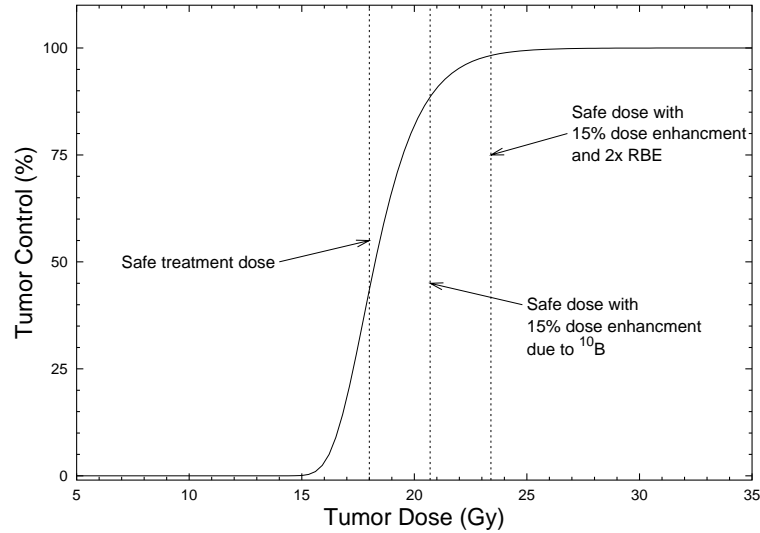


Figure 1: Plot of the tumor control probability. The plot is shown only to illustrate the shape of the tumor control probability function not to indicate actual safe treatment doses.

with fast neutrons have shown success in killing the tumor but at the expense of healthy tissue [3, 21, 22]. After clinical trials performed at Fermilab, Saroja *et al.* concluded:

“... neutrons can eradicate malignant glioma cells but in the view of the severity of normal brain damage there appeared to be no identifiable therapeutic window at which local control could be achieved without lethal side effects.”

The additional of a selective dose to the tumor alone due to the boron capture reaction may lead to an identifiable therapeutic window. Studies suggest that the relative biological effectiveness (RBE) for boron neutron capture may be as high as twice the RBE for the fast neutron beam [4, 23]. Since tumor control is a steep function of tumor dose, a small increase in tumor dose may lead to a significant increase in tumor control (Fig. 1). Thus, an increase of only 10% to 15% in the total absorbed dose, when coupled with the higher RBE, could significantly reduce the tumor survival probability.

Investigations into the use of BNCEFNT are currently in progress at several FNT facilities worldwide, including the University of Washington (UW), Harper Hospital Fast

Neutron Therapy Facility, and the Biomedical Cyclotron of Nice. The University of Washington has recently designed and installed a new target specifically for BNCEFNT studies. The University of Washington BNCEFNT beam uses a cyclotron to accelerate protons to 50.5 MeV. The protons are directed onto a laminated target with a 5-mm layer of beryllium, followed by a 2.5-mm layer of tungsten. This new target design produces essentially the same neutron flux above 40-MeV as their unmodified FNT beam, but leads to a decreased fluence rate in the 10 to 40-MeV range, and an increased fluence rate below 10 MeV. The new target produces a boron dose enhancement of 13% to 14% per 100-ppm ^{10}B for a $10 \times 10 \text{ cm}^2$ beam. The unmodified FNT target resulted in a boron dose enhancement of about 7% [24].

The Harper Hospital Fast-Neutron Therapy Facility uses a superconducting cyclotron to produce a 48.5-MeV deuteron beam that is incident on a thick beryllium target [25]. Studies at this facility have investigated the use of steel, tungsten, lead, and aluminum as possible filter materials for a BNCEFNT beam [26]. They found that steel and tungsten provided the highest dose enhancements. The unmodified beam of this facility has a boron dose enhancement of 2.5% to 5% per 100-ppm ^{10}B [27].

The Nice Biomedical Cyclotron produces 60-MeV protons that are incident on a laminated target of 15-mm of beryllium followed by 9-mm of graphite. A FLUKA/MCNP-4A study of the Nice facility calculated a percent dose enhancement (PDE) of 4.6% per 100-ppm ^{10}B for a $10 \times 10 \text{ cm}^2$ beam. A $20 \times 20 \text{ cm}^2$ beam produced a dose enhancement of 10.4% per 100-ppm ^{10}B [28]. Further studies by Paquis and Pignol to increase the PDE for the Nice Biomedical Cyclotron have focused on the addition of high Z material collimation near the patients head [23, 29]. The head was assumed to be surrounded by a block of graphite. These studies concluded that a lead collimator placed near the head can produce dose enhancements of 22% per 100-ppm ^{10}B . Pignol assumed that the gamma from the boron capture reaction is deposited locally, thus resulting in 2.79-MeV per neutron capture [30]. If the gamma is not assumed to be deposited locally the PDE reduces to 18% per

100-ppm ^{10}B .

2.4 Fermilab Neutron Therapy Facility

The Fermilab Neutron Therapy Facility, located at the Fermi National Accelerator Laboratory, has been treating patients using fast neutrons since 1976. The facility produces neutrons by bombarding a 2.21-cm-thick beryllium target with 66-MeV protons. The protons lose 49 MeV in the beryllium target and are stopped by a 0.5-mm gold backing [31]. This projectile target combination is abbreviated p(66)Be(49). The incident proton beam on the target is focused to 5-mm in diameter. The beryllium target is cooled by conduction to a water-cooled aluminum block. The resulting neutron beam is initially collimated by a low carbon steel primary collimator, located adjacent to the target assembly. Dual parallel plate ionization chambers are located on the downstream side of the primary collimator. These transmission chambers are used to monitor the neutron flux during experiments and therapy. The chambers are made of aluminum and filled with air. When calibrated against tissue-equivalent ionization chambers the transmission chambers have an error of $\pm 0.2\%$ [32]. The output of the transmission chambers are automatically corrected for temperature and pressure by the treatment monitoring computer and converted to monitor units (MU). The transmission chambers are calibrated such that one monitor unit produces a dose of one gray at 10-cm deep in tissue for a $10 \times 10 \text{ cm}^2$ collimator. A diagram of the target, primary collimator, and transmission chamber is shown in Figure 2.

The secondary collimator employs 79-cm long concrete-polyethylene collimators. Different collimators are used to produce different treatment field sizes. The removable collimators are inserted inside concentric Benelex [33] liners. The Benelex liners can be removed to accommodate different size collimators. A diagram of the target and collimators is shown in Figure 3. The downstream face of the collimators is 109 cm from the center of the beryllium target. The target to isocenter distance is 190 cm.

The Fermilab proton Linac supplies the Fermilab Neutron Therapy facility protons at a

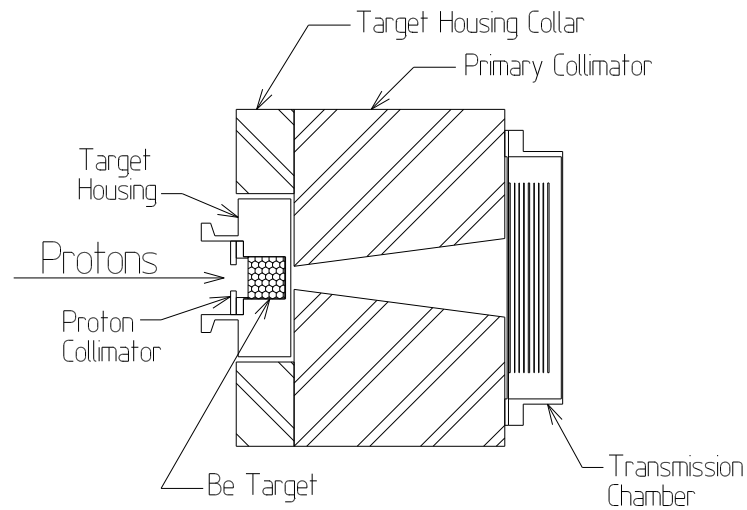


Figure 2: Diagram of the Fermilab Neutron Therapy Facility beryllium target, primary collimator, and transmission chamber.

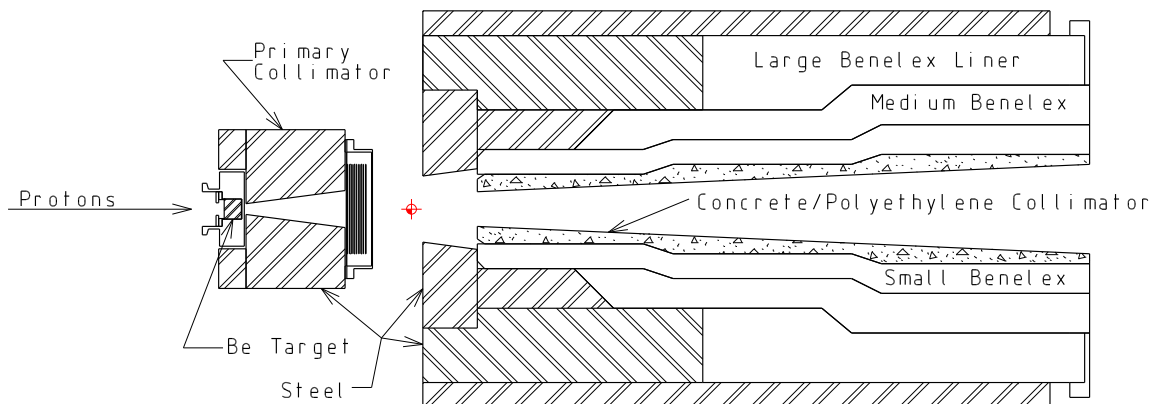


Figure 3: Diagram of the Fermilab Neutron Therapy Facility target and collimator.

pulse rate of 15 Hz. Each of the 15 Hz macropulses is 57 microseconds long and is composed of one-nanosecond micropulses. The micropulses are spaced five nanoseconds apart. The length of the macropulse can be decreased to reduce the dose rate.

The percent dose enhancement (PDE) of the Fermilab Neutron Therapy Facility has been measured by Katja Langen using a tissue-equivalent proportional counter loaded with 200-ppm ^{10}B [34]. These measurements were performed in a head-shaped Lucite phantom filled with water at a depth of 5 cm. Langen measured a PDE of $(1.5 \pm 0.1)\%$ per 100-ppm ^{10}B for the $10 \times 10 \text{ cm}^2$ field of the standard treatment beam. Langen also attempted to modify the beam to increase the dose enhancement by using 9.0-cm of tungsten filtration. The tungsten filter was placed near the head phantom and produced a dose enhancement of $(2.5 \pm 0.1)\%$ for 100-ppm ^{10}B . Langen was able to obtain a dose enhancement of $(6.0 \pm 0.2)\%$ by reducing the proton energy to 37-MeV, using 20-cm thick steel blocks to form a $12 \times 12 \text{ cm}^2$ beam, and by filtering the beam with 9.0-cm of tungsten. She estimated a 20% increase in the RBE for the modified beam.

CHAPTER III

METHODS AND EQUIPMENT

The measurements of the standard therapy beam and the boron neutron capture enhanced fast neutron therapy (BNCEFNT) beam concentrated on the use of a borated and a non-borated tissue equivalent (TE) ionization chamber. These chambers were used to measure the fast neutron and gamma dose, and the dose due to the boron capture reaction.

3.1 Tissue Equivalent Ion Chambers

Ionization chambers provide a method of measuring absorbed dose that is both straightforward and precise. For these reasons they are the most commonly used detectors for measuring absorbed dose. The alternatives, such as calorimeters and proportional counters, are more difficult to use. Since ionization chambers are used in the course of regular patient treatment at Fermilab, they provide a direct method of comparing the dose measurement of the BNCEFNT beam to the standard treatment beam.

3.1.1 Ion Chamber Design and Composition

The two tissue-equivalent (TE) ionization chambers used in this work were 0.5-cm³ Spokas thimble chambers manufactured by Exradin [35], now Standard Imaging, Inc. A diagram of the chambers is given in Figure 4. The chambers are composed of A-150 tissue-equivalent plastic. A-150 tissue-equivalent plastic is an electrical conductive plastic formulated to have the same constituents as muscle. A-150 plastic is composed of polyethylene,

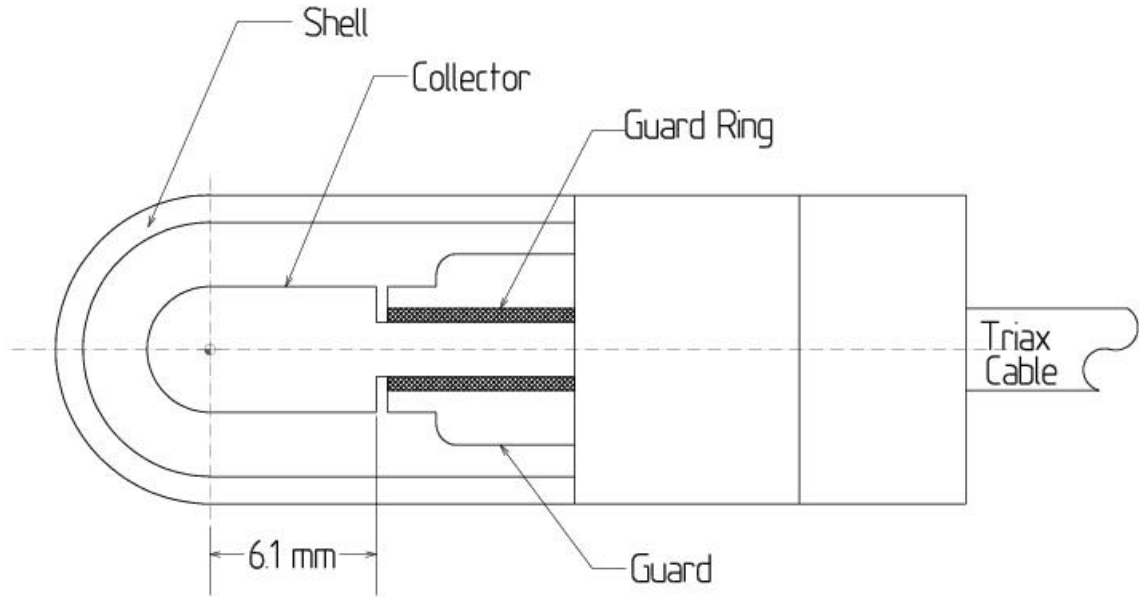


Figure 4: Exradin Model T2 tissue-equivalent ion chamber.

nylon, carbon, and calcium fluoride [36, 37]. The density of molded A-150 plastic is $1.127 \pm 0.005 \text{ g/cm}^3$ [38]. The composition of A-150 plastic is not identical to the composition of ICRU muscle because of the large addition of carbon to the plastic. The compositions of A-150 and ICRU muscle are listed in Table 1.

The two ion chambers are identical except that the borated chamber contains 1000-ppm natural boron in the tissue equivalent material. Since ^{10}B comprises 18.4 weight percent of natural boron, the borated detector contains 184-ppm ^{10}B . However, all results of this work are normalized to 100-ppm ^{10}B . Boron is used in the wall material of the chamber in order to measure the absorbed dose due to the $^{10}\text{B}(n,\alpha)^7\text{Li}$ reaction. This is the reaction of interest in BNCEFNT. MCNP models of the borated and non-borated ion chambers did not show flux depression due to ^{10}B .

The borated and non-borated A-150 materials were analyzed by the Georgia Tech Research Institute Materials Analysis Center. The materials were analyzed by inductively coupled plasma atomic emission. The borated material was found to have 989-ppm boron.

Table 1: Composition of various tissue equivalent materials (weight percent).

Material	Ref.	H	C	N	O	Others
A-150 plastic (nominally)	(1)	10.1	77.6	3.5	5.25	1.8 Ca 1.7 F
A-150 plastic	(2)	10.2 ± 0.1	76.8 ± 0.5	3.6 ± 0.2	5.9 ± 0.2	1.8 ± 0.1 Ca 1.7 ± 0.1 F
A-150 plastic	(3)	10.3 ± 0.1	76.9 ± 0.2	3.3 ± 0.1	6.9 ± 0.5	1.1 ± 0.6 Ca 1.4 ± 0.1 F
ICRU soft tissue	(4)	10.1	11.1	2.6	76.2	
ICRU muscle tissue	(5)	10.2	12.3	3.5	72.9	1.1 Na, Mg, P, S, K, Ca
Total Body	(6)	10.0	22.9	2.6	61.4	1.4 Ca, 1.1 P, 0.6 others
Brain Tissue	(7)	10.7	14.5	2.2	71.2	0.2 Na, 0.4 P, 0.2 S, 0.3 Cl, 0.3 K

(1) ICRU 26 [39].

(2) Measured, Smathers *et al* [36].

(3) Measured, Goodman [38].

(4) ICRU 33 [40].

(5) ICRU 10b [41].

(6) ICRP (1975) [42].

(7) ICRU 44 [43].

The deviation from 1000-ppm boron was less than the error of the procedure, thereby confirming that the detectors were constructed with 1000-ppm boron. The non-borated sample was measured to have less than 2-ppm boron, the detection limit of the procedure.

For all measurements and calibrations in this work the ionization chambers were filled with air.

3.1.2 Absorbed Dose Measurement

In order to convert the measured charge collected from the ionization chamber to a dose in tissue a conversion coefficient must be applied. This conversion coefficient is found by calibrating the detectors in a known gamma radiation field. This calibration coefficient converts energy deposited in air to energy deposited in tissue. The factors for converting energy deposited in air to energy deposited in tissue are determined by the theory governing ion chamber operation, Bragg-Gray theory. Ion chambers work on the principle of collecting charge liberated in the fill gas, chamber walls, and surrounding media. The charge collected, Q_x , is proportional to the absorbed dose in the chamber gas, which is in turn proportional to the absorbed dose in the chamber wall, $D_{w,x}$. Adopting the notation used by the American Association of Physicists in Medicine (AAPM) Protocol for Neutron Beam Dosimetry [37], the absorbed dose can be related to the charged collected by

$$D_{w,x} = \frac{Q_x}{M_g} \cdot \frac{\bar{W}_x}{e} \cdot (S_{w,g})_x \quad (1)$$

where

- M_g = the mass of the gas in the cavity
- $(S_{w,g})_x$ = ratio of stopping powers of wall to gas for secondary charged particles
- \bar{W}_x/e = the average energy required to produce an ion pair in the gas cavity
- e = the charge of the electron (1.60×10^{-19})

The subscript x denotes the type of radiation environment where the detector is used. If the detector is calibrated in a ^{60}Co beam the subscript is C . If the detector is used to measure a mixed radiation beam the subscript is T , for total. The subscript N is often used in place of T when the neutron component predominates the radiation field.

Since absorbed dose in tissue is the desired end-point, the ratio of the mass-energy absorption coefficient of tissue to that of A-150 (K_x) must be included in Equation 1, giving

$$D_{t,x} = D_{w,x} \cdot K_x = \frac{Q_x}{M_g} \cdot \frac{\bar{W}_x}{e} \cdot (S_{w,g})_x \cdot K_x \quad (2)$$

where $D_{t,x}$ is the absorbed dose to tissue.

For measuring the absorbed dose in a phantom for a mixed fast neutron and gamma radiation environment Equation 2 becomes

$$D_{t,T} = \frac{Q_T}{M_g} \cdot \frac{\bar{W}_N}{e} \cdot (S_{w,g})_N \cdot K_N \cdot d_{NG} \quad (3)$$

where $K_N = K_t/K_w$ is the ratio of neutron kerma factor for tissue to that for A-150, d_{NG} is the chamber displacement correction factor which accounts for the perturbation of the radiation field by the displacement of phantom material by the chamber, and Q_T is the charge collected by the detector. For measurements in this work, the dose due to fast neutrons and gammas is measured with the non-borated detector and Q_T is replaced by Q_{NB} . For calibrating a detector in a known ^{60}Co beam Equation 2 becomes,

$$D_{t,C} = X_C \cdot f_{t,C} \cdot A_{w,C} = \frac{Q_C}{M_g} \cdot \frac{\bar{W}_C}{e} \cdot (S_{w,g})_C \cdot K_C \quad (4)$$

where X_C is the known exposure from the ^{60}Co beam, $f_{t,C}$ is the muscle tissue dose-to-exposure conversion for ^{60}Co , and $A_{w,C}$ is the attenuation and scattering correction factor for ^{60}Co for the chamber.

Dividing Equation 3 by Equation 4

$$\frac{D_{t,T}}{X_C \cdot f_{t,C} \cdot A_{w,C}} = \frac{\frac{Q_T}{M_g} \cdot \frac{\bar{W}_N}{e} \cdot (S_{w,g})_N \cdot K_N \cdot d_{NG}}{\frac{Q_C}{M_g} \cdot \frac{\bar{W}_C}{e} \cdot (S_{w,g})_C \cdot K_C} \quad (5)$$

Table 2: AAPM recommend values and uncertainties of the constants for Equation 7. Alternate values are also listed.

Constant	AAPM Value (1)	Uncertainty (%)	Ref.	Alt. Value	Uncertainty (%)
$A_{w,C}$	0.985	0.5			
$f_{t,C}$	0.00957 Gy/R	0.2			
d_{NG}	0.981	1	(2)	0.985	0.6
$(S_{w,g})_N$	1.157	4-5			
$(S_{w,g})_C$	1.142	1.0			
\bar{W}_N/e	35.8 J/C	6-8			
\bar{W}_C/e	33.7 J/C	0.4			
K_N	0.952	2	(3)	0.926	3
K_C	1.004	0.2			

(1) AAPM Protocol for Neutron Beam Dosimetry [37].

(2) Awschalom *et al.* [44].

(3) Awschalom *et al.* [45].

and rearranging, Equation 6 is obtained

$$D_{t,T} = \frac{X_C}{Q_C} \cdot A_{w,C} \cdot f_{t,C} \cdot d_{NG} \cdot \frac{(S_{w,g})_N}{(S_{w,g})_C} \cdot \frac{\bar{W}_N}{\bar{W}_C} \cdot \frac{K_N}{K_C} \cdot Q_T \quad (6)$$

Substituting the ion chamber ^{60}Co calibration factor, N_C (R/C) = X_C/Q_C

$$D_{t,T} = N_C \cdot A_{w,C} \cdot f_{t,C} \cdot d_{NG} \cdot \frac{(S_{w,g})_N}{(S_{w,g})_C} \cdot \frac{\bar{W}_N}{\bar{W}_C} \cdot \frac{K_N}{K_C} \cdot Q_T \quad (7)$$

This equation is referred to later in this work as the Bragg-Gray equation. The AAPM recommended values and uncertainties for the factors of Equation 7 are shown in Table 2 specific to the Fermilab Neutron Therapy facility. Using these values, Equation 7 becomes

$$\begin{aligned} D_{t,T} &= N_C \text{ (R/nC)} \cdot 0.985 \cdot 0.00957 \text{ (Gy/R)} \cdot d_{NG} \cdot \frac{1.157}{1.142} \cdot \frac{35.8 \text{ (J/C)}}{33.7 \text{ (J/C)}} \cdot \frac{0.952}{1.004} \cdot Q_T \text{ (nC)} \\ &= 9.620 \times 10^{-3} \text{ (Gy/R)} \cdot N_C \text{ (R/nC)} \cdot d_{NG} \cdot Q_T \text{ (nC)} \end{aligned} \quad (8)$$

The proper use of the chamber displacement correction factor d_{NG} is not universally defined. The AAPM [37] and the European protocols [46] are at odds with each another. The AAPM suggest a multiplicative displacement correction factor while the European protocol suggest applying a point of measurement correction. The AAPM suggest that the

multiplicative displacement correction factor be used only on the descending portion of the depth-dose curve. Applying this correction on the descending portion of the curve leads to a discontinuous depth-dose curve. The AAPM bases its recommendations on the work of Shapiro *et al.* [47], who found that the chamber displacement correction factor had no dependence on field size. The European protocol adjusts for the displacement of phantom material by the ionization chamber by assigning the location of the detector to a point upstream of the actual measured location.

Awschalom *et al.* [44] performed measurements of the displacement factor on the Fermilab Neutron Therapy Facility Beam and found that the correction factor generally did have a dependence on field size in contrast to the recommendations of the AAPM. However, for a 0.5-cm³ thimble chamber Awschalom's results do not vary significantly by field size. He measured a chamber displacement correction factor of 0.984 ± 0.006 for a 7.5×7.5 cm² field and 0.985 ± 0.004 for a 35-cm diameter field. Both measurements for the 0.5-cm³ chamber were only performed at a depth of 10 cm. Awschalom did show that the chamber displacement correction factor is a function of the local field gradient and therefore is not necessarily constant for all depths. Awschalom also measured the point of measurement correction for a 0.5-cm³ chamber and found that it was 0.26 ± 0.1 cm for the 7.5×7.5 cm² field and 0.35 ± 0.1 cm for the 35-cm diameter field.

The advantage of the point of measurement correction is that it can be applied to all points equally. It is uncertain how to correct the thermal neutron response of the borated chamber for displacement of the phantom material. Since the difference between the borated and non-borated chambers is used to calculate the boron dose, the displacement factor is set to unity for this work. The resulting expression for the fast neutron and gamma dose is

$$D_{t,T} = 9.620 \times 10^{-3} \text{ (Gy/R)} \cdot N_C(\text{R/nC}) \cdot Q_T(\text{nC}) \quad (9)$$

All of the measured depth-dose data of this work is tabulated in Appendix C to allow the reader to apply the displacement factor as they desire.

The detector response is a function of the mass of the gas in the chamber volume. Since the mass of the gas varies with temperature and pressure a correction must be applied to all measurements. The measurements are corrected to a standard temperature and pressure of 0°C and 760 Torr. The correction factor (K_{TP}) to correct to these conditions is defined as

$$K_{TP} = \frac{273.15 + T_M \text{ (C)}}{273.15} \cdot \frac{760 \text{ Torr}}{P_M \text{ (Torr)}} \quad (10)$$

where T_M is the measurement temperature and P_M is the measurement pressure.

3.2 Borated Ion Chamber Thermal Neutron Response

The dose due to the boron capture reaction can be expressed as a function of the difference between the borated TE ionization chamber and the non-borated TE ionization chamber. Since alpha particles and lithium ions have a very short range in air, large chambers that have dimensions greater than the range of the alpha particles and lithium ions do not satisfy the Bragg-Gray principle. In order to overcome this problem the borated ion chamber was calibrated in a thermal neutron field. The thermal neutron fluence is proportional to the difference in the borated and non-borated ion chamber readings multiplied by a calibration factor.

$$\phi_{th} = N_{th} \cdot \left[Q_B - Q_{NB} \left(\frac{N_C^{NB}}{N_C^B} \right) \right] \quad (11)$$

where ϕ_{th} = the thermal neutron fluence (n/cm²)

N_{th} = the ionization chamber thermal neutron calibration factor (n/cm²/nC)

Q_B = the charge collected by the borated chamber (nC)

Q_{NB} = the charge collected by the non-borated chamber (nC)

N_C^{NB} = non-borated detector ⁶⁰Co calibration factor (R/nC)

N_C^B = borated detector ⁶⁰Co calibration factor (R/nC)

If the thermal neutron fluence is known then the ionization chamber thermal neutron calibration factor can be calculated from

$$N_{th} = \frac{\phi_{th}}{\left[Q_B - Q_{NB} \left(\frac{N_C^{NB}}{N_C^B} \right) \right]} \quad (12)$$

The boron capture reaction rate per unit mass, and thus the boron dose, is proportional to the thermal neutron flux. Following a methodology similar to Waterman [4], who related the response of a BF_3 detector to boron dose, the boron dose can be calculated from the boron capture reaction rate:

$$\begin{aligned} D_{boron}(Gy) &= \frac{\phi_{th} \sigma_{a_{th}}^{B-10} N_{B-10} Q (\text{Volume})}{\text{Mass}} \\ &= \frac{\phi_{th} \sigma_a^{B-10} N_{B-10} Q}{\rho_{wall}} \end{aligned} \quad (13)$$

where $\sigma_{a_{th}}^{B-10}$ = the average microscopic (n, α) cross section for thermal neutrons (cm^2).

N_{B-10} = the atom density of ^{10}B (atoms/ cm^3).

Q = the energy imparted to the alpha and lithium ions from the (n, α) reaction (2.34 MeV).

ρ_{wall} = the density of wall material (g/cm^3).

The (n, α) cross section averaged for a thermal neutron distribution ($\sigma_{a_{th}}^{B-10}$) is related to the (n, α) cross section for 2200 m/s neutrons (0.0253 MeV) by

$$\sigma_{a_{th}}^{B-10} = \frac{\sqrt{\pi}}{2} \left(\frac{T_0}{T_n} \right)^{1/2} \sigma_a^{B-10}(E_0) \quad (14)$$

where T_0 = temperature of the tabulated cross section, typically 293.46 K.

T_n = temperature of the moderator for the measurement (K).

$\sigma_a^{B-10}(E_0)$ = the microscopic (n, α) cross section for neutrons of energy E_0 , typically 0.0253 MeV or 2200 m/s (cm^2).

Assuming that the calibration is made near room temperature (293.46 K) equation 14 reduces to

$$\sigma_{a_{th}}^{B-10} = \frac{\sqrt{\pi}}{2} \sigma_a^{B-10}(E_0) \quad (15)$$

From the ENDF-VI [48] evaluation for ^{10}B , $\sigma_a^{B-10}(0.0253\text{eV}) = 3839 \pm 6$ barns, and therefore $\sigma_{a_{th}}^{B-10} = 3402 \pm 5$ barns.

The ^{10}B atom density can be found from

$$N_{B-10} = \frac{\frac{w_{B-10}}{100} \rho_{wall} N_a}{W_{B-10}} \quad (16)$$

where w_{B-10} = weight percent of ^{10}B .

N_a = Avogadro's number.

W_{B-10} = atomic weight of ^{10}B .

Combining equations 11, 13 ,and 16

$$\begin{aligned} D_{boron}(Gy) &= N_{th} \cdot \left[Q_B - Q_{NB} \left(\frac{N_C^{NB}}{N_C^B} \right) \right] \cdot \sigma_{a_{th}}^{B-10} \cdot \frac{\left(\frac{w_{B-10}}{100} \right) \rho_{wall} N_a}{W_{B-10}} \cdot \frac{1}{\rho_{wall}} \cdot Q \\ &= N_{th} \cdot \left[Q_B - Q_{NB} \left(\frac{N_C^{NB}}{N_C^B} \right) \right] \cdot \sigma_{a_{th}}^{B-10} \cdot \frac{\left(\frac{w_{B-10}}{100} \right) N_a}{W_{B-10}} \cdot Q \end{aligned} \quad (17)$$

for the borated chamber with 184-ppm ^{10}B , Equation 17 becomes

$$\begin{aligned} D_{boron}(Gy) &= N_{th} \left(\frac{\text{n}}{\text{cm}^2 \cdot \text{nC}} \right) \cdot \left[Q_B(\text{nC}) - Q_{NB}(\text{nC}) \left(\frac{N_C^{NB}(\text{R/nC})}{N_C^B(\text{R/nC})} \right) \right] \times \\ &\quad (3402 \times 10^{-24} \text{ cm}^2) \cdot \frac{\left(\frac{184}{1 \times 10^6} \right) (6.022 \times 10^{23} \text{ atoms/mole})}{(10.01293 \text{ g/mole})} \cdot (2.34 \text{ MeV}) \times \\ &\quad (1.602177 \times 10^{-13} \text{ J/MeV}) (1000 \text{ g/kg}) \\ &= 1.404 \times 10^{-11} \left(\frac{\text{Gy}}{\text{n/cm}^2} \right) \times \\ &\quad N_{th} \left(\frac{\text{n}}{\text{cm}^2 \cdot \text{nC}} \right) \left[Q_B(\text{nC}) - Q_{NB}(\text{nC}) \left(\frac{N_C^{NB}(\text{R/nC})}{N_C^B(\text{R/nC})} \right) \right] \end{aligned} \quad (18)$$

3.3 Dose Enhancement

The percent dose enhancement (PDE) is defined as

$$\text{PDE} = \frac{D_{boron}}{D_{n+\gamma}} \times 100 \text{ (\%)} \quad (19)$$

where $D_{n,\gamma}$ is the dose due to fast neutron and gammas. Substituting Equations 9 and 18 into Equation 19 yields

$$\begin{aligned}
 \text{PDE} &= \frac{1.404 \times 10^{-11} \left(\frac{\text{Gy}}{\text{n/cm}^2} \right) N_{th} \left(\frac{\text{n}}{\text{cm}^2 \cdot \text{nC}} \right) \cdot \left[Q_B(\text{nC}) - Q_{NB}(\text{nC}) \left(\frac{N_C^{\text{NB}}(\text{R/nC})}{N_C^{\text{B}}(\text{R/nC})} \right) \right]}{9.620 \times 10^{-3} (\text{Gy/R}) \cdot N_C^{\text{B}}(\text{R/nC}) \cdot Q_{NB}(\text{nC}) \left(\frac{N_C^{\text{NB}}(\text{R/nC})}{N_C^{\text{B}}(\text{R/nC})} \right)} \times 100 (\%) \\
 &= 1.459 \times 10^{-9} \left(\frac{\text{R}}{\text{n/cm}^2} \right) \cdot \left(\frac{N_{th} \left(\frac{\text{n}}{\text{cm}^2 \cdot \text{nC}} \right)}{N_C^{\text{B}}(\text{R/nC})} \right) \times \\
 &\quad \left\{ \frac{Q_B(\text{nC}) - Q_{NB}(\text{nC}) \left(\frac{N_C^{\text{NB}}(\text{R/nC})}{N_C^{\text{B}}(\text{R/nC})} \right)}{Q_{NB}(\text{nC}) \left(\frac{N_C^{\text{NB}}(\text{R/nC})}{N_C^{\text{B}}(\text{R/nC})} \right)} \right\} \times 100 (\%) \tag{20}
 \end{aligned}$$

After calibration of the detectors in both a ^{60}Co field and in a thermal neutron field, N_C^{B} and N_{th} are known. Then Equation 20 can be simplified to

$$\text{PDE} = C_{\text{PDE}} \frac{\left[Q_B - Q_{NB} \left(\frac{N_C^{\text{NB}}}{N_C^{\text{B}}} \right) \right]}{Q_{NB} \left(\frac{N_C^{\text{NB}}}{N_C^{\text{B}}} \right)} \times 100 (\%) \tag{21}$$

where C_{PDE} is the PDE correction factor. This correction factor accounts for the over-response of the borated detector to thermal neutrons. C_{PDE} is defined as

$$C_{\text{PDE}} = 1.459 \times 10^{-9} \left(\frac{\text{R}}{\text{n/cm}^2} \right) \cdot \left(\frac{N_{th} \left(\frac{\text{n}}{\text{cm}^2 \cdot \text{nC}} \right)}{N_C^{\text{B}}(\text{R/nC})} \right) \tag{22}$$

3.4 Ionization Chamber Calibration

Calibration of the ion chambers was performed to determine their response to ^{60}Co and ^{137}Cs gamma rays as well as thermal neutrons. The borated and non-borated ion chambers were calibrated at the University of Wisconsin-Madison Radiation Calibration Laboratory to determine their response to ^{60}Co gamma-rays. The Radiation Calibration Laboratory is a National Institute of Standards and Technology (NIST) accredited secondary standards laboratory and is also accredited by the American Association of Physicists in Medicine (AAPM). The detectors were calibrated against a NIST traceable source to determine the ^{60}Co calibration factor, $N_C(\text{R/nC})$. The borated TE ion chamber had a calibration factor

Table 3: Gamma calibration results of the ^{60}Co and the ^{137}Cs calibrations.

	TE Detector (R/nC)	Borated TE Detector (R/nC)	Ratio (TE/Borated TE)
UW Calibration (Co) 4/6/01	6.709	7.055	0.9510
NTF Calibration (Cs) 5/6/96	6.743	7.072	0.9535
NTF Calibration (Cs) 1/26/01	6.885	7.279	0.9459
UW Calibration (Cs) 4/6/01	6.846	7.180	0.9535
NTF Calibration (Cs) 11/30/01	6.714	7.097	0.9460
Average	6.779	7.137	0.9499
St. Dev.	0.081	0.093	0.0038
Percent Error	1.2%	1.3%	0.4%

UW - University of Wisconsin-Madison Radiation Calibration Laboratory

NTF - Fermilab Neutron Therapy Facility.

of $7.055 \text{ R/nC} \pm 2\%$. And, the non-borated TE ion chamber had a calibration factor of $6.709 \text{ R/nC} \pm 2\%$. The differing sensitivities of the two detectors implies that the gas volume of the non-borated TE ion chamber is larger than the gas volume of the borated chamber. In order to correct for this difference in the volume of the gas a correction factor must be applied. The correction factor is given by

$$\frac{N_C^{\text{NB}}}{N_C^{\text{B}}} = \frac{6.709 \text{ (R/nC)}}{7.055 \text{ (R/nC)}} = 0.9510 \quad (23)$$

where, N_C^{NB} is the ^{60}Co calibration factor of the non-borated detector, and N_C^{B} is the ^{60}Co calibration factor of the borated detector.

Before each set of measurements, the detectors were checked with a ^{137}Cs source located in the treatment room of the Fermilab Neutron Therapy Facility (Fig. 5). This source was used to verify proper operation of the detectors before each set of measurements. The calibration factors determined with the ^{137}Cs source (Table 3) were not used in this work. However, they do show that the detectors responded consistently during the period of operation.

Since the short-ranged alpha particles generated in the boron neutron capture reaction



Figure 5: ^{137}Cs calibration source located in the Fermilab Neutron Therapy Facility treatment room. The source was used for checking the proper operation of the ionization chambers before use.



Figure 6: Thermal neutron calibration of the TE ionization chambers at the Oregon State University Research Reactor. Here a detector has been placed on a plastic holder and inserted into the thermal column of the reactor.

violate the Bragg-Gray principle, calibration in a known thermal neutron field was required. Both the borated and non-borated ion chambers were calibrated at the Oregon State University (OSU) Research Reactor. The OSU reactor is a TRIGA reactor with a maximum power of 1.1-MW. The reactor is moderated by light water and has a graphite moderated thermal column with a well-known thermal neutron fluence rate. The detectors were placed on plastic holders and inserted into the thermal column (Fig. 6). The detectors were placed in the thermal column on separate runs to prevent any interference between the detectors. The calibrations were performed at a reactor power of 1.5 kW, which provided a nominal fluence rate of 1.2×10^8 n/(cm²·s) 2200 m/s equivalent thermal fluence rate.

The thermal fluence rate of the reactor was confirmed by gold foil activation. A bare

gold foil and a cadmium covered gold foil were used. The activated foils were counted using a high-purity germanium (HPGe) detector. The measured activities of the foils were corrected to the saturated activity, and were converted to thermal neutron fluence rate using the expression for the saturation activity due to thermal neutron activation [49]

$$\phi_0 g \sigma_o = \frac{1}{G_{th}} \left[R_s - R_{s,Cd} \left(1 + \frac{g \sigma_0}{G_{res} I_0} f_1 + \frac{\sigma_0 w'}{G_{res} I_0} \right) \right] \quad (24)$$

where ϕ_0 = the equivalent 2200 m/s thermal fluence rate.

σ_0 = the 2200 m/s cross section.

G_{th} = the thermal neutron self shielding factor.

G_{res} = the epithermal neutron self shielding factor.

R_s = the reaction rate per atom for the bare foil.

$R_{s,Cd}$ = the reaction rate per atom for the cadmium-covered foil.

g = Westcott g factor, correction factor that accounts for the departure from the ideal $1/v$ cross section in the thermal energy range.

I_0 = the resonance integral for an ideal dilute detector.

f_1 = the epithermal activation of a $1/v$ detector in the energy range $5kT$ to the cadmium cutoff E_{cd} ($E_{cd}=0.55\text{eV}$) [49].

w' = the departure of the cross section from the $1/v$ law in the energy range $5kT$ to E_{cd} ($E_{cd}=0.55\text{eV}$).

The values of the coefficients for Equation 24 are taken from ASTM E 262-97 [49] (Table 4). The value of G_{th} was found by an MCNP simulation of the gold foil. The error for G_{th} listed in Table 4 is the Monte Carlo statistical error.

The true thermal neutron fluence rate is found from the equivalent 2200 m/s thermal fluence rate by

$$\phi_{th} = \frac{2}{\sqrt{\pi}} \left(\frac{T_n}{T_0} \right)^{1/2} \phi_0 \quad (25)$$

The true thermal flux in the thermal column during the calibration was 1.39×10^8 n/cm²/sec \pm 13% at a reactor power of 1.5 kW (It is important to note that this is the

Table 4: Coefficients used to determine the saturated activity due to thermal neutron activation of gold foil from ASTM E 262-97.

	Value
σ_0	98.69 ± 0.14 barns
G_{th}	0.9609 ± 0.0004
G_{res}	0.572 ± 0.010
g	1.0051
w'	0.0500
$I_0/(g\sigma_0)$	157 ± 0.3
f_1	0.468

total thermal flux at room temperature, not the 2200-m/s equivalent thermal flux). At 1.5 kW the borated TE ion chamber had an average thermal neutron response of 5.33 nC/min \pm 1.3%; while the non-borated TE ion chamber had an average thermal neutron response of 0.580 nC/min \pm 1.4 %. These values are used to determine the ionization chamber thermal neutron calibration factor N_{th} using equation 12.

$$\begin{aligned}
 N_{th} &= \frac{1.39 \times 10^8 \frac{n}{cm^2 s}}{(5.33 \text{ nC/min} - 0.580 \text{ nC/min})} 60 \text{ sec/min} \\
 &= 1.76 \times 10^9 \frac{n/cm^2}{nC} \pm 13\%
 \end{aligned} \tag{26}$$

The dose due to the 184-ppm ^{10}B in the borated detector can now be quantified from Equation 18 as the

$$D_{boron}(Gy) = 0.0247 \text{ (Gy/nC)} \cdot \left[Q_B \text{ (nC)} - Q_{NB} \text{ (nC)} \left(\frac{N_C^{NB}}{N_C^B} \right) \right] \tag{27}$$

and the PDE correction factor can now be determined, from Equation 22:

$$\begin{aligned}
 C_{PDE} &= 1.459 \times 10^{-9} \left(\frac{\text{R}}{\text{n/cm}^2} \right) \cdot \left(\frac{N_{th} \left(\frac{\text{n}}{\text{cm}^2 \cdot \text{nC}} \right)}{N_C \text{ (R/nC)}} \right) \\
 &= 1.459 \times 10^{-9} \left(\frac{\text{R}}{\text{n/cm}^2} \right) \frac{1.79 \times 10^9 \left(\frac{\text{n/cm}^2}{\text{nC}} \right)}{7.055 \times 10^9 \text{ (R/nC)}} \\
 &= 0.364 \pm 16\%
 \end{aligned} \tag{28}$$

The 16% error associated with the PDE correction factor comes from two major sources, the HPGe detector efficiency and \bar{W}_N/e . The error for the thermal fluence rate for the

thermal neutron calibration is 13% which is limited by the error of the HPGe detector efficiency used to count the gold foils. However, the measured thermal fluence rate varied only 2.5% from the known value of the thermal fluence rate of the OSU reactor, so the true error of the thermal fluence rate may be much lower. The error associated with the Bragg-Gray equation (9%) is the second major source of error. In particular, the error associated with \bar{W}_N/e is on the order of 6-8%.

CHAPTER IV

DESIGN OF A NEUTRON BEAM FOR BNCEFNT

4.1 Benchmarking MCNPX for BNCEFNT.

All simulations of the new filter and collimation system were performed with the Monte Carlo radiation transport code MCNPX [50]. MCNPX is an extension of MCNP4B [51] and incorporates the high energy physics models of LAHET [52] and CEM [53, 54]. MCNPX is used to calculate the neutron source spectra from 66-MeV protons on the beryllium target, as well as transport neutrons through the filter and collimation system.

MCNP and LAHET have been previously used to design facilities for BNCEFNT. Pignol and Nigg have demonstrated that MCNP calculations of boron dose enhancement of fast neutron therapy agree with measurements [24, 28]. Specifically, Nigg used LAHET to calculate the neutron source spectrum from protons incident on a beryllium target.

To further verify the use of MCNPX to predict the boron dose enhancement, depth-dose measurements were performed using the Fermilab Neutron Therapy Facility treatment beam. In these initial measurements the depth-dose was measured with the borated and non-borated detectors for 3 field sizes: $20 \times 20 \text{ cm}^2$, $10 \times 10 \text{ cm}^2$, and 55.3-cm diameter.

For the depth-dose measurements the borated and non-borated chambers were placed simultaneously in the water phantom with an off-axis separation distance of 5 cm. The off-axis direction is perpendicular to the beam direction. The detectors were placed at the isocenter and the tank was moved to adjust the depth of the detectors in the phantom.

Placement of the water tank was controlled remotely using a stepper motor system. The error in the positioning of the detectors was ± 1 mm. The detector distance from the central axis was controlled by a second stepper motor.

4.1.0.1 20×20 cm² Beam Measurements

The 20×20 cm² beam was created by inserting a specially molded concrete/polyethylene collimator inside of the medium Benelex liner. This beam is a standard treatment beam at Fermilab, i.e. it has not been modified for BNCEFNT. The depth-dose distribution (Fig. 7) of the 20×20 cm² beam was measured a total of three times with the borated chamber and twice with the non-borated chamber. These measurements were performed on different days and, therefore, provided an error estimate that included the error in positioning the detectors. As a result of these multiple measurements, the maximum error of any single measurements was estimated at less than 2%. This 2% maximum error is subsequently used where only one measurement was made at each depth.

The depth-dose measurements show that the addition of 100-ppm ¹⁰B causes the maximum total dose, including the dose due to the boron capture reaction to shift from 2-cm deep to 3-cm deep in the water phantom. The percent dose enhancement (PDE) is calculated using Equation 21 and re-normalized for a 100-ppm ¹⁰B detector loading. The PDE reaches a maximum of $(9.2 \pm 1.5)\%$ at a depth of 7 cm (Fig. 8).

4.1.0.2 10×10 cm² Beam Measurements

The depth-dose distribution for the 10×10 cm² field (Fig. 9) was only measured once, so the associated error is estimated as 2% at all depths and should generally be much smaller. The PDE (Fig. 10) reaches a maximum of $(4.8 \pm 0.8)\%$ at a depth of 6 cm in the water phantom.

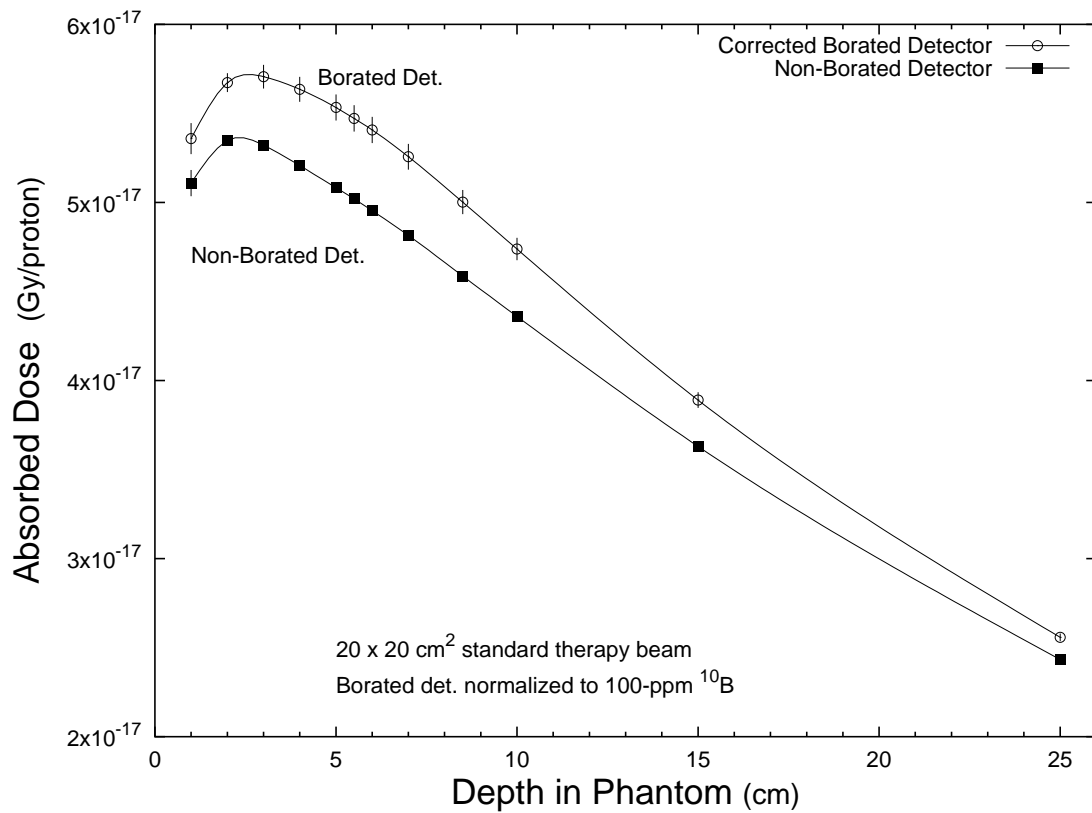


Figure 7: Depth-dose measurement of the $20 \times 20 \text{ cm}^2$ standard therapy beam as measured with the borated and non-borated TE ionization chambers. The borated detector measurements have been normalized to 100-ppm ^{10}B . The errors shown do not include the 9% error associated with the coefficients of the Bragg-Gray equation.

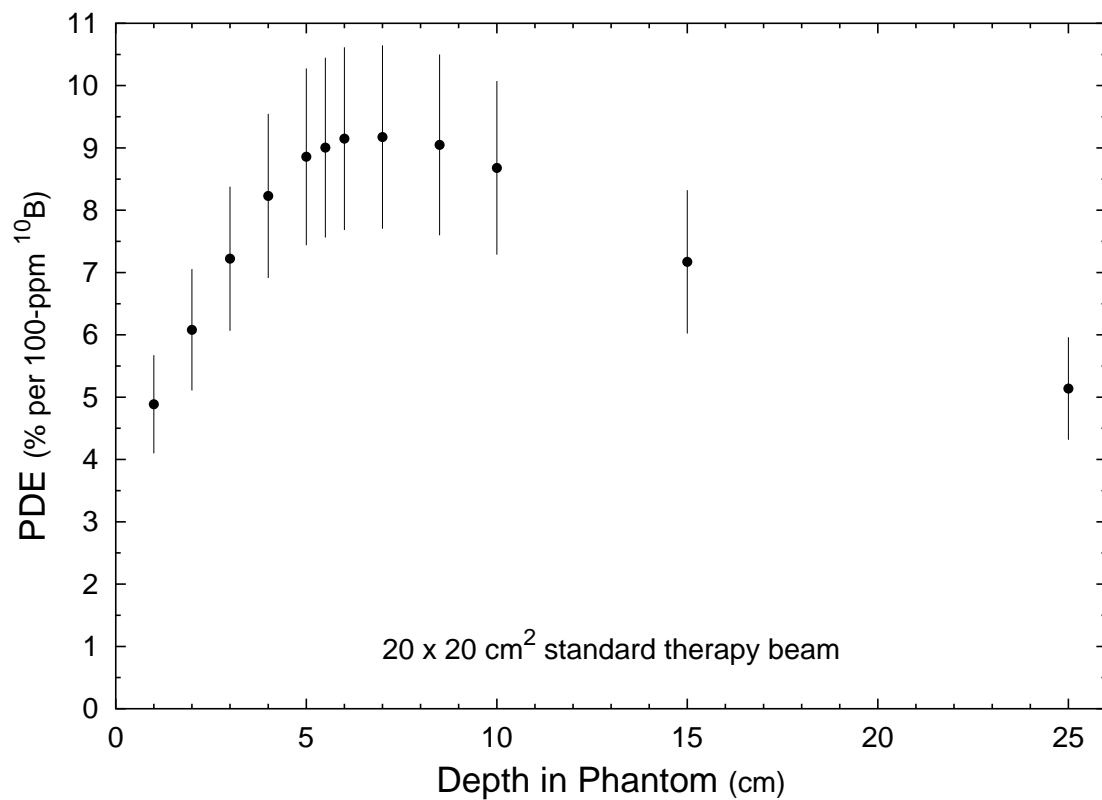


Figure 8: PDE of the $20 \times 20 \text{ cm}^2$ standard therapy beam as measured with the borated and non-borated TE ionization chambers. The PDE has been normalized to 100-ppm ^{10}B . The error shown is the total experimental and systematic error.

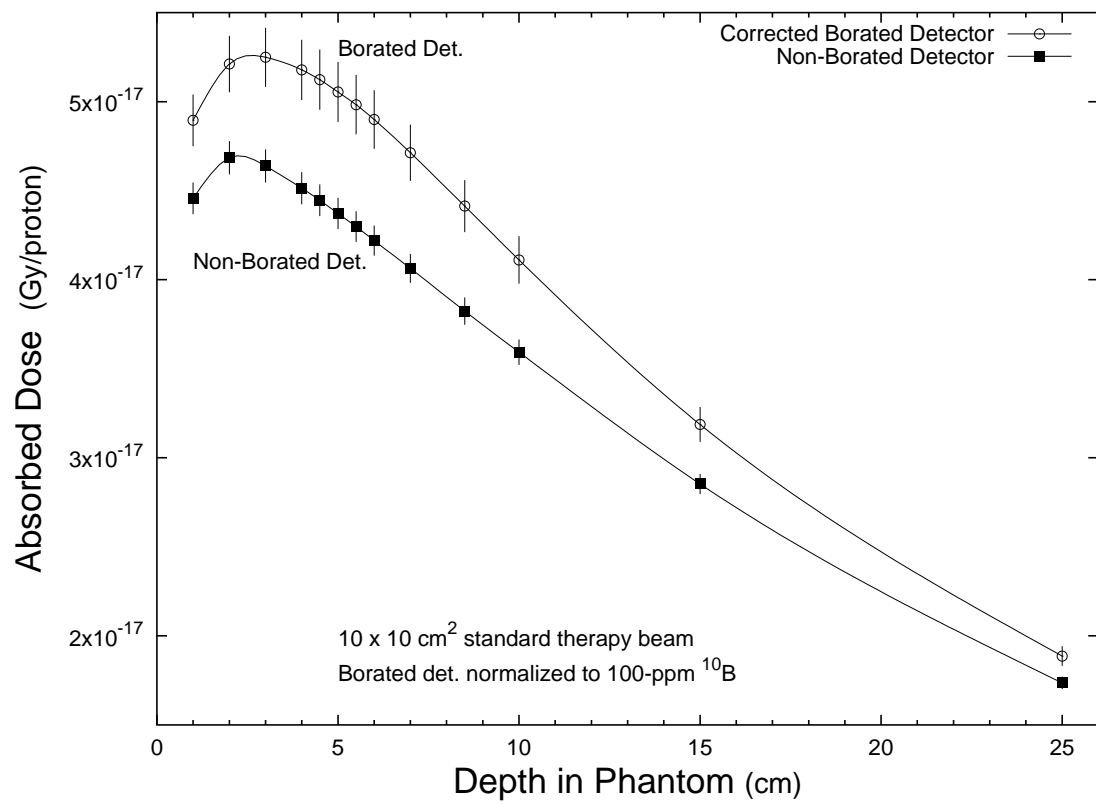


Figure 9: Depth-dose measurement of the $10 \times 10 \text{ cm}^2$ standard therapy beam as measured with the borated and non-borated TE ionization chambers. The borated detector measurements have been normalized to 100-ppm ^{10}B . The experimental errors are shown.

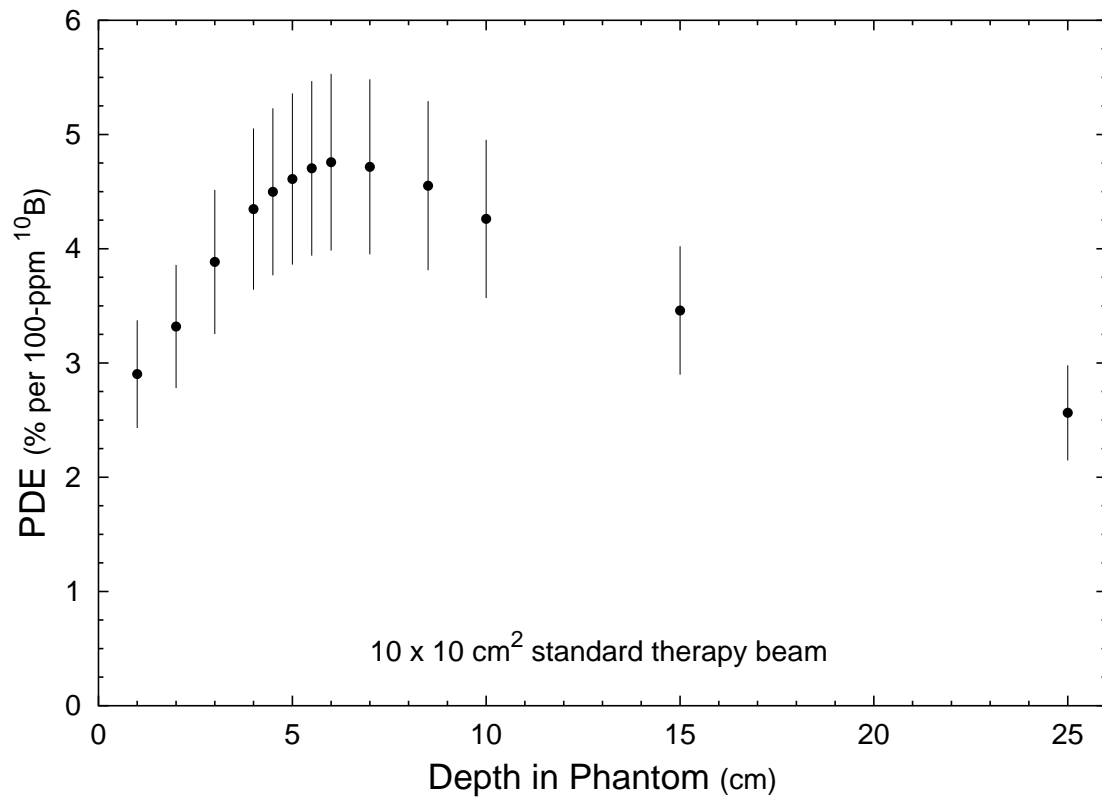


Figure 10: PDE of the $10 \times 10 \text{ cm}^2$ standard therapy beam as measured with the borated and non-borated TE ionization chambers. The PDE has been normalized to 100-ppm ^{10}B . The total experimental and systematic errors are shown.

4.1.0.3 55.3-cm Diameter Beam Measurements

To create the 55.3-cm diameter beam both the small and medium Benelex liners were removed. This provided an opening diameter of 31.75 cm at 109 cm from the center of the beryllium target. At the isocenter the field is approximately 55.3-cm in diameter. The depth-dose distribution measurement (Fig. 11) shows that the maximum (n+ γ) dose is 17% higher than the maximum (n+ γ) dose for the 20 \times 20 cm² beam measurement. The relative dose of the 55.3-cm diameter beam decreases slower with depth than the relative dose of the 20 \times 20 cm² beam. In fact at 25 cm the dose is still 52% of the maximum dose, while the 20 \times 20 cm² dose is projected to fall to 50% of the maximum dose at 23 cm. These measurements were performed in a water phantom and the relative dose rate will decrease faster in higher density material such as A-150 plastic or tissue. The PDE reaches a maximum of (14.8 \pm 2.4)% at a depth of 7 cm (Fig. 12).

4.1.1 MCNPX Comparison to Measurements

The experiments on the standard treatment beam were modeled using MCNPX and the LA-150 [55] neutron libraries. In the calculations the square collimator openings were modeled using equivalent area cylindrical openings and the rectangular water phantom was modeled as a cylinder with an equivalent cross-sectional area. The source for the MCNPX calculations was generated by simulating 66-MeV protons on the beryllium target using the Bertini intranuclear cascade (INC) model. The neutrons incident on the collimator face were written to a surface source file that was used for all subsequent calculations. A total of 6.0 \times 10⁹ source protons were tracked resulting in 9.0 \times 10⁶ neutrons incident on the face of the collimator. The generation of the surface source file represented considerable computational time, requiring 400 hours on 16 800-MHz Pentium machines for a total run-time of 266.7 CPU-days.

Comparison of the depth-dose measurements to the calculations indicated that MCNPX underestimated the fast neutron and gamma dose by about a factor of 3 (See Table 5).

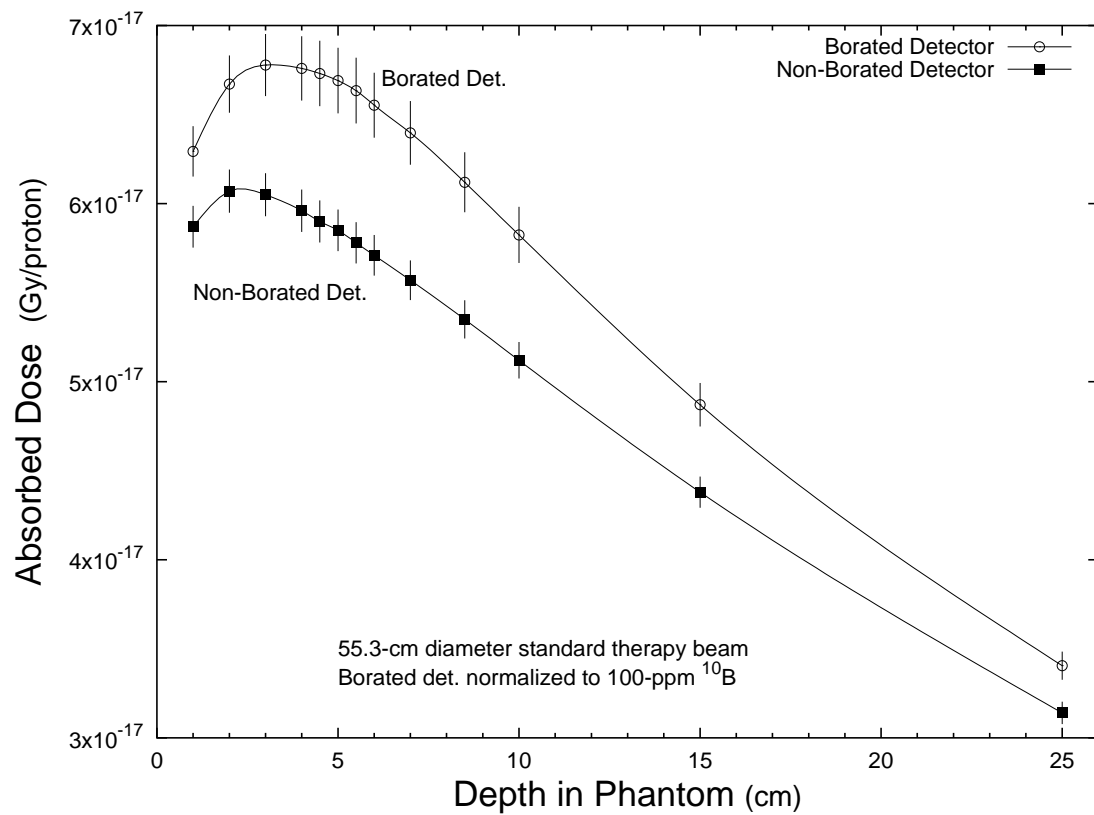


Figure 11: Depth-dose measurement of the 55.3-cm diameter beam as measured with the borated and non-borated TE ionization chambers. The borated detector measurements have been normalized to 100-ppm ^{10}B . Only the experimental errors are shown.

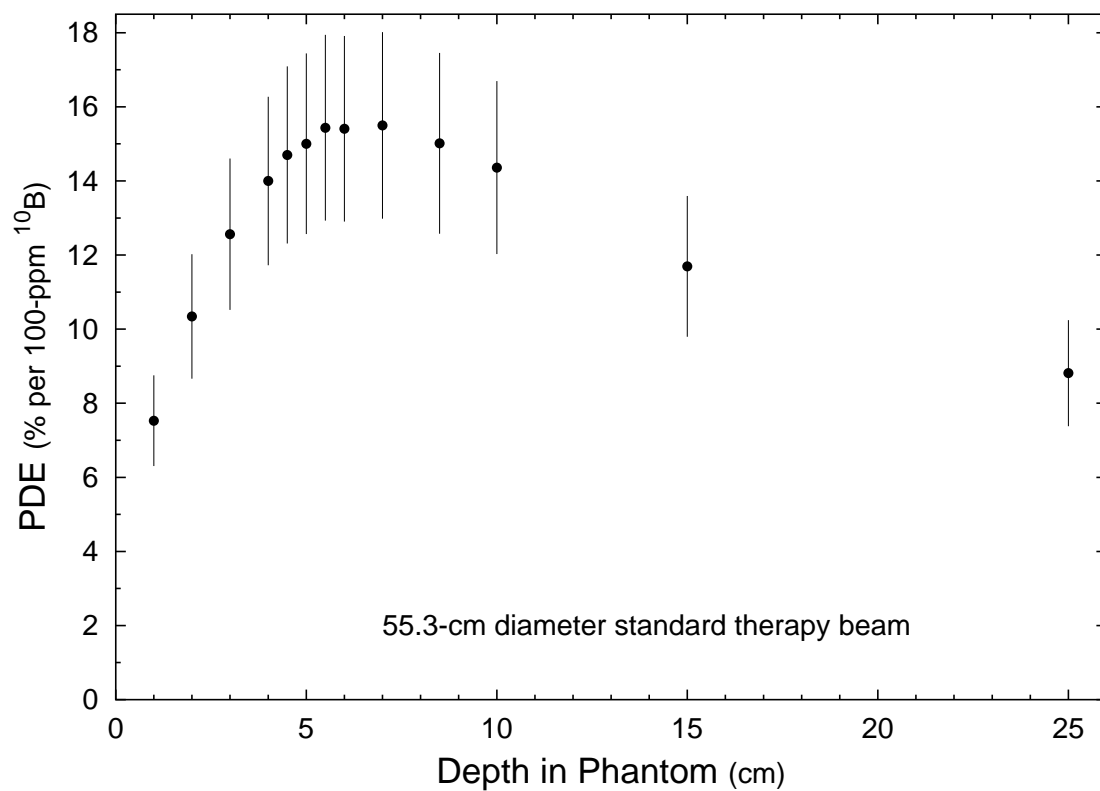


Figure 12: PDE of the 55.3-cm diameter beam as measured with the borated and non-borated TE ionization chambers. The PDE has been normalized to 100-ppm ^{10}B . The total experimental and systematic errors are shown.

Table 5: Experiment-to-calculated ratios (E/C) of the (n+ γ) dose and percent dose enhancement (PDE) at 5-cm deep in a water phantom.

Field Size	PDE E/C	(n+ γ) Dose E/C
55.3-cm dia.	1.00 ± 0.16	2.73 ± 0.08
20cm x 20cm	0.89 ± 0.14	2.69 ± 0.07
10cm x 10cm	1.06 ± 0.17	2.96 ± 0.10

However, the calculated shape of dose as a function of depth in the phantom agreed well with the measurements. The MCNPX calculations of the depth dose for the 20×20 cm², 10×10 cm², and the 55.3-cm diameter beam are shown normalized to the measurements in Figures 13, 14, and 15, respectively.

The normalization factor was found by the ratio of the calculated and measured responses of the non-borated detector at a depth of 3-cm in the phantom. Since the borated chambers are not used in the calculation of the normalization factor, the ability of MCNPX to estimate the boron dose can be evaluated. The likely cause of this discrepancy is an underestimation of the calculated neutron source strength by the Bertini INC model. Since the shape of the depth-dose curves calculated with MCNPX match the measurements well, the neutron spectrum is assumed to be an adequate representation of the actual neutron spectrum. Therefore, the total neutron yield and the neutron yield in the forward direction reported by MCNPX are in question. MCNPX calculations with the ISABEL INC model produced similar results. Since the Bertini and ISABEL INC models were optimized for higher Z targets, the failure to produce the correct neutron yield is not surprising. In fact, a study of the neutron yield of 100-MeV protons on lithium targets has shown that both the Bertini and ISABEL INC models underestimate the total neutron yield by greater than a factor of 2 [56].

In the development of a BNCEFNT beam the ability to predict the fractional increase in absorbed dose due to the boron reaction is critical. Comparison of the measured and

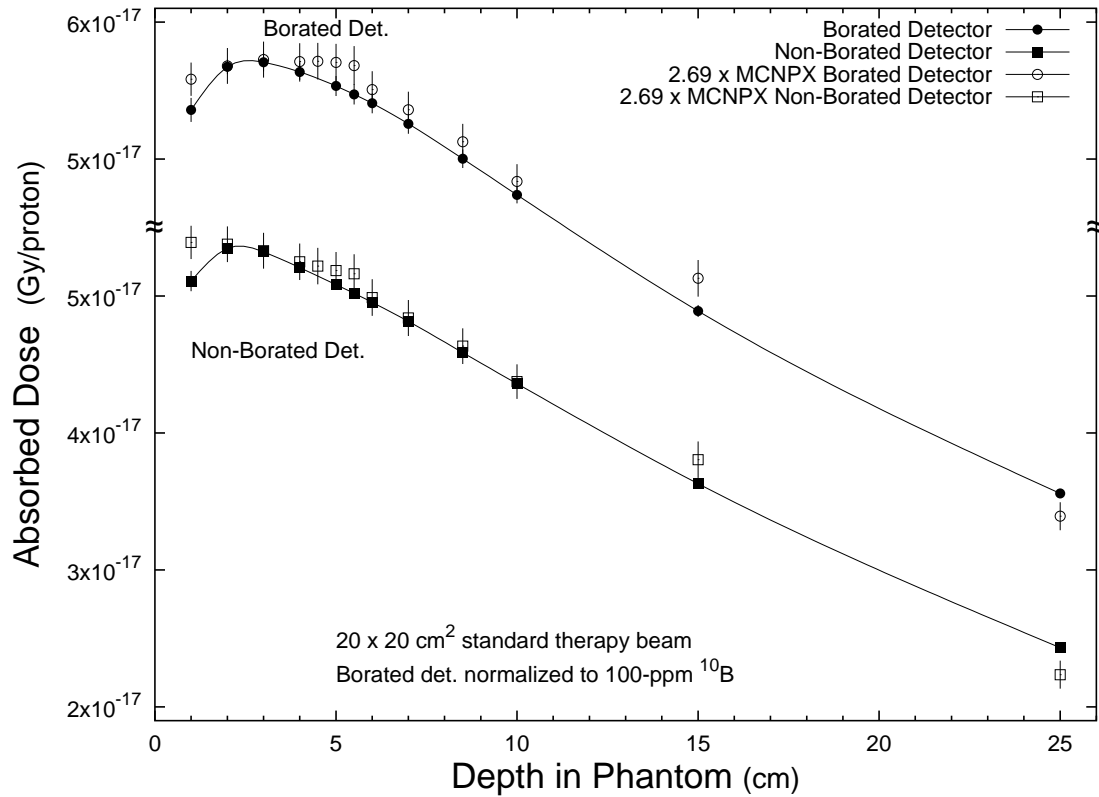


Figure 13: Depth-dose measurement and MCNPX calculation of the Fermilab Neutron Therapy Facility standard treatment beam ($20 \times 20 \text{ cm}^2$ field). The non-borated detector represents fast neutron and gamma dose. The borated detector represents fast neutron, gamma, and boron capture dose for 100-ppm ^{10}B . The MCNPX calculation has been normalized to the non-borated detector measurement at 3-cm deep, resulting in a 2.69 normalization factor.

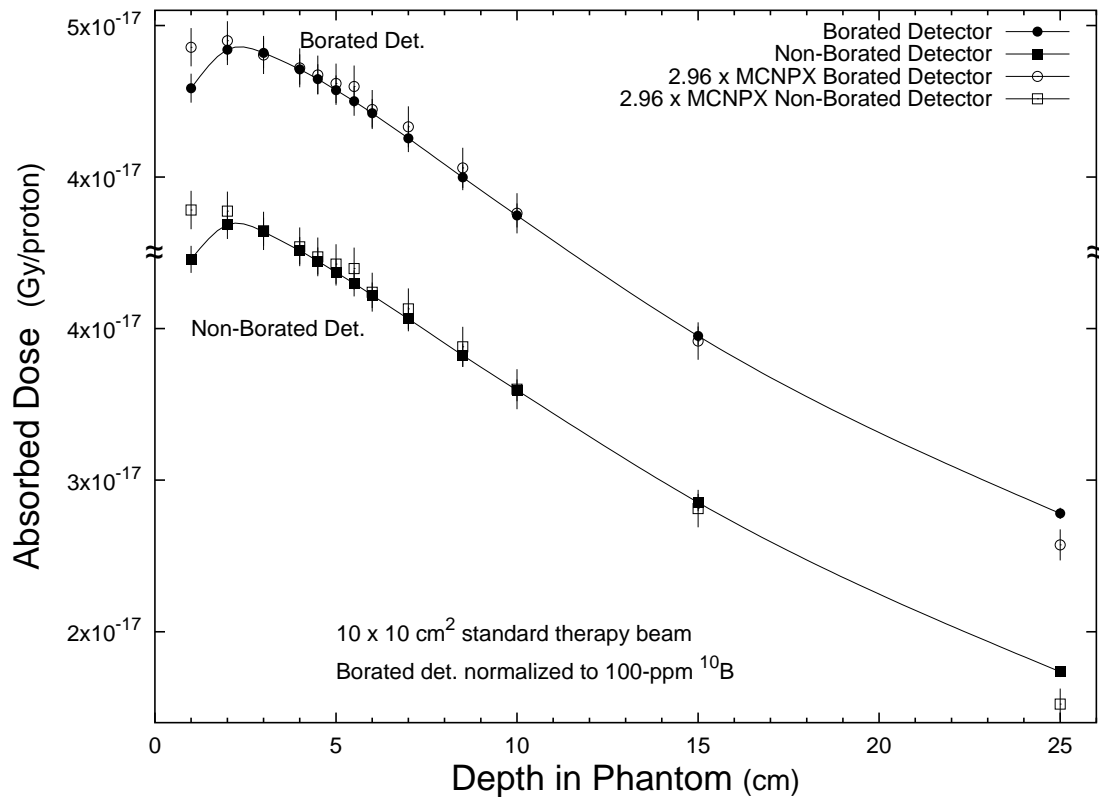


Figure 14: Depth-dose measurement and MCNPX calculation of the Fermilab Neutron Therapy Facility standard treatment beam ($10 \times 10 \text{ cm}^2$ field). The non-borated detector represents fast neutron and gamma dose. The borated detector represents fast neutron, gamma, and boron capture dose for 100 ppm ^{10}B . The MCNPX calculation has been normalized to the non-borated detector measurement at 3-cm deep, resulting in a 2.96 normalization factor.

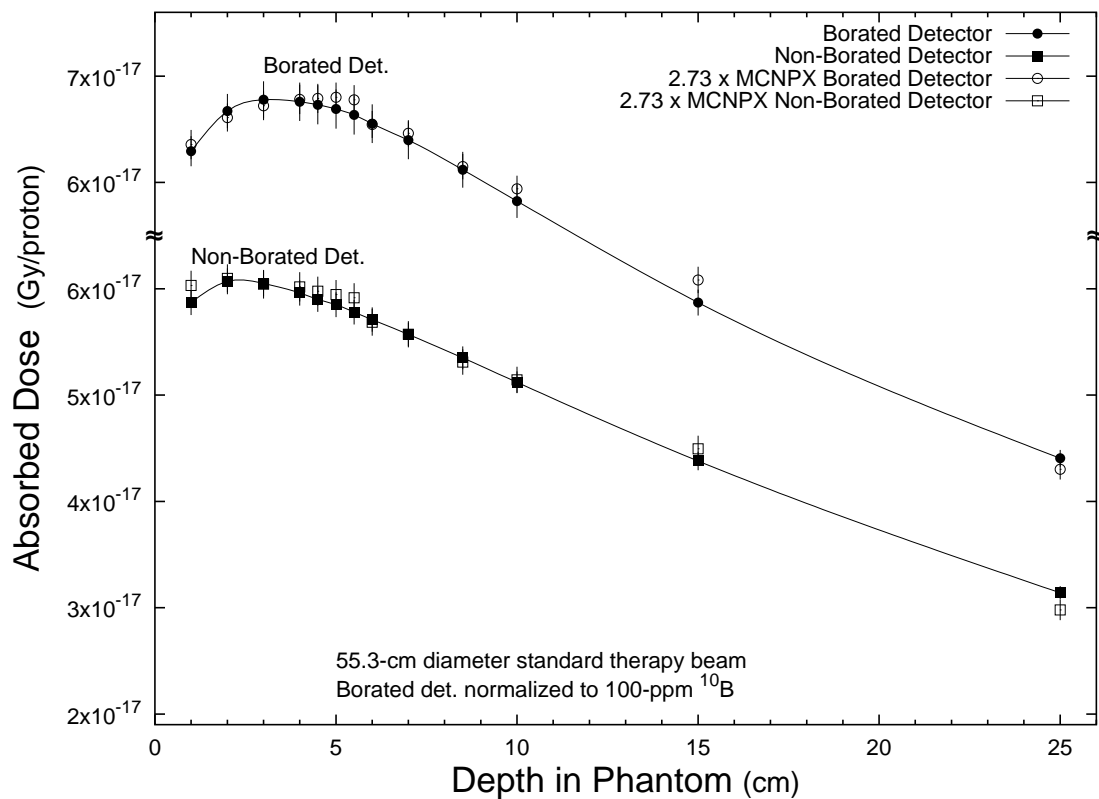


Figure 15: Depth-dose measurement and MCNPX calculation of the Fermilab Neutron Therapy Facility standard treatment beam (55.3-cm dia. field). The non-borated detector represents fast neutron and gamma dose. The borated detector represents fast neutron, gamma, and boron capture dose for 100-ppm ^{10}B . The MCNPX calculation has been normalized to the non-borated detector measurement at 3-cm deep, resulting in a 2.73 normalization factor.

calculated PDE shows that MCNPX does a good job of estimating the PDE at all field sizes (Fig. 16). These calculations show that the neutron source generated with the Bertini INC model performed better than the neutron source generated by the ISABEL INC model. The Bertini INC model tends to overestimate the maximum PDE and the PDE at depths greater than the maximum PDE, while under predicting the PDE at depths shallower than the maximum PDE. The ISABEL INC neutron source generally underestimated the PDE at all depths.

The failure of the MCNPX results to predict the PDE at very shallow depths is not unexpected. MCNPX fails to track the proton recoil from neutron elastic scattering with hydrogen. MCNPX instead uses kerma factors to calculate the energy deposition at the point of interaction. Therefore, MCNPX will overestimate the energy deposition until proton recoil equilibrium is obtained. This overestimation can be seen in the depth-dose calculations at 1-cm deep for the non-borated detector in Figures 13, 14, and 15. This overestimation of the $(n+\gamma)$ dose leads to an underestimation in the PDE.

The discrepancies between the measured and calculated values of the PDE must be considered in terms of their uncertainties. The differences between the measured and calculated values of the PDE vary from -6% to +11%. And, the experimental errors of the measured PDE values are about 1.4% to 2.8%. The Monte Carlo errors for the calculations are 2.7% to 6.4%. Therefore, the minimum expected differences between the measured and calculated PDE values should vary from 3% to 7%. Since the differences in the measured and calculated PDE values are less than the total error of the measured PDE values, it is concluded that MCNPX is an adequate design tool for BNCEFNT beam systems.

4.2 Filter and Collimation Design

Investigations in optimizing a fast neutron therapy beam for BNCEFNT have occurred at several neutron therapy facilities worldwide. These studies provide an important base of knowledge in the modification of the Fermilab beam. Most importantly they provide

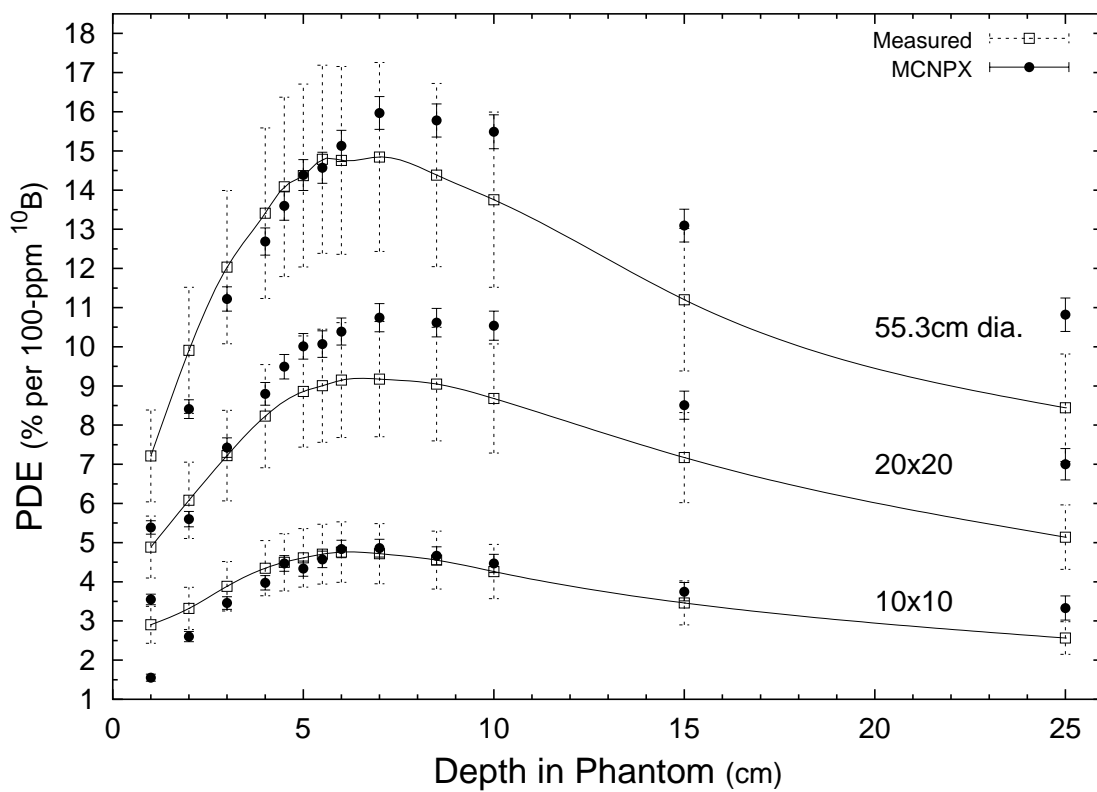


Figure 16: Measurements and MCNPX calculations of the Percent Dose Enhancement (PDE) for three fields: $10 \times 10 \text{ cm}^2$, $20 \times 20 \text{ cm}^2$, and 55.3-cm diameter. The results have been normalized to $100\text{-ppm } ^{10}\text{B}$. The MCNPX calculations are performed using the Bertini INC model.

information on material selection. At Harper Hospital in Detroit, Kota *et al.* measured the boron dose rates of the $d(48.5 \text{ MeV})+\text{Be}$ beam filtered with 25-cm of steel, 25-cm of lead, 25-cm of aluminum, and 18.7-cm of tungsten [26]. They concluded that steel and tungsten filters produced the best beams for BNCEFNT. Pignol *et al.* studied the effect of collimator material in the optimization of the fast neutron therapy beams at Nice, France and Orleans, France. They calculated the thermal neutron flux from the $p(60)+\text{Be}$ and a $p(34)+\text{Be}$ beams collimated with steel, tungsten, bismuth, and lead [29]. Pignol concluded that the lead collimator produced the largest thermal flux for both facilities.

4.2.1 Material Selection

The new BNCEFNT filter and collimation system was designed in an iterative process. This process had three major steps and all steps were performed twice. The three major steps were: optimization of the filter material, optimization of the filter thickness, and optimization of the collimator material. The first iteration of the design process focused mainly on material selection of the filter and collimator, while the second iteration focused on implementing a workable design.

The first step in the first iteration was the selection of the filter material. In this step the Fermilab Neutron Therapy Facility, with the concrete/polyethylene collimator and the inner Benelex liner replaced with lead, was modeled with MCNPX. Lead was chosen as a likely candidate for the collimator material due to investigations by Pignol in the optimization of the $p(60)+\text{Be}$ beam at Nice and the $p(34)+\text{Be}$ beam at Orleans [29]. Six thicknesses of each tested filter material were modeled on the upstream side of the collimator. The thicknesses examined were 5, 10, 15, 20, 25, and 30 cm. A diagram of the model is shown in Figure 17. Eighty-seven different materials were tested as possible filter materials. Of the eighty-seven materials, sixty-three were pure elements of natural atomic abundances, eighteen were compounds or mixtures, and six were enriched isotopes. The results of these calculations showed that iron was the best filter material (Table 6).

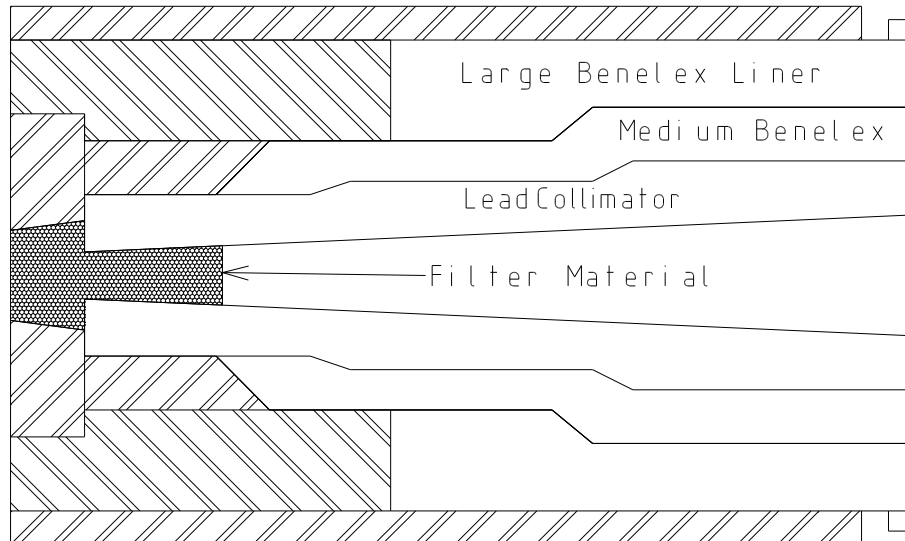


Figure 17: MCNPX model geometry for the first iteration of the filter material testing. The filter was tested for 6 thicknesses of 83 materials. The thicknesses tested were 5, 10, 15, 20, 25, and 30 cm.

Tungsten also produced a large dose enhancement but the reduction in dose rate was too great. Lead had a very small reduction in the dose rate, but with a 30-cm thick lead filter the PDE only reached a maximum of 14%. For lead to be used, more than a 30-cm length would be needed and such a large mass of lead would be difficult to insert in the collimator.

The second step in the filter optimization was to determine the thickness of the iron filter. Fourteen different thicknesses of iron were modeled using MCNPX ranging from 0 to 25 cm. The results indicated that the goal of 15% PDE with only $1/15^{th}$ reduction in dose rate could not be attained with this configuration (Fig. 18). Since the goal of a 15% PDE is more limiting than the goal of $1/15^{th}$ reduction in dose rate, the iron filter thickness was chosen as the thinnest filter that could attain a 15% PDE. The range of possible thicknesses

Table 6: Results of selected material for the first iteration of the filter material testing. The “(n+ γ) dose ratio” is the ratio of the intensity of the (n+ γ) dose rate without any filter over the (n+ γ) dose rate of the filter under investigation. The PDE listed is the maximum PDE.

Material	Thickness (cm)	Max. PDE (%)	(n+ γ) Dose Ratio (No Filter/Tested Filter)
Pt	30	48 ± 19	822 ± 279
Fe	30	34 ± 5	79 ± 10
W	30	25 ± 14	450 ± 211
Pb	30	14 ± 2	52 ± 7
Bi	30	9 ± 1	49 ± 5
Al	30	7 ± 1	26 ± 3

included 19 to 22 cm, with 20 cm selected as the filter thickness.

With the filter set to 20-cm of iron the collimator material was selected. The same eighty-seven materials were tested as possible collimator materials. Each collimator material was tested by replacing the concrete/polyethylene collimator and the small Benelex insert with the test material. The materials that produced the highest PDE with high intensities are listed in Table 7. Iron collimation produced that highest PDE at 19.5% but not the highest dose rate. Potassium produced the second highest PDE at 16.7% and one of the highest dose rates. A closer review of potassium as a filter material indicated that potassium is in fact a poor selection as a collimator material due to its poor shielding properties.

4.2.2 Design Implementation: Second Iteration

The selection of iron as a possible filter and collimator material allow for a very practical design. Iron is inexpensive, easy to machine, and non-toxic. Additionally, its neutron cross section is known over the range of interest [55]. The major activation reaction from the irradiation of iron is the $^{56}\text{Fe}(n,p)^{56}\text{Mn}$ reaction ($T_{1/2} = 2.6$ hours).

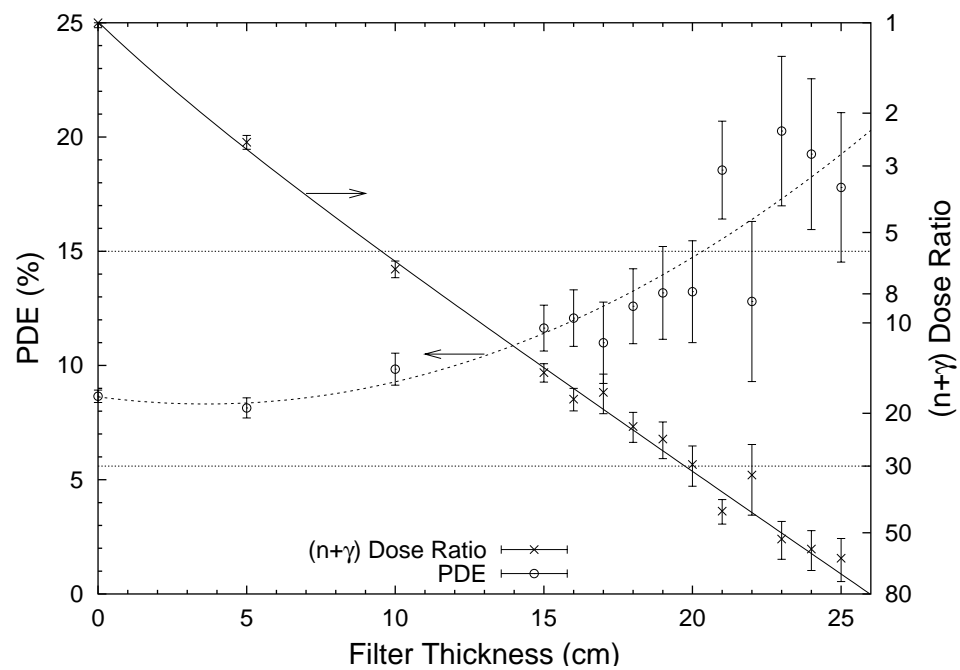


Figure 18: MCNPX calculated values for the PDE and the $(n+\gamma)$ dose ratio. The $(n+\gamma)$ dose ratio is the ratio of the $(n+\gamma)$ dose rate of the beam without any filter over the $(n+\gamma)$ dose rate of the filter under investigation. The plotted PDE is the PDE at 7-cm in depth.

Table 7: Results of the collimator material optimization for selected materials. The results shown here are materials with a PDE greater than 13% and an $(n+\gamma)$ dose rate less than that of the iron collimator. The “ $(n+\gamma)$ dose ratio” is the ratio of the $(n+\gamma)$ dose rate of the beam without any filter over the $(n+\gamma)$ dose rate of the system under investigation. The PDE listed is the maximum.

Collimator Material	Max. PDE (%)	$(n+\gamma)$ Dose Ratio (No Filter/Tested Filter)
Fe	20.3 ± 1.4	32 ± 2
K	17.4 ± 0.7	15 ± 1
S	17.0 ± 1.0	26 ± 1
Pb	15.5 ± 1.1	31 ± 2
Sn	15.3 ± 1.0	29 ± 2
Cr	15.1 ± 1.1	31 ± 2
UO ₂	14.8 ± 1.0	31 ± 2
Ca	14.8 ± 0.7	16 ± 1
Th	14.8 ± 1.1	31 ± 2
Ti	14.1 ± 1.0	31 ± 2
I	14.0 ± 0.9	25 ± 1
As	13.8 ± 1.0	31 ± 2
Bi	13.8 ± 0.9	27 ± 2
Li	13.5 ± 0.8	23 ± 1

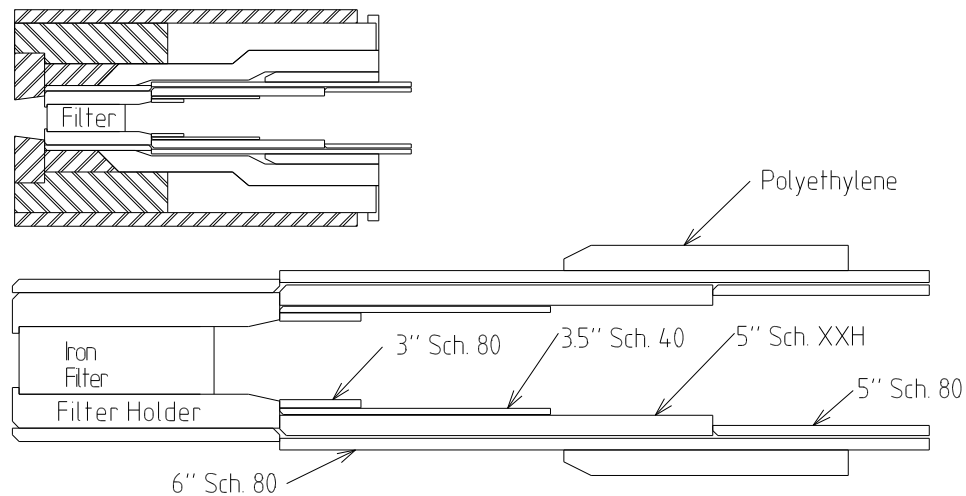


Figure 19: Diagram of the iron filter and filter holder, along with the 20-cm-diameter-field steel collimator. The field size is the projected size of the collimated field at the isocenter. The diagram in the upper left depicts the collimator inserted in the Fermilab facility.

In the second phase of the design a practical model was developed for the further optimization. Since iron was the material of choice the collimator was developed using standard steel pipe. Concentric pieces of steel pipe are fitted together to provide the desired collimator diameter.

The filter was designed to be easily removed and variable in thickness. This allowed for experiments to study the effects of different materials and thicknesses. The filter is held by an iron filter holder with an inside diameter of 5.08-cm. The filter holder can hold up to 21.5-cm of filter material. A diagram of the filter and collimator is shown in Figure 19.

To ensure that iron was the best filter material for this new configuration, the performance of a select number of materials were compared with iron. The materials were chosen based on the results of the first iteration of filter material selection. Iron again proved to be the superior filter material (Table 8). Iron produced a higher $(n+\gamma)$ dose rate for the new configuration than for the preliminary model.

In order to optimize the filter thickness to meet the goal of 15% dose enhancement and $1/15^{th}$ of the original $(n+\gamma)$ dose rate, the filter was varied for thicknesses ranging from 0

Table 8: PDE and (n+ γ) dose ratio for selected filter materials in the final geometry. The “(n+ γ) dose ratio” is the ratio of the (n+ γ) dose rate of the beam without any filter over the (n+ γ) dose rate of the filter under investigation. The PDE listed is the maximum PDE.

Material	Thickness (cm)	PDE at 5cm Deep (%)	(n+ γ) Dose Ratio (No Filter/Tested Filter)
Fe	17.0	16.5 \pm 1.2	20.5 \pm 1.4
W	20.0	15.9 \pm 2.0	78.2 \pm 8.7
Hf	25.0	15.6 \pm 1.4	93.4 \pm 7.3
Pt	12.5	14.8 \pm 1.4	35.6 \pm 2.8
Pb	30.0	12.6 \pm 1.1	55.9 \pm 4.7
^{235}U	10.0	12.6 \pm 0.9	11.0 \pm 0.7

to 25 cm. The results of the MCNPX calculations show that 15% dose enhancement can be obtained for iron filter thicknesses in the range of 15 to 17 cm (See Fig. 20). However, the (n+ γ) dose rate drops below $1/15^{th}$ of the original (n+ γ) dose rate for thicknesses over 15 cm. A fit of the calculated intensities as a function of filter thickness produces a macroscopic effective removal cross section of $0.174 \pm 0.005 \text{ cm}^{-1}$ or a relaxation length of 5.8 cm. A projected filter thickness of 17 cm ensured that the primary goal of 15% dose enhancement for the 20-cm diameter field was attained. The (n+ γ) dose rate of a beam filtered with 17-cm of iron was estimated to be $1/19^{th}$ of the unfiltered beam (n+ γ) dose rate. If the 15% dose enhancement due to 100-ppm ^{10}B was also taken into account, the reduction in the total dose rate was decreased to $1/17^{th}$ of the original dose rate.

With the filter set at 17 cm of iron, the 83 possible collimator materials were again tested. With the larger volume filter the PDE and the dose rate showed little dependence on collimator material. The results showed no reason to discount iron as the selected collimator material.

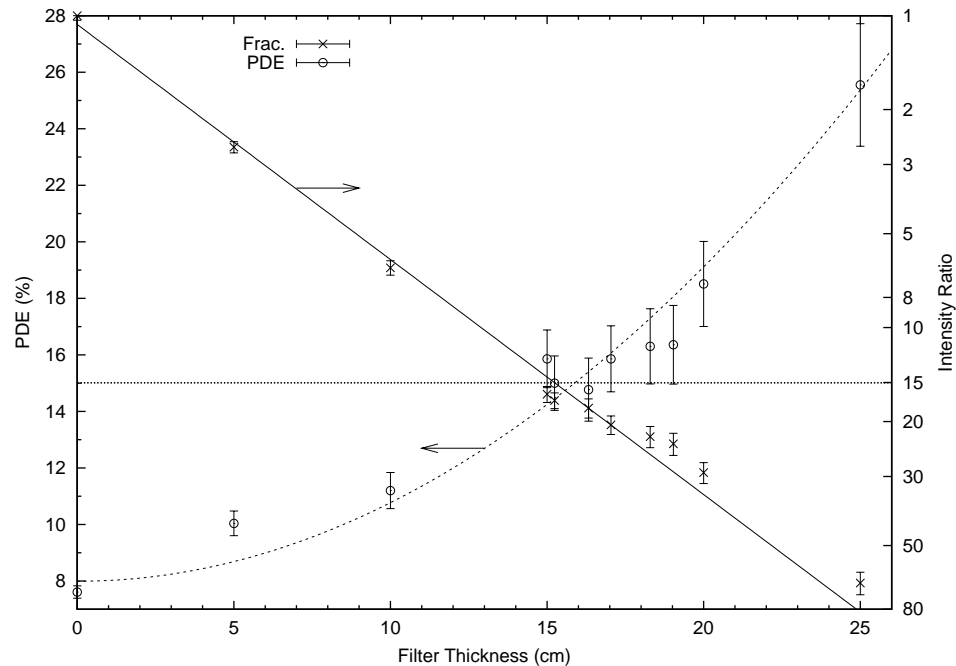


Figure 20: PDE and intensity vs the iron filter thickness for the proposed design.

4.3 Final Design of the BNCEFNT Beam

Since the optimum filter thickness as calculated with MCNPX was somewhat ambiguous for the preliminary estimate of a 17-cm thickness, the filter was designed to be variable and composed of several filter thicknesses stacked together. This allowed the final optimization of the filter thickness to be performed experimentally. Therefore, a filter holder was designed that could accommodate a range of filter thicknesses. The final design of the iron filter and collimator system fits into the Fermilab facility by removing the small Benelex liner. It is composed of three main sections: the base, the filter and filter holder, and the collimator.

The base was designed to provide an interface to the Fermilab Neutron Therapy Facility. It provides the same outer dimensions as the small Benelex liner that it replaces. The parts of the base are shown in Figure 21. The outer filter holder is made from low carbon steel and was machined to an outside diameter of 6.0" and an inside diameter of 5". The 6" schedule 80 steel pipe is welded to the outer filter holder. The polyethylene is pressed onto

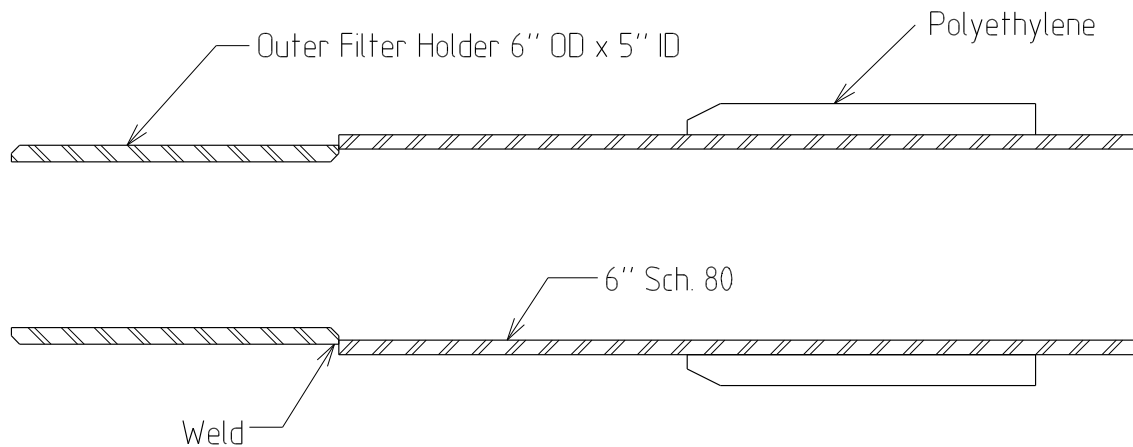


Figure 21: Diagram of the base section of the BNCEFNT filter and collimator. The base section provides an interface to the Fermilab FNT facility collimator geometry. This base section is inserted in place of the small Benelex liner.

the 6" diameter pipe.

The filter holder is designed to contain various lengths of filter material and prevents the filter from damaging the transmission chamber or other equipment in the beam line. The filter holder was machined from low carbon steel. (Fig. 22). The filter consists of various thicknesses low carbon steel. The pieces, which are 2.5 inches in diameter, were designed with a $1/2$ " diameter \times $1/2$ " deep threaded hole to allow easy insertion and removal with a threaded rod (Fig. 23).

The collimator is made from standard steel pipe. Pieces of pipe were cut to provide a stepped collimator. The collimator pieces were designed to provide two field sizes, 20-cm diameter (Fig. 24) and 10-cm diameter (Fig. 25). The size and lengths of the pipe are listed in Table 9.

The filter and collimator was machined and constructed at Fermilab. A photograph of the filter and collimator prior to installation is shown in Figure 26. The 20-cm diameter collimator installed in the Fermilab Neutron Therapy Facility is shown in Figure 27.

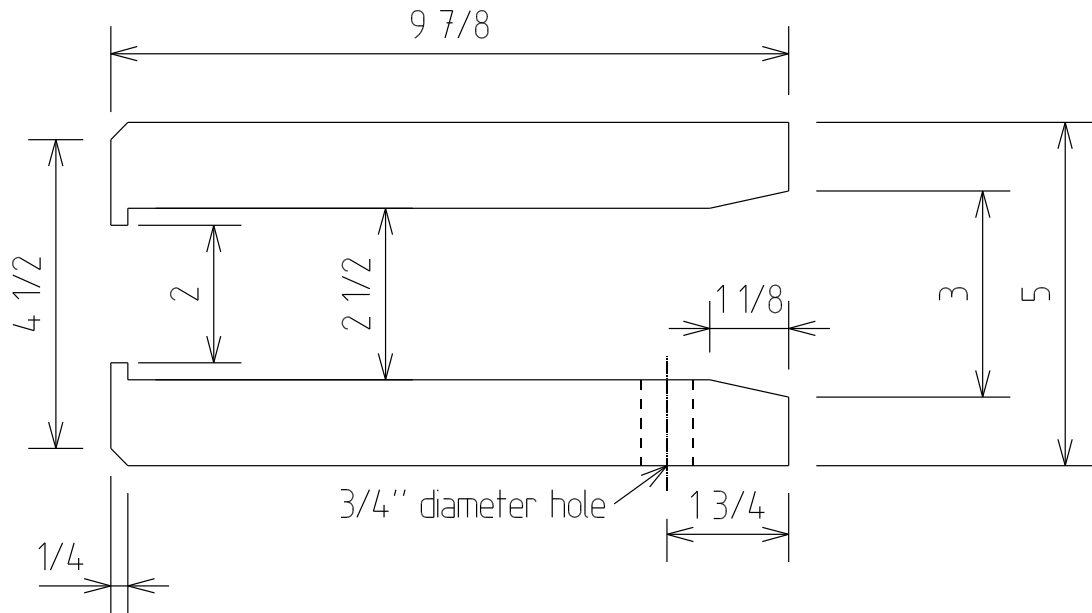


Figure 22: Diagram of the filter holder. All dimensions are in inches.

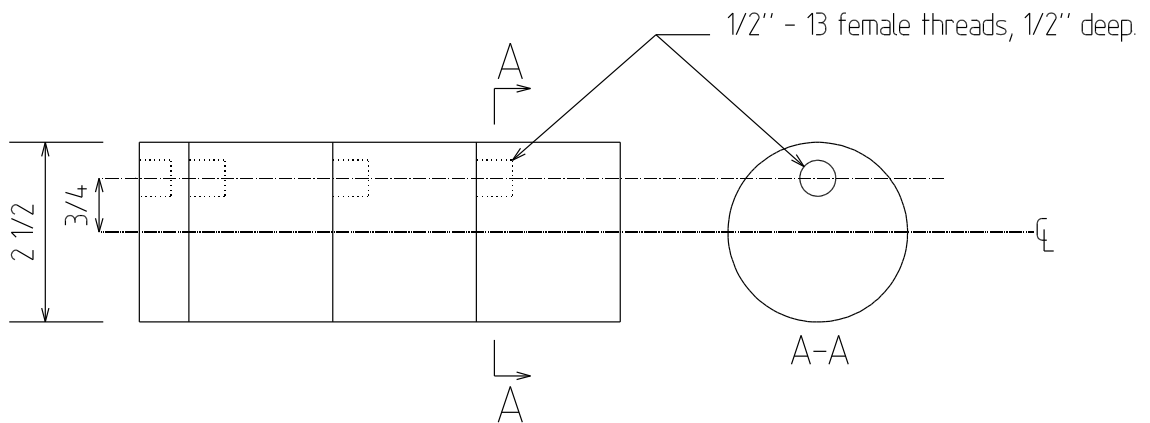


Figure 23: Diagram of the iron filter. All dimensions are in inches.

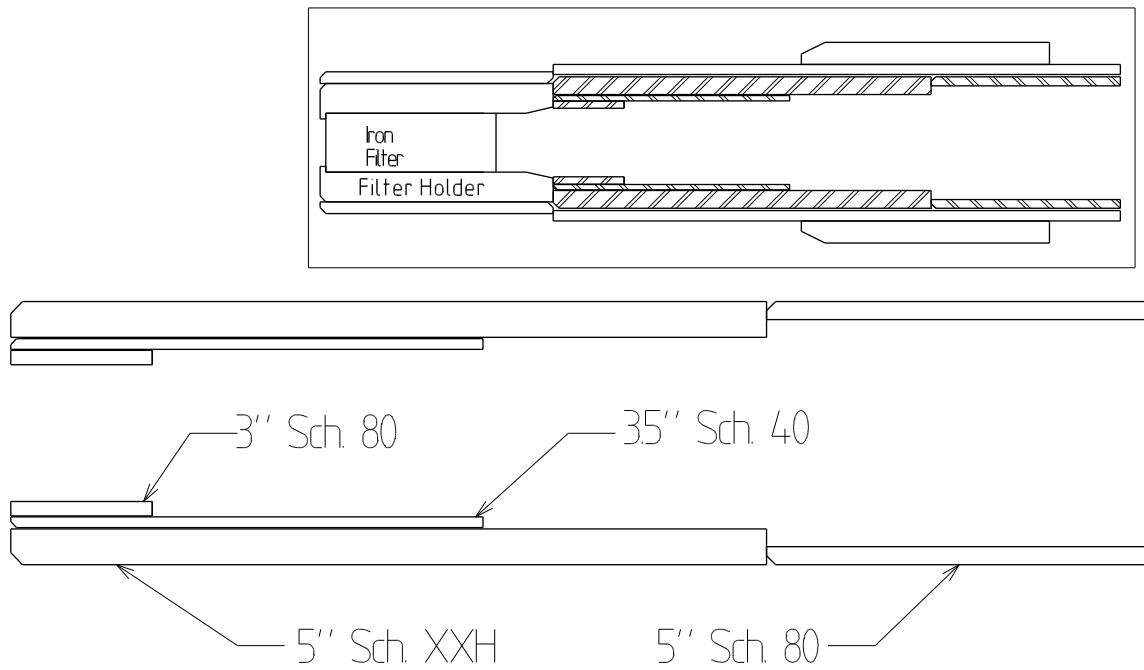


Figure 24: Diagram of the BNCEFNT 20-cm diameter collimator. The insert in the upper right shows the 20-cm diameter collimator (hatched) inserted into the base section.

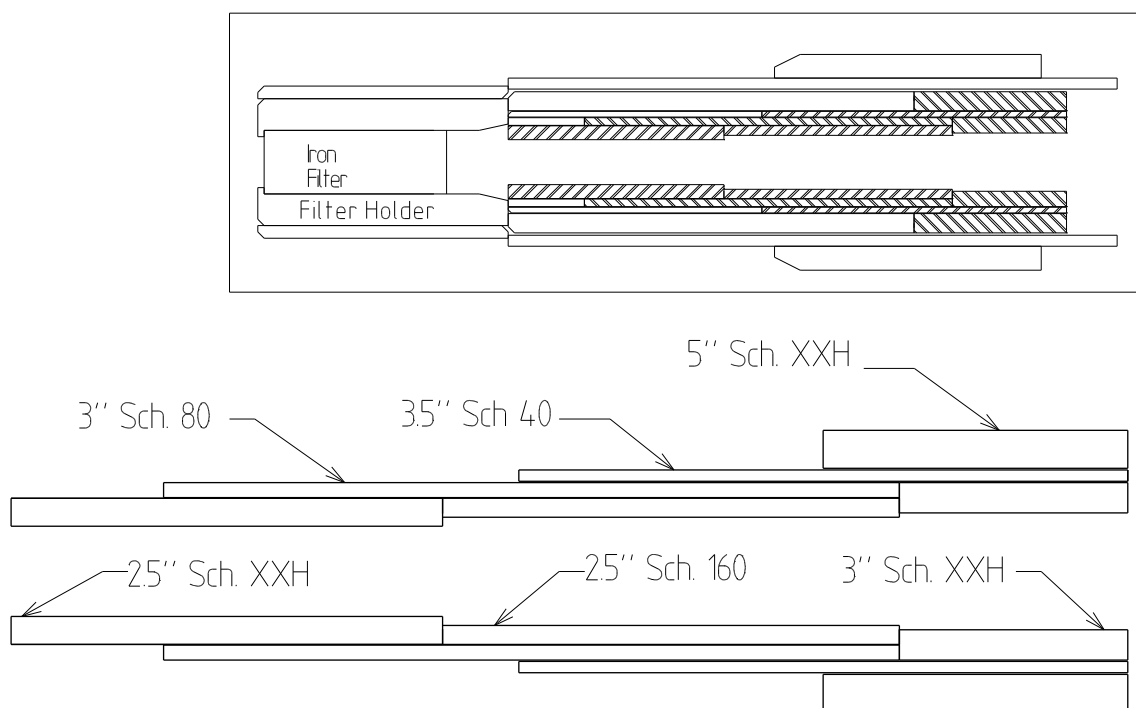


Figure 25: Diagram of the BNCEFNT 10-cm diameter collimator. The boxed insert in the upper right shows the 10-cm diameter collimator (hatched) inserted into the BNCEFNT 20-cm collimator.

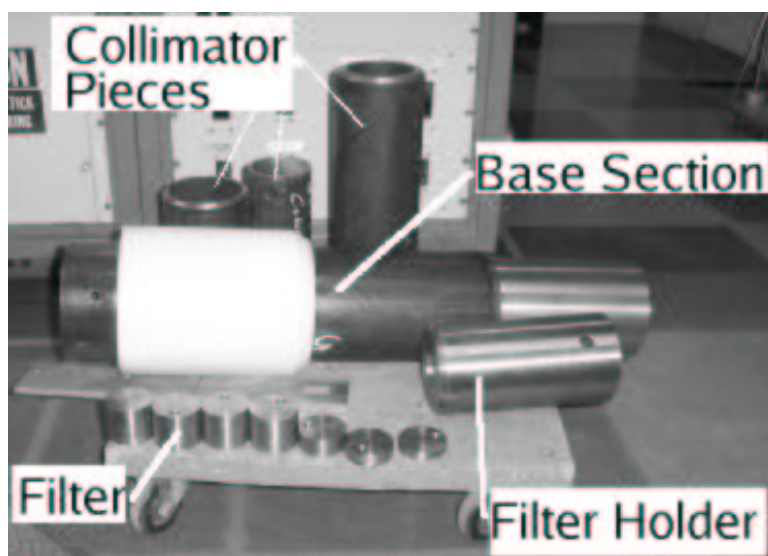


Figure 26: Photograph of the BNCEFNT filter and collimator.

Table 9: Dimensions of the filter and collimator components. All units are in inches.

Section	Component	Length (in)	Outside Radius (in)	Inside Radius (in)
Base Section				
	Small Collimator Sleeve	9.875	3.000	2.000
	6" Sch. 80	24.0	3.313	2.881
	Polyethylene Sleeve	10.5	4.250	3.313
20-cm Diameter Collimator				
	5" Sch. XXH	16.0	2.782	2.032
	5" Sch. 80	8.0	2.782	2.407
	3.5" Sch. 40	10.0	2.000	1.774
	3" Sch. 80	3.0	1.750	1.450
10-cm Diameter Collimator				
	5" Sch. XXH	6.0	2.782	2.032
	3.5" Sch. 40	12.0	2.000	1.774
	3" Sch. 80	14.5	1.750	1.450
	2.5" Sch. XXH	8.5	1.438	0.886
	2.5" Sch. 160	9.0	1.438	1.063
	3" Sch. XXH	4.5	1.750	1.150



Figure 27: Photograph of the 20-cm diameter collimator inserted into the Fermilab Neutron Therapy Facility.

CHAPTER V

MEASUREMENTS OF THE BNCEFNT BEAM

Depth-dose measurements were performed using the prototype boron neutron capture enhanced fast neutron therapy (BNCEFNT) beam filter/collimator system described in Chapter IV. These measurements were designed to verify that the BNCEFNT beam reached the goal of 15% dose enhancement (PDE) with minimal loss in dose rate. The depth-dose measurements were performed with both the borated and non-borated tissue equivalent (TE) ionization chambers and served to provide a measure of the percent dose enhancement, dose rate, depth-dose, and beam collimation.

5.1 Corrections and Uncertainties

The errors shown for the non-borated detector in all depth-dose plots do not include the uncertainty in the factors associated with the Bragg-Gray equation (Equation 7). The errors shown are only the measurement error (2%). The response of the non-borated detector has been converted to absorbed dose in tissue using Equation 9.

The results that are termed the “borated detector” are not the borated chamber readings but the response that would occur if the detector did not violate the Bragg-Gray principle, and contained 100-ppm ^{10}B rather than 184-ppm of ^{10}B . Therefore, the borated detector is the absorbed dose due to fast neutrons, gammas, and boron neutron capture. The boron neutron capture dose for a 100-ppm ^{10}B tissue equivalent wall can be calculated by summing

Equation 9 and Equation 27 corrected to 100-ppm ^{10}B .

$$\begin{aligned}
D_B &= D_{\text{NB}} + \left(\frac{100 \text{ ppm}}{184 \text{ ppm}} \right) D_{\text{boron}} \\
&= 0.0645 \text{ (Gy/nC)} \cdot Q_{\text{NB(nC)}} + \\
&\quad \frac{100}{184} \cdot 0.0247 \text{ (Gy/nC)} \cdot \left[Q_B \text{ (nC)} - Q_{\text{NB (nC)}} \left(\frac{N_C^{\text{NB}}}{N_C^{\text{B}}} \right) \right] \\
&= 0.0645 \text{ (Gy/nC)} \cdot Q_{\text{NB(nC)}} + \\
&\quad \frac{100}{184} \cdot 0.0247 \text{ (Gy/nC)} \cdot [Q_B \text{ (nC)} - Q_{\text{NB (nC)}}(0.951)] \\
&= 0.0517 \text{ (Gy/nC)} \cdot Q_{\text{NB(nC)}} + 0.0134 \text{ (Gy/nC)} \cdot Q_B \text{ (nC)} \quad (29)
\end{aligned}$$

where D_B is the corrected reading of the borated detector, D_{NB} is the corrected reading of the non-borated detector, and D_{boron} is the contribution of the boron neutron capture dose to the borated detector reading. The errors of D_B shown on all depth-dose plots do not include uncertainties associated with D_{NB} but uncertainties associated with D_{boron} (16%) and the measurement error (2%) are shown.

The percent dose enhancement (PDE) is calculated from Equation 21. The errors shown in the plots of the PDE include the error associated with the PDE correction factor (16%) and the measurement errors unless otherwise noted. The lines in the depth-dose plots are provided to allow the reader to easily group the data. The lines are not meant to provide interpolation between points.

5.2 Measurements of the BNCEFNT beam

Measurements of the new BNCEFNT filter and collimation system were performed for five iron filter thicknesses to provide percent dose enhancement (PDE) and dose rate data as a function of iron filter thickness. The filter thickness experiments were performed using the 20-cm diameter iron collimator. The five filter thicknesses of iron were 0, 15.24, 17.04, 18.3, and 19.03 cm. For these filter thicknesses a minimum of three depths in the water phantom were used to measure the PDE: 3, 5, and 7-cm (Fig. 28). The maximum PDE shifts from 7 cm for no filtration to a depth of 5 cm for the thickest iron filtration. The

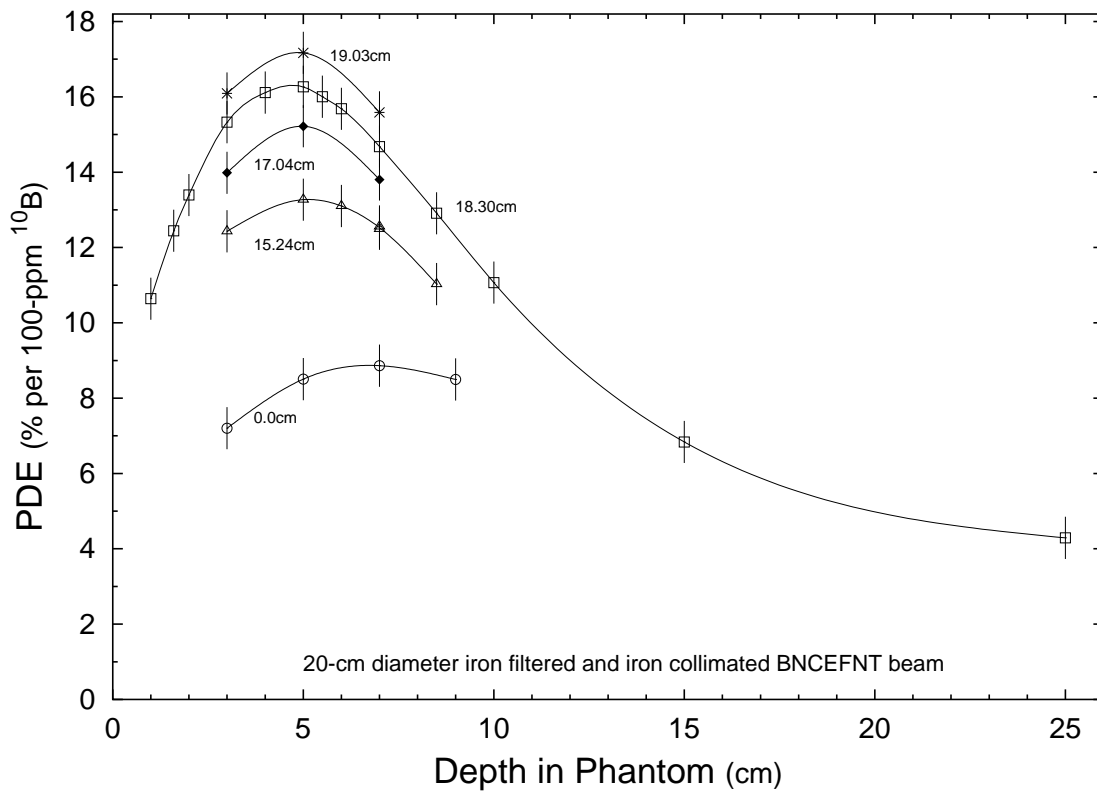


Figure 28: Measurements of the PDE as a function of depth in the water phantom for five iron filter thickness. The beam was collimated with the 20-cm diameter iron collimator. The PDE is normalized to 100-ppm ^{10}B . The errors shown do not include errors in the PDE correction factor. Only the experimental errors are shown.

PDE at 5-cm deep is plotted as a function of iron filter thickness in Figure 29.

The reduction in dose rate as a function of iron filter thickness is expressed in two different ways. One expression for the reduction in dose rate is the “ $(n+\gamma)$ dose ratio”. The $(n+\gamma)$ dose ratio is the ratio of the non-borated detector response at 5-cm deep for the standard $20 \times 20 \text{ cm}^2$ beam divided by the same response for the filtered beam. The 5-cm point is chosen to coincide with the point of maximum PDE. This ratio is a measure of the loss in absorbed dose rate due to fast neutrons and gammas. As this number becomes larger the dose rate of the beam decreases. For example, filtration causing a 95% loss in dose rate would result in a $(n+\gamma)$ dose ratio of 20.

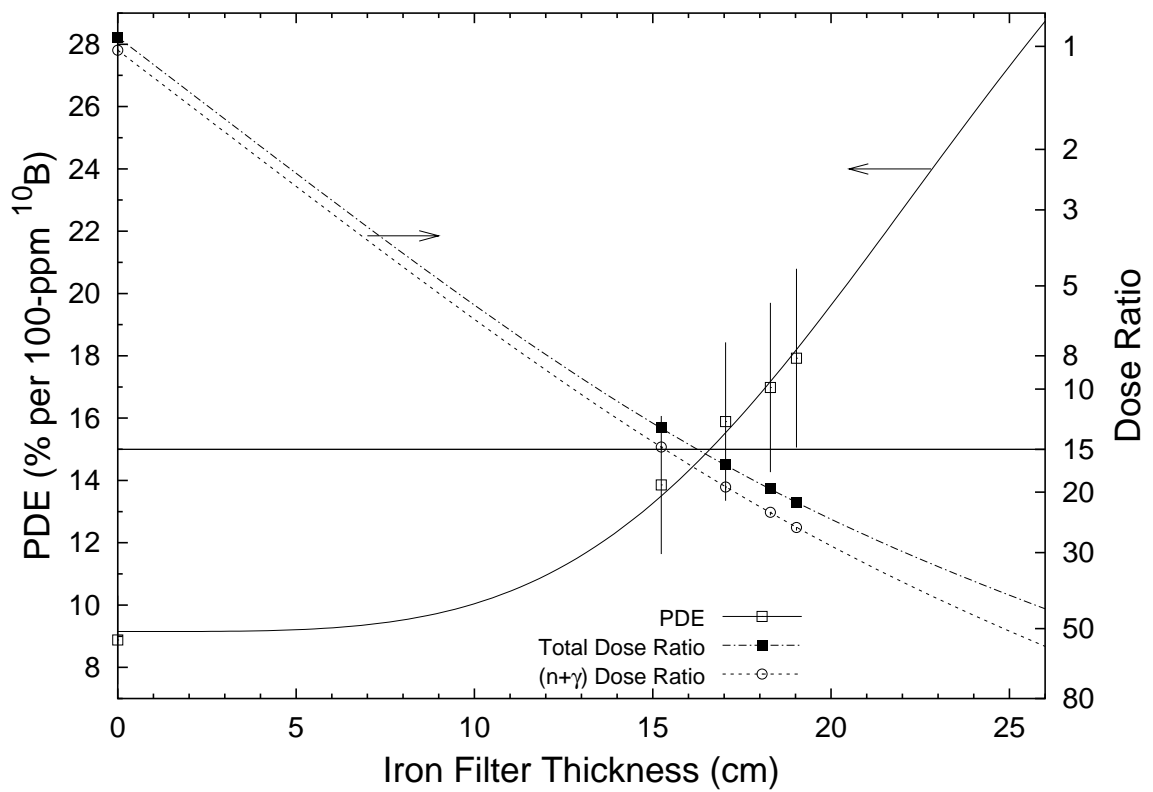


Figure 29: Measurements of the PDE at 5-cm deep and measurements of the dose rate ratios as a function of iron filter thickness. The beam was collimated with the 20-cm diameter iron collimator.

The other expression for the reduction in dose rate is the “total dose ratio”. The total dose ratio is the ratio of the non-borated detector response at 5-cm deep for the standard $20 \times 20 \text{ cm}^2$ beam divided by the borated detector response at 5-cm deep for the filtered beam. The borated detector response is normalized to 100-ppm ^{10}B . This ratio is a measure of the total dose rate for a BNCEFNT treatment as compared to the total dose rate for a standard fast neutron therapy treatment.

The total dose ratio and the $(n+\gamma)$ dose ratio are exponential functions of the filter thickness (Fig. 29). These ratios as a function of filter thickness have been found to fit to the form

$$\frac{1}{R_z(x)} = \frac{1}{R_z(0)}(1 + a_z x^4)e^{-\mu x} \quad (30)$$

Where $R_z(x)$ is the total dose ratio or the $(n+\gamma)$ dose ratio at a given depth for a filter of thickness x . The value of $R_z(0)$ is the ratio for no filtration. The subscript z is t for the total dose ratio and ng for the $(n+\gamma)$ dose ratio. μ is the effective macroscopic removal cross section and the term $(1 + a_z x^4)$ is analogous to the buildup expression used in photon shielding. The effective macroscopic removal cross section is found from the fit of $(n+\gamma)$ dose ratio and held constant for the fit of the total dose ratio. The fits to Equation 30 for the total dose ratio and the $(n+\gamma)$ dose ratio are listed in Table 10. It is important to note that the values listed in Table 10 are the results of mathematical fits to Equation 30 and do not necessarily reflect physical quantities.

The percent dose enhancement (PDE) can be defined in terms of the coefficients of Equation 30.

$$\text{PDE}(x) = \left(\frac{R_{ng}(0)}{R_t(0)} \cdot \frac{1 + a_t x^4}{1 + a_{ng} x^4} - 1 \right) \times 100 \text{ (\%)} \quad (31)$$

5.2.1 18.3-cm thick iron filter - 20 cm diameter iron collimator

The PDE and the $(n+\gamma)$ dose ratio measured for the five filter thickness provided a basis for optimizing the filter thickness. The optimum thickness was chosen during the course of the measurements performed on the BNCEFNT beam in order to perform more detailed

Table 10: Coefficients resulting from a least squares fit of Equation 30. These coefficients describe the loss in dose rate as a function of filter thickness. WSSR/ndf is also known as the reduced chi-square. WSSR is the weighted sum of squared residuals and ndf is the number of degrees of freedom.

$$1/R(x) = (1/R(0))(1 + ax^4)e^{-\mu x}$$

Constant	(n+ γ) Dose Ratio	Total Dose Ratio
μ	0.1832 ± 0.0005	-
$R(0)$	1.027 ± 0.003	0.941 ± 0.003
a	$(2.48 \pm 0.11) \times 10^{-6}$	$(3.32 \pm 0.05) \times 10^{-6}$
WSSR/ndf	0.16	0.24

measurements on the optimized filter. A filter thickness of 18.3-cm of iron was chosen as the optimum based on an incorrect estimate of the PDE correction factor at the time of the measurements. The 18.3-cm is not the optimum filter based on the final estimate of the PDE correction factor and the design goal of obtaining a minimum dose enhancement of 15% while minimizing the reduction in dose rate. However, the additional measurements performed using the 18.3-cm iron filter can be used to provide general trends that hold for all filter thicknesses. The minimal filter thickness needed to obtain a PDE of 15% is 17 cm. For 17-cm of iron the (n+ γ) dose ratio is 19.3 and the total dose ratio is 16.8.

With the 18.3-cm iron filter a maximum PDE of $(16.3 \pm 2.6)\%$ is obtained. The (n+ γ) dose ratio at 5-cm deep in the phantom is 22.9 ± 0.5 . The total dose ratio at this depth for the 18.3-cm iron filter was 19.7 ± 0.6 .

An estimate of the time that would be required to treat a brain tumor patients can be calculated using the (n+ γ) ratio and the dose rate of the standard treatment beam. Assuming that 18 Gy is given to the patient over the course of 12 fractions with 4 fields per fraction, the patient would receive an average of 0.375 Gy per field or 1.5 Gy per fraction. The standard treatment beam can deliver 0.43 monitor units (MU) per minute, assuming a

57 μsec pulse width. One MU is the beam output required to produce a dose of one gray at a depth of 10-cm in tissue for the $10 \times 10 \text{ cm}^2$ field. For the standard treatment beam the dose of one field, 0.375 Gy, can be delivered in 0.87 minutes. Or the dose of one fraction, 1.5 Gy, can be delivered in 3.49 minutes. Using the BNCEFNT filter and collimator the dose of one field can be delivered in 22.9×0.87 minutes = 19.9 minutes. And, a fraction requires 22.9×3.49 minutes = 79.9 minutes.

A complete depth-dose distribution measurement of the 18.3-cm-thick-iron-filtered beam was performed using the borated and non-borated TE ionization chambers (Fig. 30). Normalization of the depth-dose curve of the non-borated detector shows almost the same shape as the normalized depth-dose curve of the $20 \times 20 \text{ cm}^2$ standard treatment beam (Fig. 31). This normalization shows that the penetration of the modified beam is slightly greater than the penetration of the standard beam. THE PDE reaches a maximum of $(16.3 \pm 2.6)\%$ at a depth of 5 cm deep (Fig. 32). The maximum PDE occurs deeper in the water phantom than the maximum total dose which occurs at 3-cm deep where the PDE is $(15.3 \pm 2.4)\%$.

The dose was also measured off-axis. The off-axis measurements were performed at 4-cm deep in the phantom and perpendicular to the central beam axis. The dose was measured using both the borated and non-borated detectors. The off-axis measurements (Fig. 33) clearly show a sharp drop in the detector responses at ± 10 cm, confirming a collimated field size of 20-cm in diameter. The boron capture response, normalized to 100-ppm ^{10}B , does not exhibit the sharp cutoffs at the fast neutron beam edges that is exhibited by the non-borated detector response. Since the boron capture response is proportional to the thermal neutron flux, this result is not surprising since thermal neutrons are generated in the water phantom due to the slowing down of epithermal neutrons. The boron capture response is fitted to a function predicted by the one group diffusion model for the fundamental mode flux shape of a cylindrical reactor core surrounded by a reflector [57].

Inside the collimated beam the response is fitted to the solution of the diffusion model

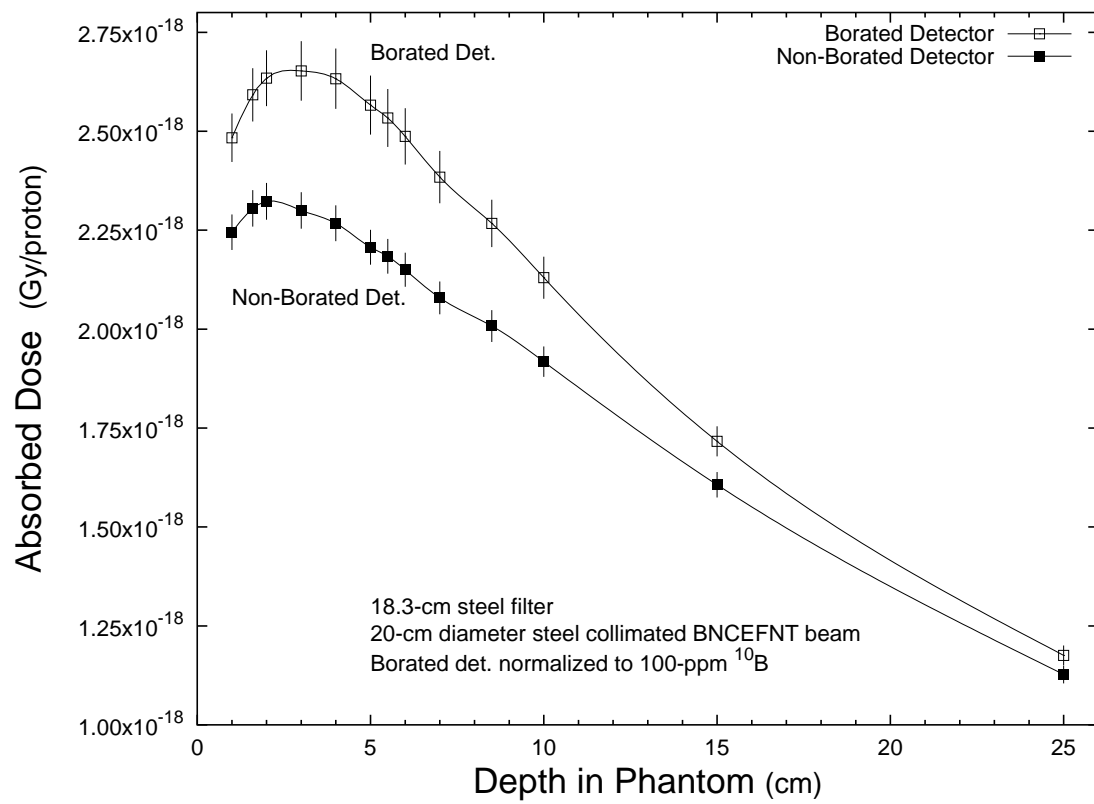


Figure 30: Depth-dose measurement of the 20-cm diameter BNCEFNT beam filtered with 18.3-cm of low carbon steel. The borated detector measurements have been normalized to 100-ppm ^{10}B .

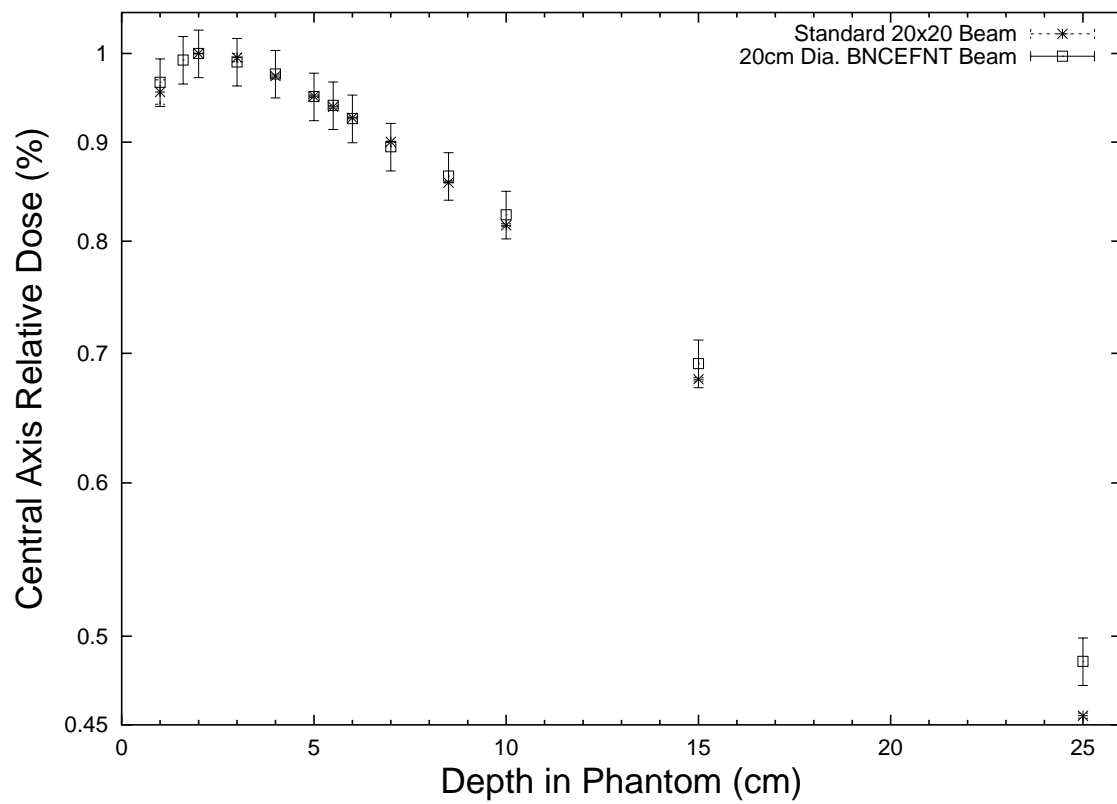


Figure 31: Central axis relative depth-dose measurement of the 20-cm diameter BNCEFNT beam filtered with 18.3-cm of low carbon steel and the $20 \times 20 \text{ cm}^2$ standard treatment beam. The measurements have been normalized at 2.0-cm deep in the water phantom.

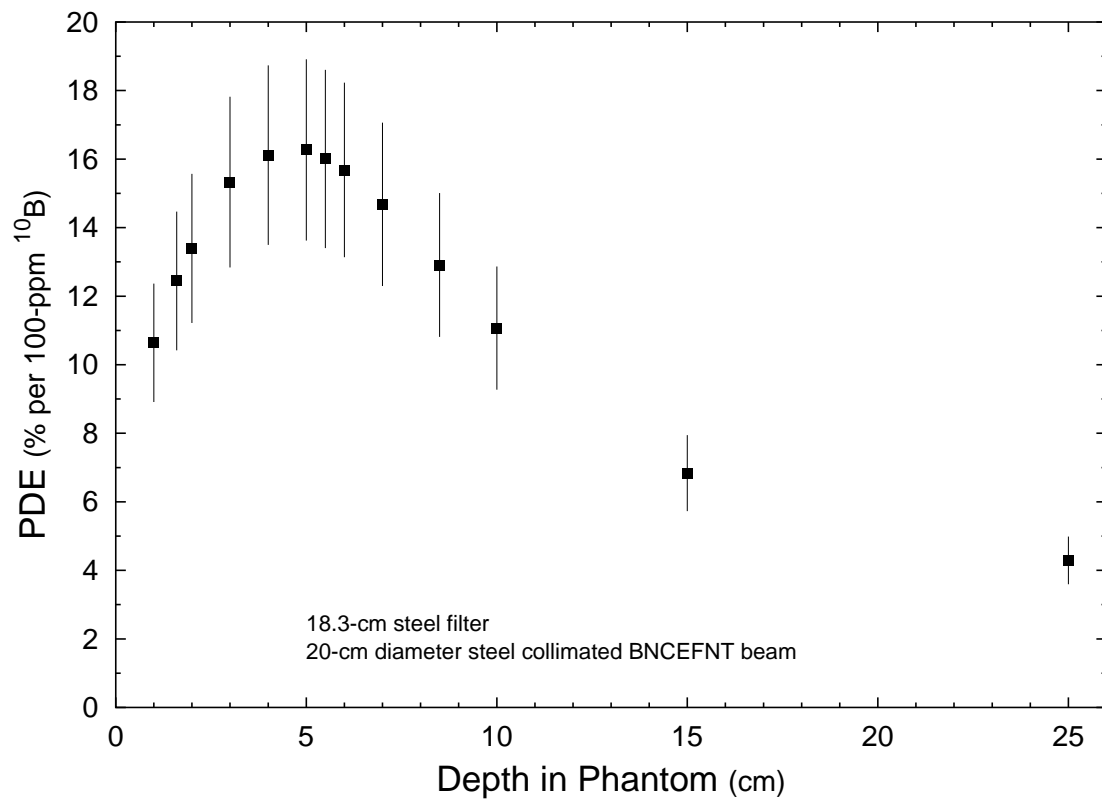


Figure 32: PDE measurements of the 20-cm diameter BNCEFNT beam filtered with 18.3-cm of low carbon steel.

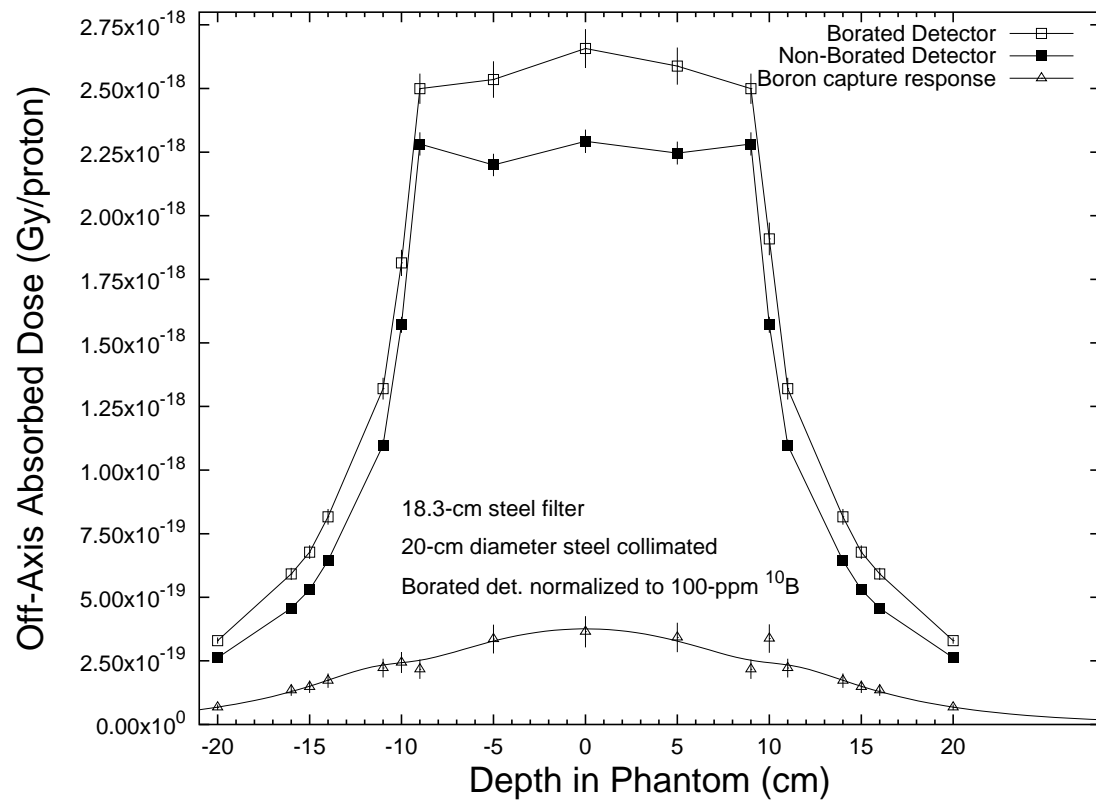


Figure 33: Off-axis measurements taken perpendicular to the beam direction at a depth of 4-cm in the water phantom for the 20-cm diameter BNCEFNT beam filtered with 18.3-cm of low carbon steel. The borated detector measurements have been normalized to 100-ppm ^{10}B .

in a reactor core

$$\phi^C(x) = A^C \cdot J_0\left(\frac{\nu_0 x}{\tilde{r}}\right) \quad (32)$$

where $\phi^C(x)$ is the neutron flux in the direct beam, A^C is the peak flux, J_0 is a Bessel function of the zero order, $\nu_0 = 2.405$, and \tilde{r} is the radius of the direct beam plus the extrapolation distance, and x is the radial distance from the center-line. Outside of the direct beam the boron capture response is fitted to the diffusion model solution of the flux in the reflector region of a reactor.

$$\phi^R(x) = A^R \cdot \sinh\left(\frac{\tilde{r} + \tilde{b} + x}{L^R}\right) \quad (33)$$

where $\phi^R(x)$ is the neutron flux in the reflector, A^R is a constant, \tilde{r} is the effective radius of the direct beam, \tilde{b} is the effective thickness of the reflector, and L^R is the diffusion length in the phantom.

The parameter A^C , A^R , \tilde{r} , \tilde{b} , and L^R of equations 32 and 33 are fitted to the measured boron capture response using a nonlinear least-squares Marquardt-Levenberg algorithm (Fig. 34). Equations 32 and 33 are not required to meet the interface boundary conditions, instead the two equations are connected using a joining function.

The diffusion theory approximation works well in the collimated beam and far outside of the beam. However, it does a poor job of estimating the thermal flux in the interface region between the collimated beam and the reflector. The detector readings change rapidly near the edge of the beam and small errors in the off-axis position will lead to large errors in the boron capture response.

An additional confirmation of the collimation of the 20-cm diameter beam was performed by exposing a piece of x-ray film in the beam (Fig. 35). From the x-ray, the beam profile is measured as 20.5-cm horizontally and 20.0-cm vertically. Three of the threaded holes used for inserting and removing the filter pieces can easily be seen as dark circles in the x-ray. Two of the dark circles are near the top and one of the circles is nearer the bottom. The white spot in the bottom half of the x-ray is a defect in the film. The x-ray confirmed that no significant leakage past the collimator pieces occurred.

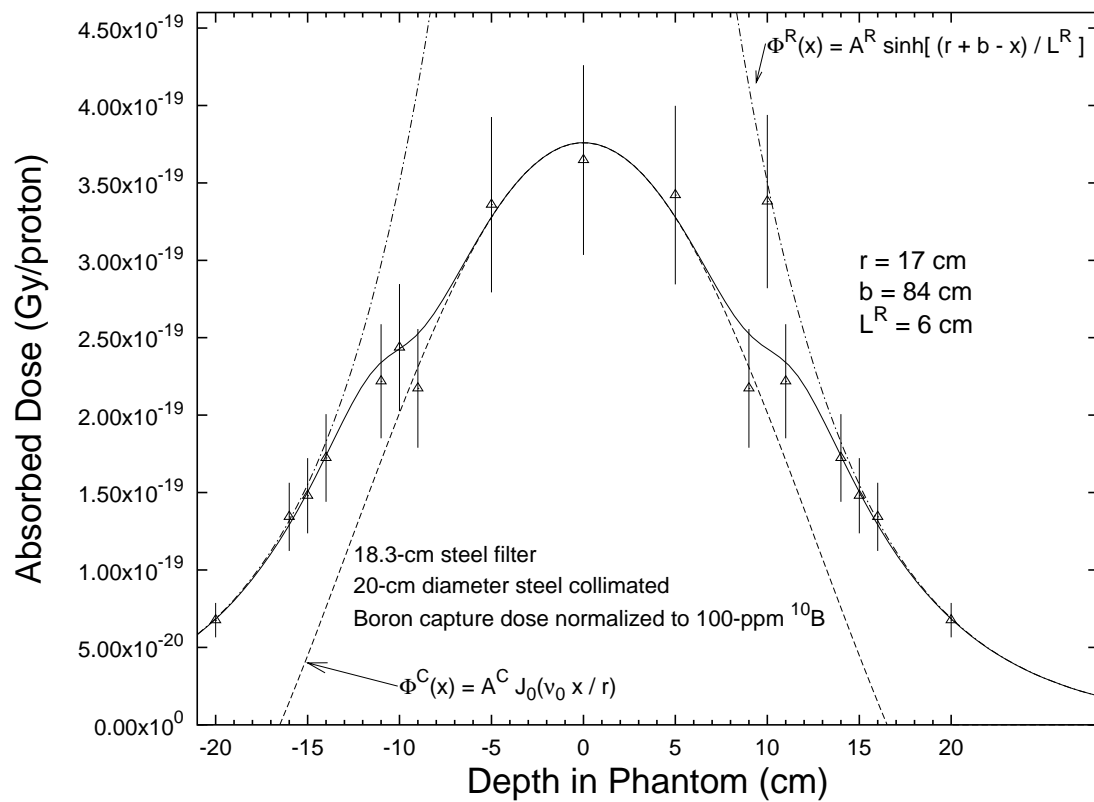


Figure 34: Off-axis boron capture dose measured perpendicular to the beam direction at a depth of 4-cm in the water phantom for the 20-cm diameter BNCEFNT beam filtered with 18.3-cm of low carbon steel. The boron capture dose has been normalized to 100-ppm ^{10}B .

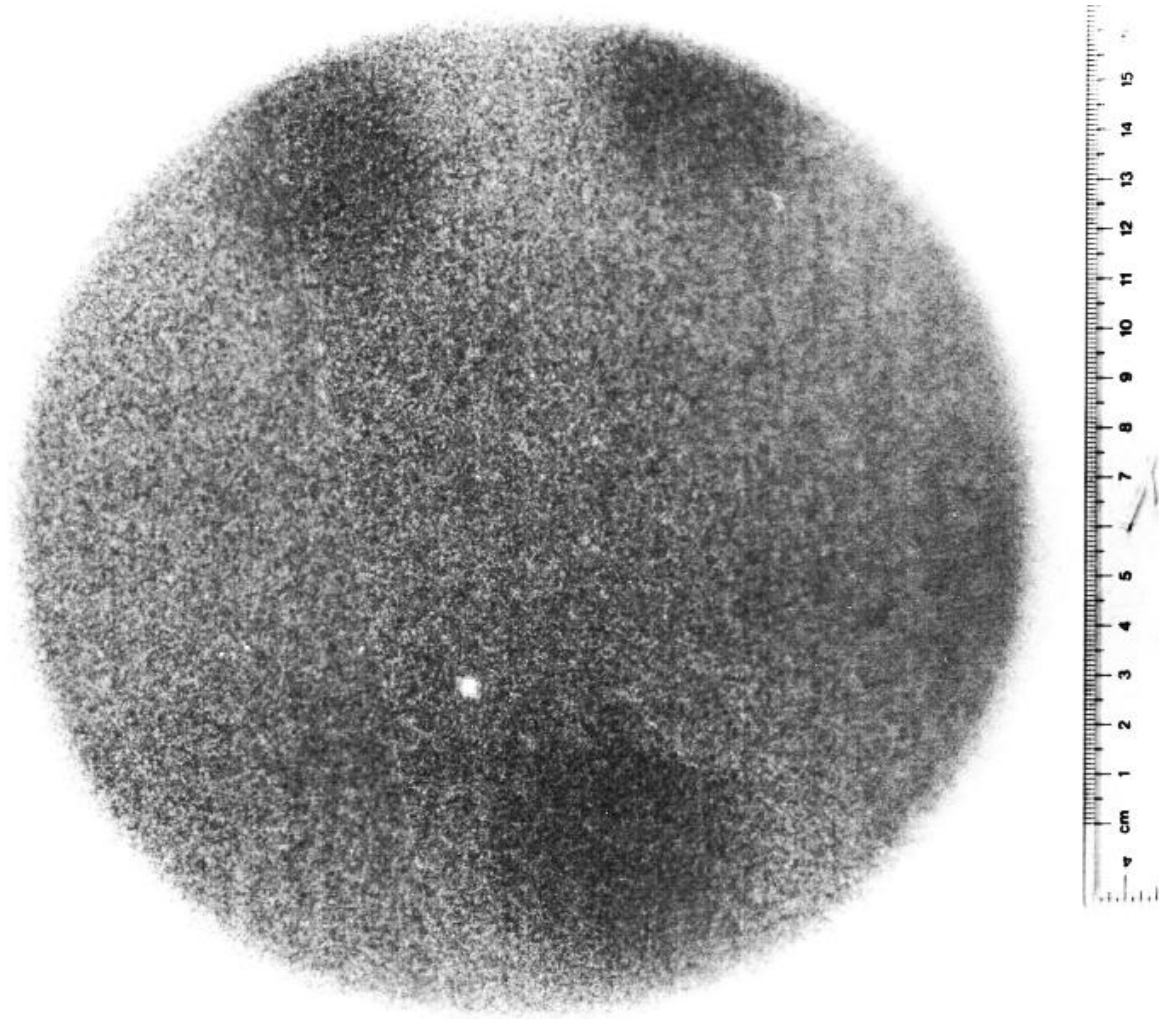


Figure 35: X-ray film irradiated with the 20-cm diameter iron collimator and the 18.3-cm thick low carbon steel filter. Three of the threaded holes used for inserting and removing the filter pieces can be seen as dark circles. The image has been contrasted to show the effects of the threaded holes. The width of the beam is 20.5 cm and the height of the beam is 20.0 cm

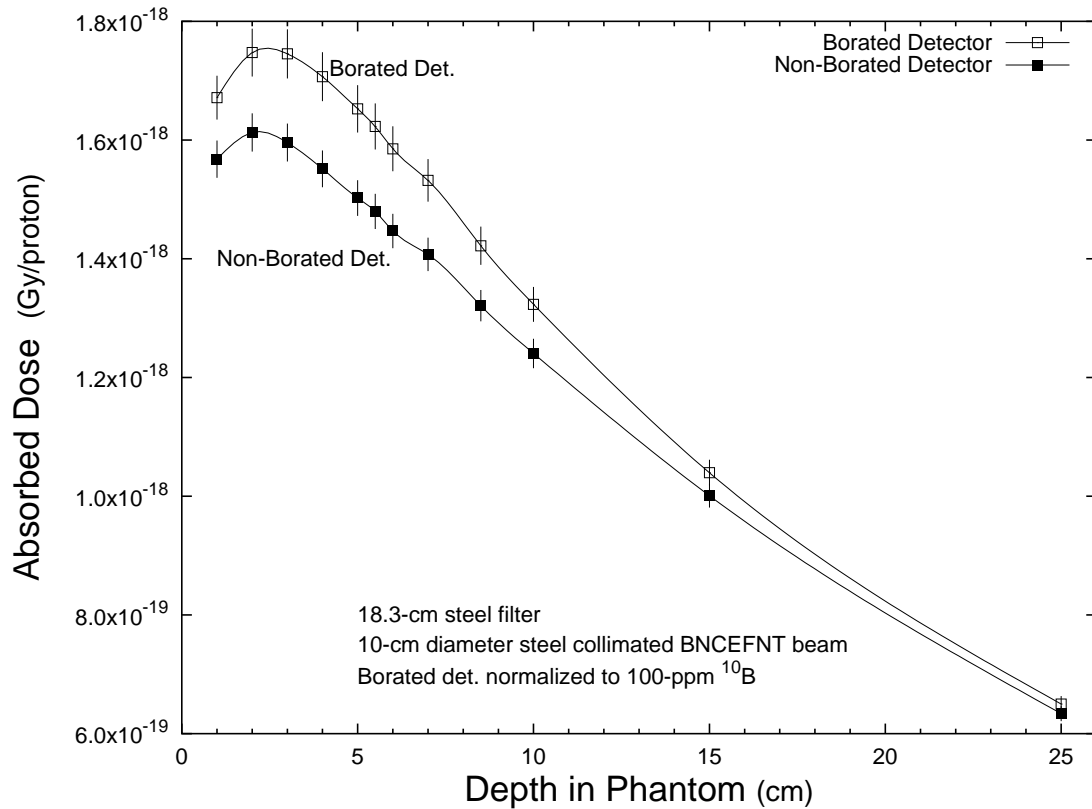


Figure 36: Depth-dose measurement of the 10-cm diameter BNCEFNT beam filtered with 18.3-cm of low carbon steel. The borated detector measurements have been normalized to 100-ppm ^{10}B .

5.2.2 10-cm diameter iron collimator

Depth dose measurements were also performed with the 10-cm diameter steel collimator and the 18.3-cm thick low carbon steel filter (Fig. 36). The percent dose enhancement (PDE) per 100-ppm ^{10}B for the 10-cm diameter iron collimator reached $(10.0 \pm 1.6)\%$ between 4-cm and 5-cm deep (Fig. 37). This is the shallowest depth at which the peak PDE was observed for all filter/collimator combinations. Normalization of the depth-dose curve of the non-borated detector shows almost the same shape as the depth dose curve of the $10 \times 10 \text{ cm}^2$ standard treatment beam (Fig. 38).

Off-axis measurements were again performed at 4-cm deep (Fig. 39) and confirmed that

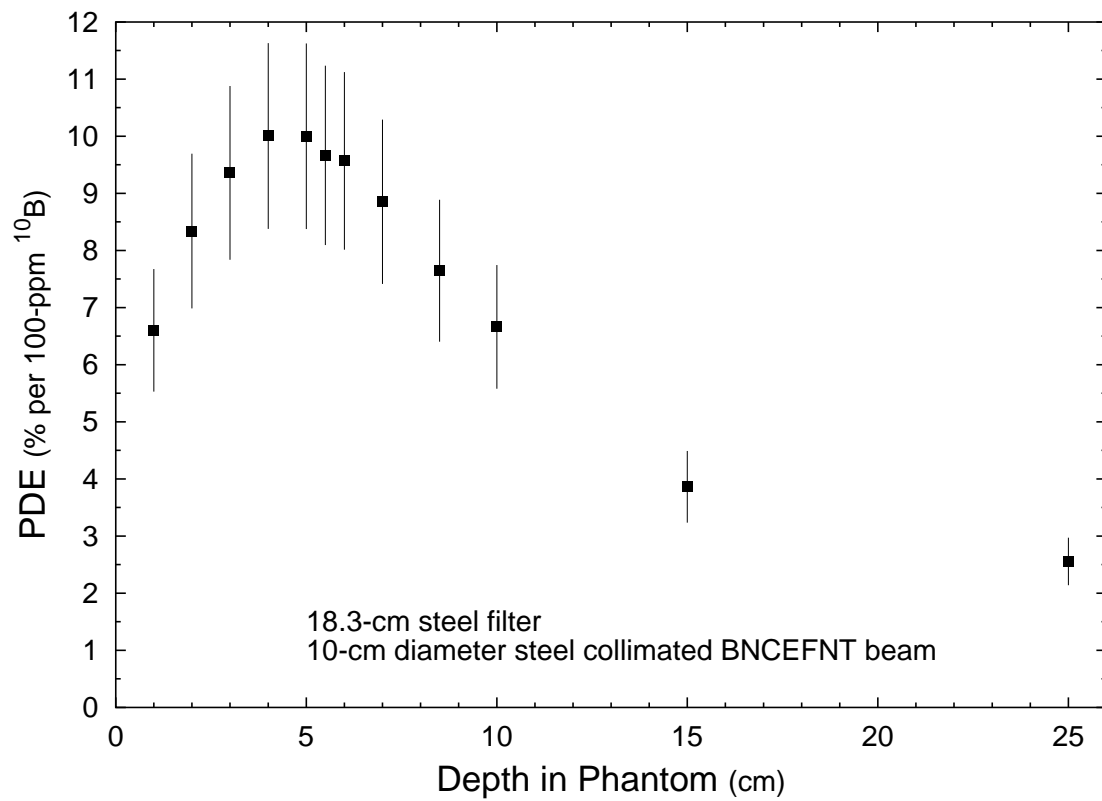


Figure 37: PDE measurements of the 10-cm diameter BNCEFNT beam filtered with 18.3-cm of low carbon steel.

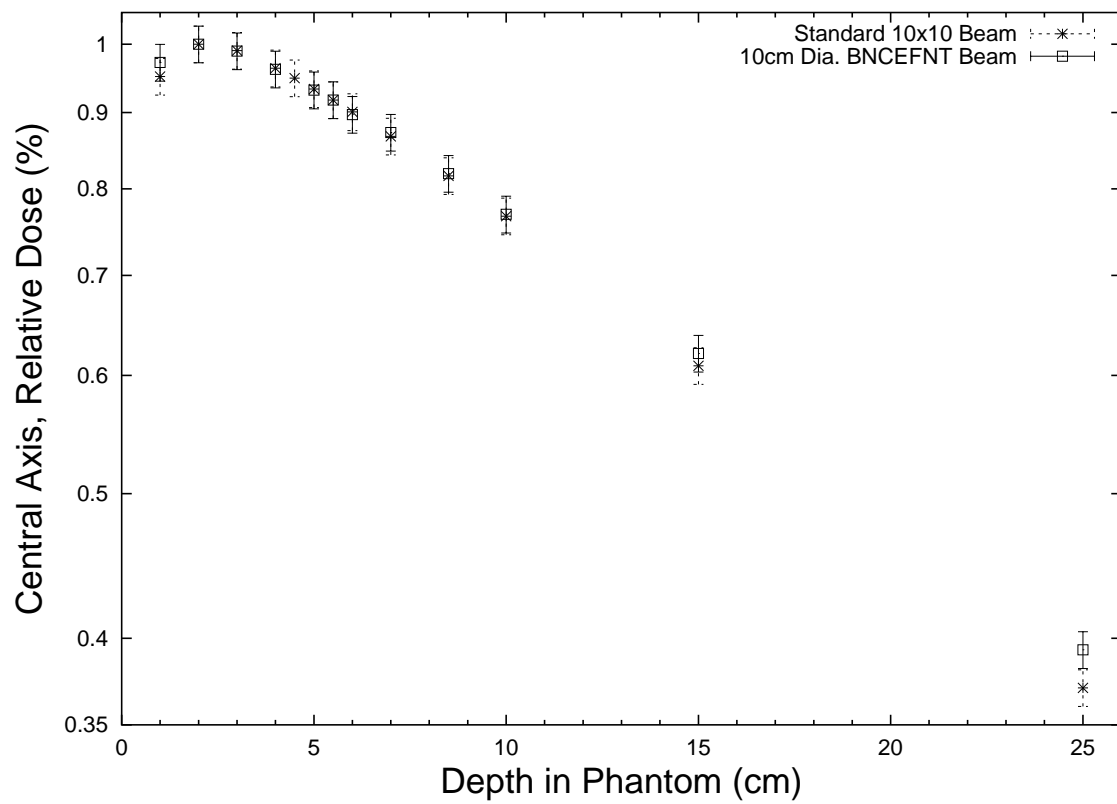


Figure 38: Central axis relative depth-dose measurement of the 10-cm diameter BNCEFNT beam filtered with 18.3-cm of low carbon steel and the $10 \times 10 \text{ cm}^2$ standard treatment beam. The measurements were normalized at 2.0-cm deep in the water phantom.

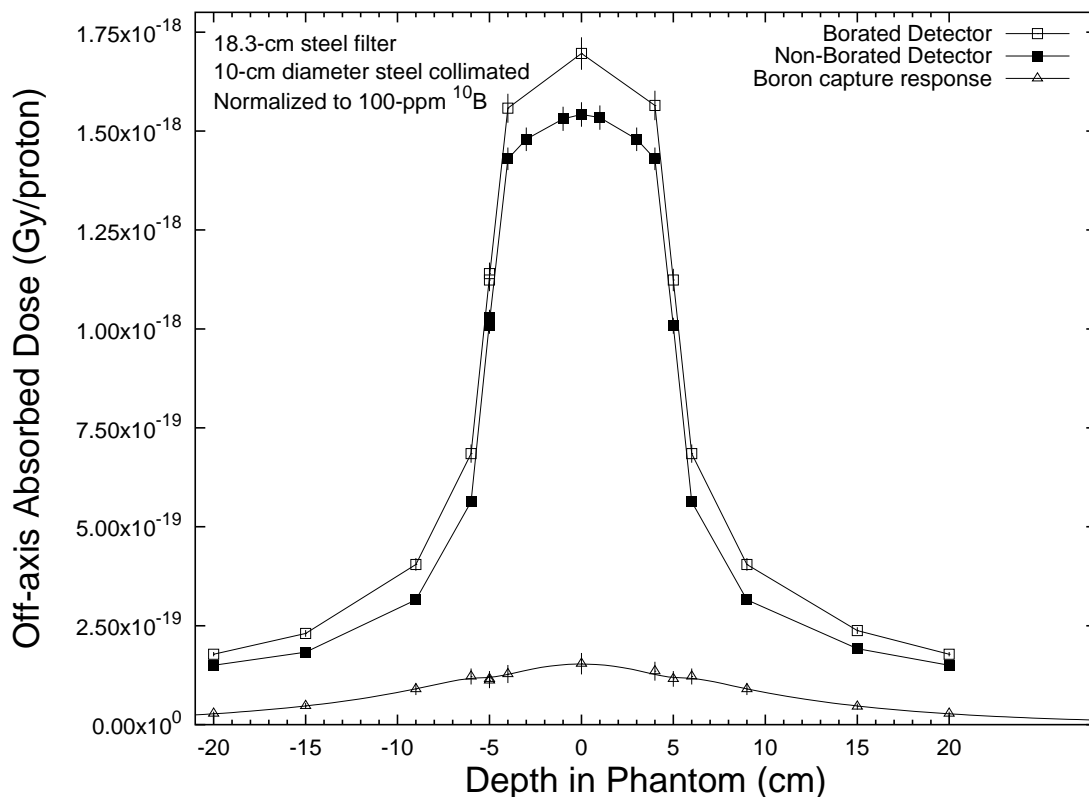


Figure 39: Off-axis measurements taken perpendicular to the beam direction at a depth of 4-cm in the water phantom for the 10-cm diameter BNCEFNT beam filtered with 18.3-cm of low carbon steel. The borated detector measurements have been normalized to 100-ppm ^{10}B .

good collimation was achieved. The boron only response again was fitted to diffusion theory parameters (Fig. 40).

5.3 MCNPX Comparison to Measurements of the BNCEFNT Beam

The results of MCNPX calculations of the depth-dose, dose rate, and percent dose enhancement (PDE) are compared to the measurements of the BNCEFNT beam. The comparison of the calculations to measurements provide verification of MCNPX for future BNCEFNT beam design. The use of these data is more applicable than measurements of the standard treatment beam since the BNCEFNT beam has more epithermal neutrons. These data

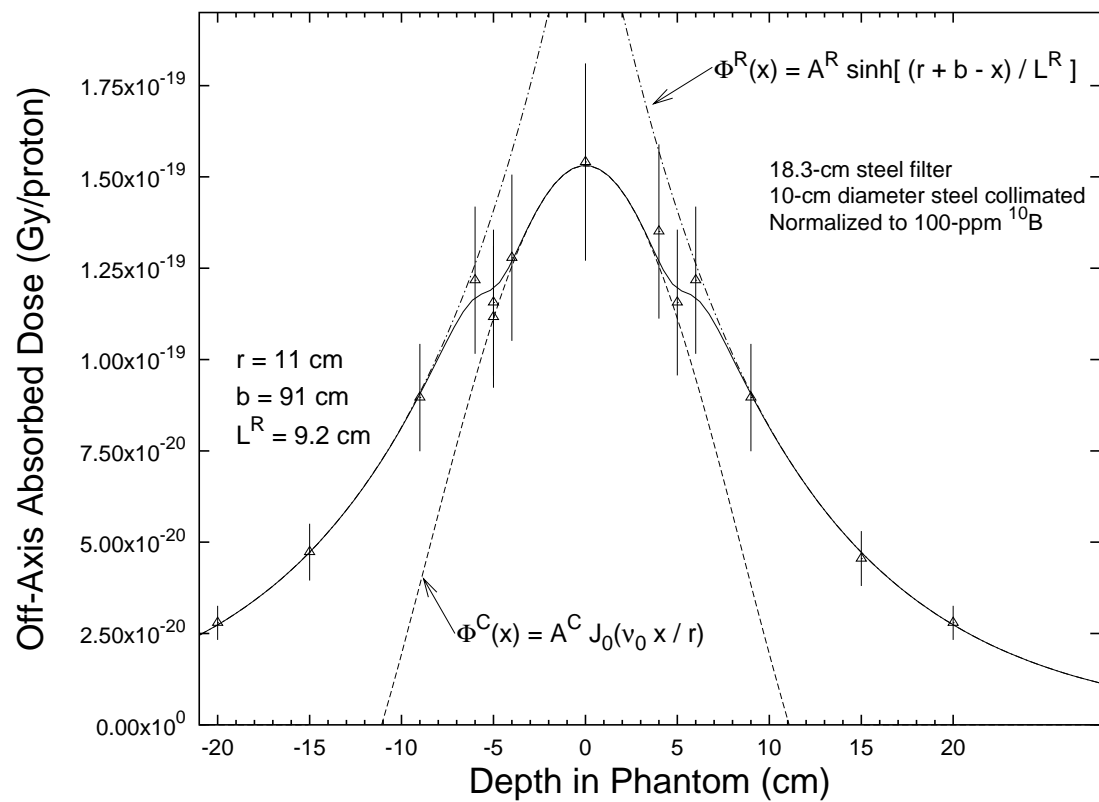


Figure 40: Off-axis boron capture dose measured perpendicular to the beam direction at a depth of 4-cm in the water phantom for the 10-cm diameter BNCEFNT beam filtered with 18.3-cm of iron. The boron capture dose has been normalized to 100-ppm ¹⁰B.

Table 11: Experiment-to-calculated ratios (E/C) of the (n+ γ) dose at 3-cm in the water phantom and the PDE at 5-cm deep in the water phantom for the BNCEFNT beam.

Field Size	PDE E/C	(n+ γ) Dose E/C
20-cm Dia.	0.85 ± 0.14	2.92 ± 0.14
10-cm Dia.	0.83 ± 0.13	2.88 ± 0.17

would be especially applicable to any designs employing filtration with iron.

MCNPX calculations of the (n+ γ) dose rate at 3-cm deep in the water phantom again underestimate the dose rate by about a factor of 3 (Table 11). The shape of the depth-dose as calculated by MCNPX is roughly the same shape as the measured depth-dose curves. The calculated depth-dose curves for the 20-cm and 10-cm diameter BNCEFNT beams are shown in Figures 41 and 42, respectively. The removal of neutrons by the filter in the calculation has resulted in an increase in the Monte Carlo error despite efforts to bias neutrons through the filter using importance weighting. The filter was broken into slabs of thickness equal to the mean free path of neutrons in the filter. The importance was increased in the slabs to maintain an equal number of neutrons in each region.

Calculations of the PDE for the 20-cm diameter beam and the 10-cm diameter beam are shown in Figures 43 and 44, respectively. These calculations show that MCNPX overestimates the peak PDE. The experiment-to-calculated ratios of the BNCEFNT 20-cm and 10-cm diameter beams are listed in Table 11. These ratios indicate that MCNPX tends to overestimate the peak PDE by 15% to 17%. However, this is on the order of the PDE measurement uncertainty (16%).

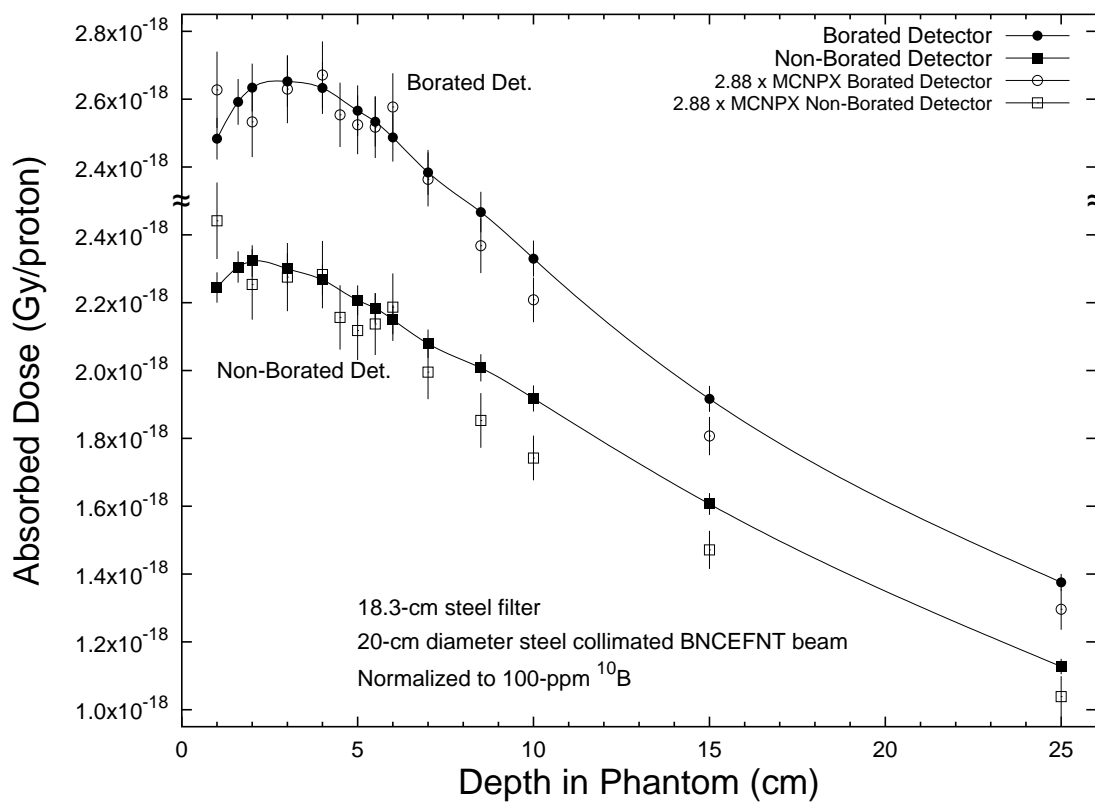


Figure 41: Depth-dose measurement and MCNPX calculation of the 20-cm diameter BNCEFNT beam. The non-borated detector represents fast neutron and gamma dose. The borated detector represents fast neutron, gamma, and boron capture dose for 100 ppm ^{10}B . The MCNPX calculation has been normalized to the non-borated detector measurement at 3-cm deep, resulting in a 2.88 normalization factor.

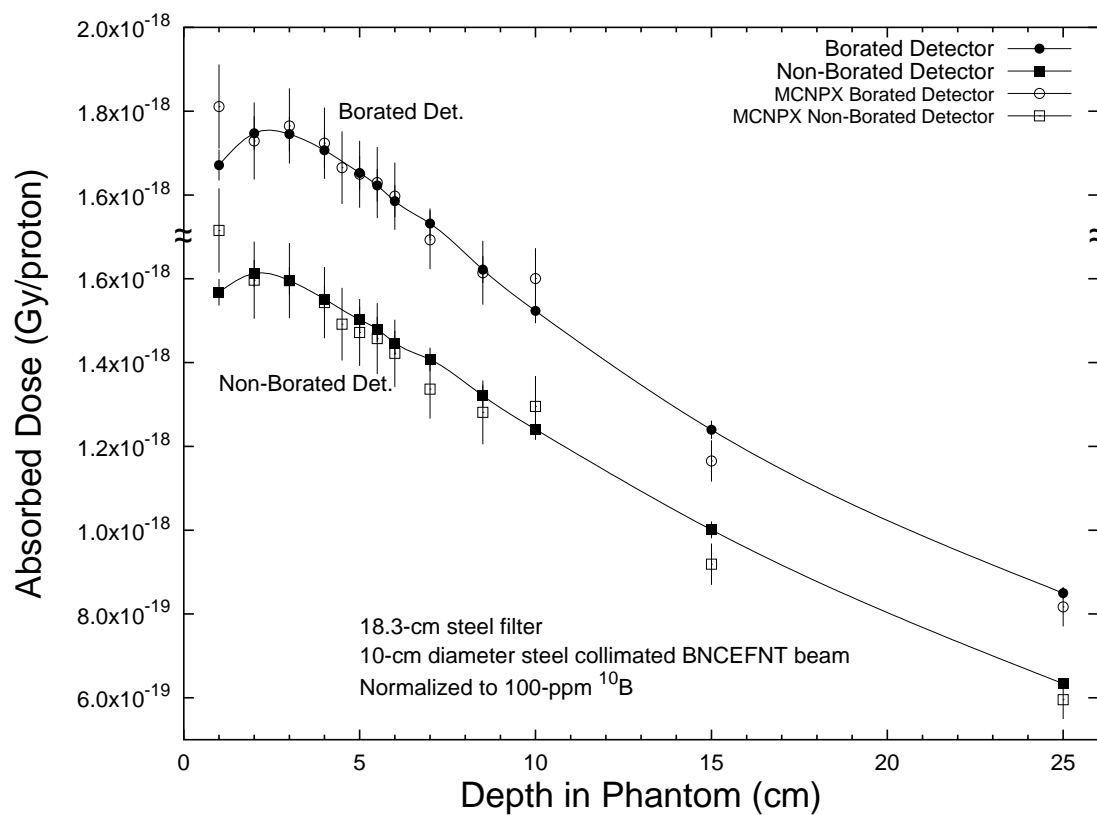


Figure 42: Depth-dose measurement and MCNPX calculation of the 10-cm diameter BNCEFNT beam. The non-borated detector represents fast neutron and gamma dose. The borated detector represents fast neutron, gamma, and boron capture dose for 100 ppm ^{10}B . The MCNPX calculation has been normalized to the non-borated detector measurement at 3-cm deep, resulting in a 2.92 normalization factor.

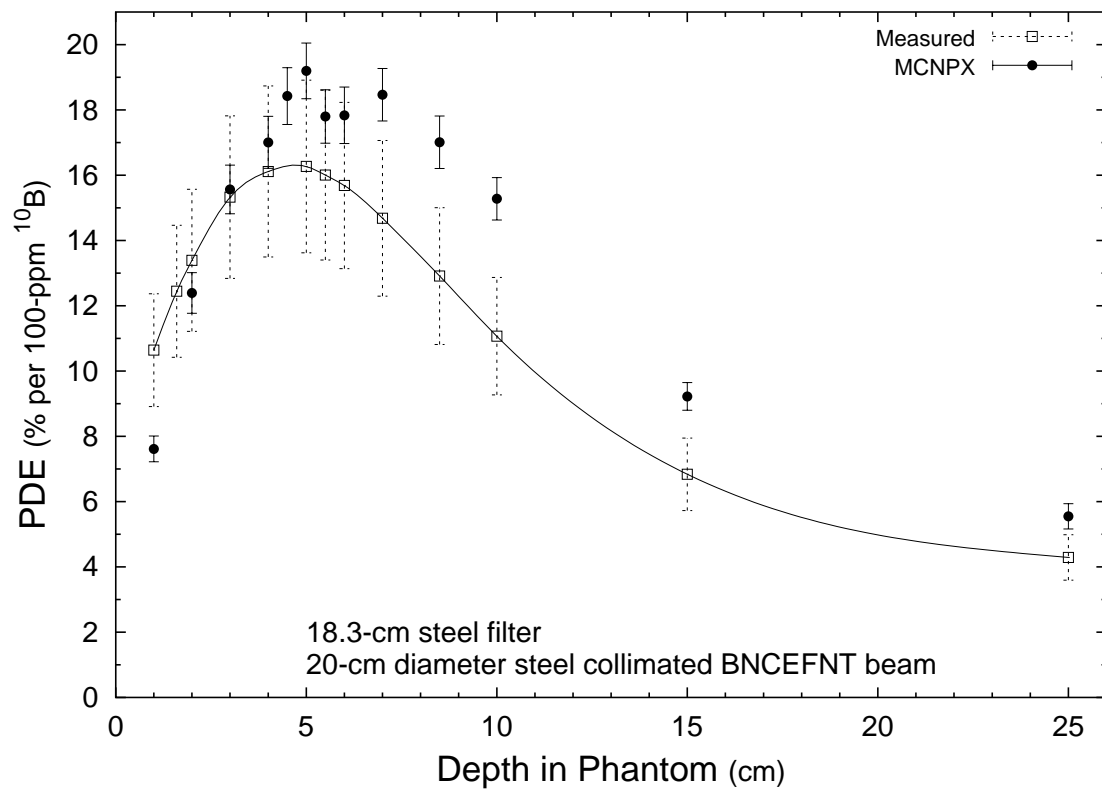


Figure 43: MCNPX calculation of the PDE vs. measurements of the 20-cm BNCEFNT beam filtered with 18.3-cm of low carbon steel.

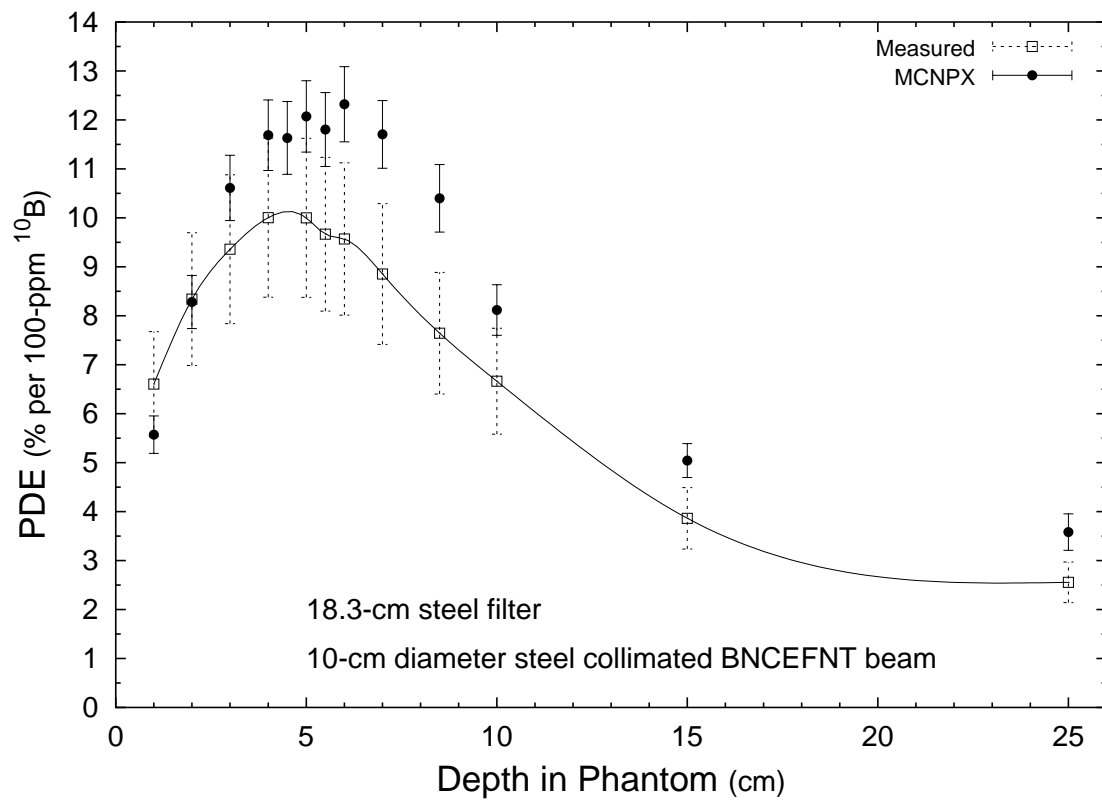


Figure 44: MCNPX calculation of the PDE vs. measurements of the 10cm BNCEFNT beam filtered with 18.3-cm of low carbon steel.

CHAPTER VI

CONCEPTUAL DESIGN: PROGRESSION TO A CLINICAL REALITY

In a clinical setting conditions will be quite different than the measurement conditions of this work. The 20-cm diameter BNCEFNT beam, while it produced a large percent dose enhancement of 16.3%, is not practical for brain tumor irradiation. The smaller 10-cm diameter field size resulted in a lower PDE of 10.0%. And, even this magnitude of percent dose enhancement will likely not be achievable in a head with this beam due to a lack of moderation as compared to the large water phantom used in this work. If the diffusion theory approximation of the thermal flux distribution is used, then the PDE will largely be a function of the volume of moderating material. If the field size is reduced further, using the current collimator approach, a further reduction in the PDE can be expected.

The ORNL mathematical head phantom, described by Eckerman [58], was used to calculate the effect the smaller volume of a typical head would have on the percent dose enhancement. In this model, the neck is described by a right circular cylinder

$$x^2 + y^2 \leq R_H^2 \quad C_T \leq z \leq C_T + C_{H0} \quad (34)$$

The head is described by a right elliptical cylinder topped by half an ellipsoid. The elliptical cylinder is defined by:

$$\frac{x^2}{A_H^2} + \frac{y^2}{B_H^2} \leq 1 \quad C_T + C_{H0} \leq z \leq C_T + C_{H0} + C_{H1} \quad (35)$$

Table 12: Constants for the mathematical head phantom.

Constant	Youth (< 15 years) or Adult Female		Adult Male
R_H (cm)	5.2	5.4	
A_H (cm)	7.77	8.00	
B_H (cm)	9.76	10.00	
C_{H0} (cm)	7.70	8.40	
C_{H1} (cm)	12.35	13.05	
C_{H2} (cm)	6.92	7.15	
Volume (cc)	4,700	5,220	
Mass (g)	5,250	5,870	

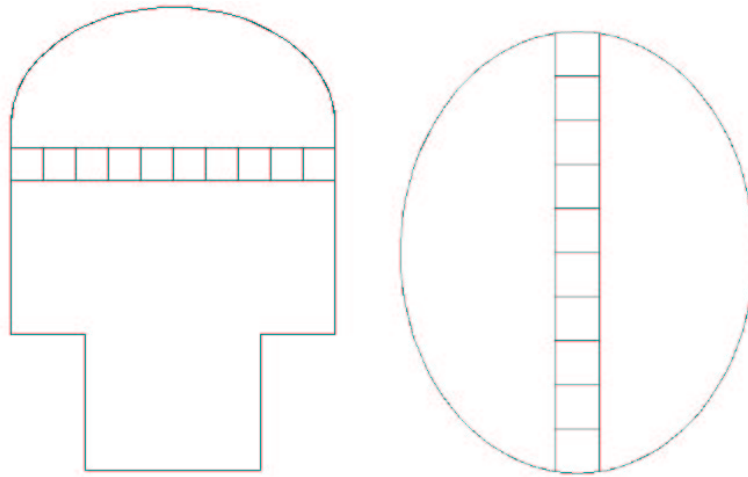


Figure 45: Diagram of the mathematical head phantom used in MCNPX to estimate dose enhancement in a head.

and the half of an ellipsoid is defined by:

$$\frac{x^2}{A_H^2} + \frac{y^2}{B_H^2} + \left(\frac{z - (C_T + C_{H0} + C_{H1})}{C_{H2}} \right)^2 \leq 1 \quad z > C_T + C_{H0} + C_{H1} \quad (36)$$

Where x , y , and z are the three Cartesian coordinates, and $z = C_T$ is the bottom of the neck.

The value of the remaining constants are listed in Table 12. The dose enhancement reduces from 19.2% per 100-ppm ^{10}B as calculated in the rectangular water phantom to 13.8% per 100-ppm ^{10}B as calculated in the mathematical head phantom for the 20-cm diameter beam.

A diagram of the mathematical head phantom is shown in Figure 45.

Moderation of neutrons using graphite, polyethylene, water, or heavy water moderator

around the head would serve to increase the dose enhancement. Pignol [29] studied the use of moderator material surrounding the head for BNCEFNT. In calculating the possible dose enhancement from high Z material collimation he used several materials to determine the best moderator. He concluded that graphite produced the largest dose enhancement. MCNPX calculations of the Fermilab facility also show that graphite is superior to water, polyethylene, and heavy water.

Following Pignol [29] and Paquis' [23] investigation of placing high Z material collimation on the face of a water phantom, the use of filtration and collimation near a head phantom has been modeled in this work. Using the standard $20 \times 20 \text{ cm}^2$ treatment beam incident on the face of a 10-cm thick, 5.64-cm diameter collimator placed near Eckerman's head phantom showed that tungsten produced the highest percent dose enhancement. Other materials studied included lead, iron, and bismuth. For a 5.64-cm diameter beam (an area equivalent to $5 \times 5 \text{ cm}^2$) and a graphite moderator, a dose enhancement of 13.5% is calculated for a tungsten collimator. Since the standard treatment beam is unfiltered for this configuration, treatment times are minimized. In fact, the dose rate increases by approximately 30% over the standard treatment beam.

The same concept can be applied to the BNCEFNT beam filtered with 18.3-cm of iron. For this beam the best collimator material to be placed near the head is iron. For a 5.64-cm diameter beam and graphite moderation of the head a dose enhancement of 15.8% is calculated for an iron collimator.

The placement of the collimator near the patient adds additional concerns to the treatment. The collimator material could become activated and pose a radiation hazard to the staff as well as increase the whole body dose to the patient. The response of the skin to low energy photons and neutron as well as charged particles produced in the heavy collimator is unknown. Langen reported that the RBE of the Fermilab Fast Neutron Therapy Facility beam filtered with 9-cm of tungsten increased by 20% [34]. It is expected that the use of a tungsten collimator would also produce a change in the RBE of the beam.

Table 13: PDE as a function of tungsten filter thickness and a 5.64-cm diameter tungsten collimator placed near the head. The head is surrounded by a moderator of varying amounts of graphite. Using the $20 \times 20 \text{ cm}^2$ standard treatment beam incident on the tungsten filter and collimator.

Moderator	Tungsten Filter Thickness (cm)	PDE (%)	(n+ γ) Dose Ratio (Standard Beam/Tested Beam)
Full Graphite Reflection			
	0.0	13.5 ± 0.4	0.67 ± 0.02
	0.5	14.8 ± 0.4	0.73 ± 0.02
	1.0	16.5 ± 0.4	0.78 ± 0.02
	1.5	17.8 ± 0.5	0.85 ± 0.02
	2.0	19.5 ± 0.5	0.90 ± 0.03
	3.0	22.6 ± 0.7	1.04 ± 0.03
	5.0	29.7 ± 1.0	1.29 ± 0.04
No Graphite Reflection			
	1.5	15.0 ± 0.4	0.86 ± 0.03
	2.0	16.4 ± 0.5	0.91 ± 0.03
	5.0	25.2 ± 1.0	1.32 ± 0.04
Partial Graphite Reflection			
	0.0	13.3 ± 0.4	0.68 ± 0.02
	0.5	14.6 ± 0.4	0.73 ± 0.02
	1.0	16.2 ± 0.4	0.79 ± 0.02
	1.5	17.6 ± 0.5	0.85 ± 0.02
	2.0	19.3 ± 0.5	0.91 ± 0.03
	3.0	22.4 ± 0.7	1.04 ± 0.03
	5.0	29.9 ± 1.0	1.30 ± 0.04

The addition of a filter placed just before the collimator material can increase the percent dose enhancement significantly. Calculations show that the dose enhancement can approach 30% for a 5.64-cm diameter beam with tungsten collimation and a 5-cm tungsten filter. The MCNPX model used to determine this places the mathematical head phantom in a graphite moderator as in Figure 46. The moderator is a practical design that could be constructed and is designed to fit the adult male head phantom. The MCNPX model results for the tungsten collimator with various thicknesses of tungsten filter are listed in Table 13. Also listed in the Table 13 are the results with no moderation and with partial moderation. A diagram for a partial moderator design is shown in Figure 47.

The calculated dose enhancements for the partial moderator system are very close to the

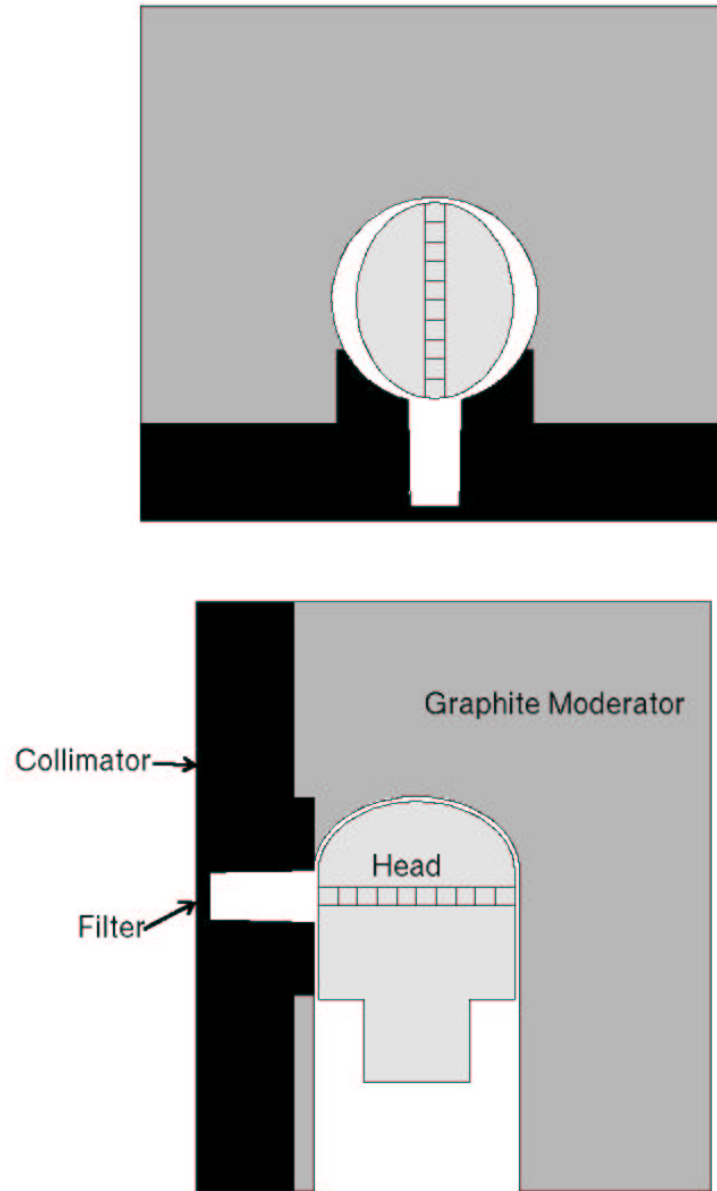


Figure 46: Diagram of the MCNPX model of a tungsten filter, tungsten collimator, full graphite moderator, and mathematical head phantom.

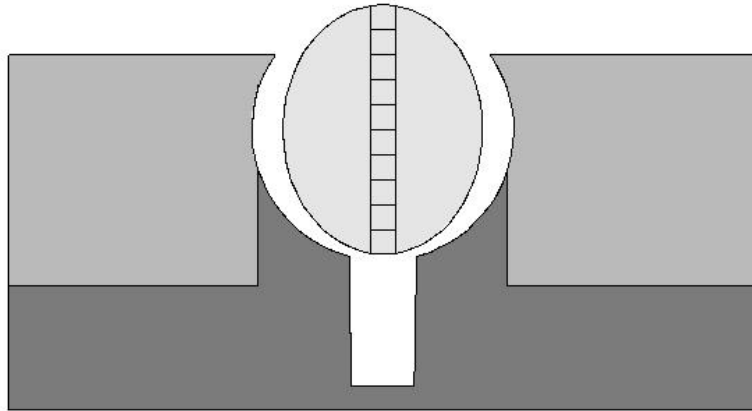


Figure 47: Diagram of the MCNPX model of the partial graphite moderator, tungsten collimator, and mathematical head phantom.

enhancement for a full moderator system. This design is a much more practical design for treatment than a full moderator system. It allows easy alignment of the patient, minimizes potential problems due to claustrophobia, and reduces the amount of material subject to activation. The major advantage of the use of a high Z collimator near the head is the time required for treatment. For a 1.5-cm tungsten filter, tungsten collimator, and partial graphite moderator, the time required administer a fraction of 1.5 Gy would take 3.0 minutes. This is considerable savings over the 79.9 minutes required by the 20-cm diameter BNCEFNT beam, that was constructed for this work.

The isodose plot of the 1.5-cm tungsten filter, tungsten collimator, and partial graphite moderator, is given in Figure 48. This plot, produced using the mesh tally feature of MCNPX shows that this design produces good collimation. The collimator projects a 5.64-cm diameter field at the isocenter, which is located at the center of the phantom.

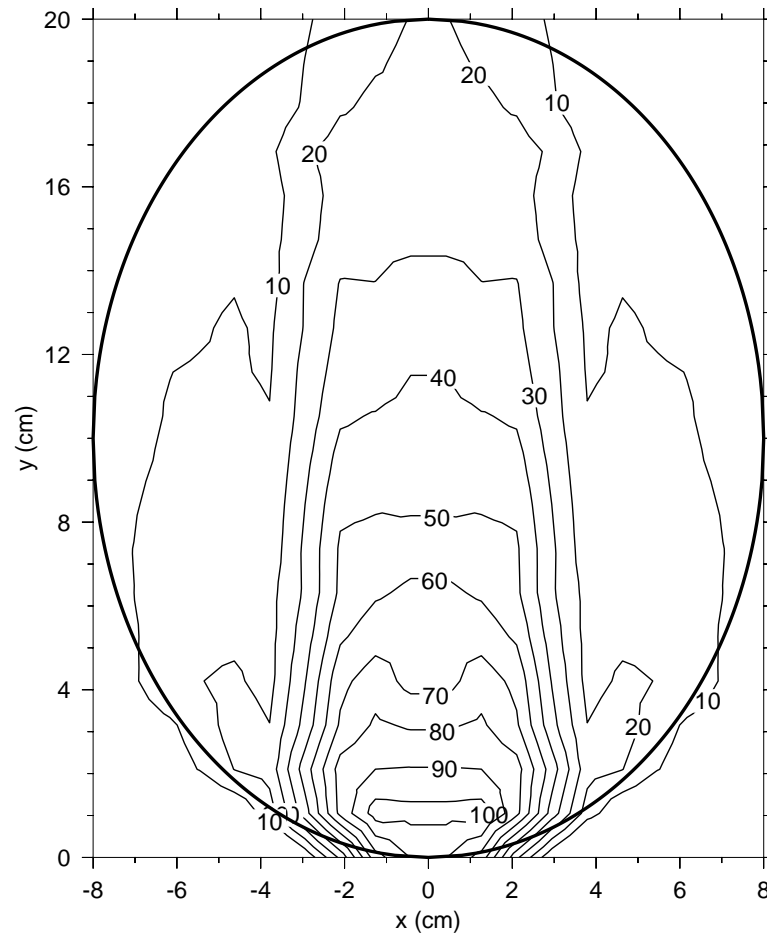


Figure 48: Calculated isodose curve of the (n,γ) dose for the partial graphite moderator, 5.64-cm diameter tungsten collimator, 1.5-cm tungsten filter, and mathematical head phantom. The thick elliptical line is the outline of the head phantom.

CHAPTER VII

CONCLUSIONS AND RECOMMENDATIONS

7.1 Conclusions

A prototypical boron neutron capture enhanced fast neutron therapy (BNCEFNT) collimator and filter assembly has been designed, constructed, and tested. This assembly consists of a 18.3-cm thick low carbon steel filter and a steel collimator. The resulting neutron beam produces a measured percent dose enhancement (PDE) of $(16.3 \pm 2.6)\%$ per 100-ppm ^{10}B for a 20-cm diameter beam and $(10.0 \pm 1.6)\%$ per 100-ppm ^{10}B for a 10-cm diameter beam. The dose rate for this new beam is reduced to 4.4% of the dose rate of the standard fast neutron treatment beam. This design has the same relative depth-dose profile as the standard treatment beam.

Calculation of the depth-dose and percent dose enhancement show that MCNPX is a viable tool for the development of fast neutron beams for BNCEFNT. However, MCNPX tends to over predict the peak dose enhancement by 15 to 17%. The use of borated tissue equivalent ionization chambers was demonstrated to provide an excellent technique for the measurement of the boron dose enhancement.

A conceptual design utilizing a tungsten collimator and a tungsten filter placed near the patient may solve the low dose rate problem. A conceptual design was presented that uses a tungsten collimator placed near the head with a 1.5-cm tungsten filter before the collimator. This design, when coupled with the partial moderation of neutrons with graphite placed

about the head results in a calculated dose enhancement of $(17.6 \pm 0.5)\%$. The resulting total dose rate of the design is higher than the dose rate of the standard treatment beam, allowing the delivery of 1.5 Gy in under 3 minutes.

7.2 Recommendations

The reported error in the PDE correction factor (16%) can be reduced by reducing the uncertainty in the ionization chamber thermal neutron calibration thermal neutron fluence rate (13%). For example the uncertainty in the thermal neutron fluence rate could be reduced to as low as 2% by using the thermal column of the NIST reactor thereby decreasing the error associated with the PDE correction factor to about 10%. The most limiting factor in the further reduction of the measurement error of the dose enhancement is the systematic error due to the AAPM reported uncertainty in \bar{W}_n/e .

Comparisons of the measurements and calculations for the BNCEFNT beam show that MCNPX tends to overestimate the dose enhancement by 15% to 17%. For future calculations that use MCNPX to calculate the neutron source it is recommended that an engineering factor of 0.84 be applied to the MCNPX calculated percent dose enhancement.

A tungsten collimator and filter placed near the head should be constructed to confirm the dose enhancement can exceed 15% for beams $5 \times 5 \text{ cm}^2$ and smaller. The measurements of the dose enhancement should be performed in a head phantom moderated on three sides by graphite. Measurements should also be performed to confirm the collimation and depth-dose distribution of this beam.

Experiments measuring the effect of different phantom materials on the dose enhancement should be performed. It is unknown how the density and composition will affect the dose enhancement. Specifically, measurements using a tissue-equivalent material with a density of brain tissue (1.04 g/cm^3) should be performed.

Experiments to measure the skin dose from the proposed tungsten collimator and the constructed iron filter and collimator should be performed. This is especially important if

heavy Z material filtration and collimation are located near the head as in the proposed conceptual design.

The availability of a ${}^9\text{Be}(p,n)$ cross section for use in MCNPX would allow the calculation of more exact neutron spectra and neutron yield. Young and Arthur [59] have compiled an ENDF-VI (p,n) cross section for ${}^9\text{Be}$, but attempts by the author to convert this cross section into ACE format failed. The conversion of this cross section to ACE format would be advantageous to the fast neutron therapy community.

APPENDIX A

LIST OF ABBREVIATIONS

AAPM American Association of Physicists in Medicine

Be Beryllium

BNCT Boron Neutron Capture Therapy

BNCEFNT Boron Neutron Capture Fast Neutron Therapy

CPU Central Processing Unit

E/C Experiment-to-Calculated Ratio

ENDF Evaluated Nuclear Data File

FNT Fast Neutron Therapy

GBM Glioblastoma Multiforme

HPGe High-Purity Germanium

ICRP International Commission on Radiological Protection

ICRU International Commission on Radiation Units and Measurements

INC Intranuclear Cascade

kW kilo-watt

LET Linear Energy Transfer

Linac Linear Accelerator

MIT Massachusetts Institute of Technology

MU Monitor Units

NIST National Institute of Standards and Technology

OER Oxygen Enhancement Ratio

ORNL Oak Ridge National Laboratory

OSU Oregon State University

PDE Percent Dose Enhancement

ppm Parts per million

RBE Relative Biological Effectiveness

TE Tissue Equivalent

UW University of Washington

APPENDIX B

TABULATED DEPTH-DOSE RESULTS

B.1 Measurement Results

Table 14: The depth-dose measurements of the 20×20 cm² standard therapy beam using the borated and non-borated chambers. The borated chamber response and the percent dose enhancement have been normalized to 100-ppm ¹⁰B.

Depth (cm)	Borated Chamber		Non-Borated Chamber		PDE (%)	PDE Error (%)
	Absorbed Dose (Gy/proton)	Exp. Error (%)	Absorbed Dose (Gy/proton)	Exp. Error (%)		
1.0	5.36E-17	1.6	5.11E-17	1.4	4.9	16
2.0	5.67E-17	0.9	5.35E-17	0.0	6.1	16
3.0	5.71E-17	1.2	5.32E-17	0.5	7.2	16
4.0	5.64E-17	1.2	5.21E-17	0.2	8.2	16
5.0	5.53E-17	1.3	5.08E-17	0.1	8.9	16
5.5	5.47E-17	1.3	5.02E-17	0.2	9.0	16
6.0	5.41E-17	1.4	4.95E-17	0.1	9.1	16
7.0	5.26E-17	1.4	4.81E-17	0.1	9.2	16
8.5	5.00E-17	1.4	4.59E-17	0.0	9.0	16
10.0	4.74E-17	1.3	4.36E-17	0.2	8.7	16
15.0	3.89E-17	1.1	3.63E-17	0.2	7.2	16
25.0	2.56E-17	0.9	2.43E-17	0.3	5.1	16

Table 15: The depth-dose measurements of the $10 \times 10 \text{ cm}^2$ standard therapy beam using the borated and non-borated chambers. The borated chamber response and the percent dose enhancement have been normalized to 100-ppm ^{10}B .

Depth (cm)	Borated Chamber		Non-Borated Chamber		PDE (%)	PDE Error (%)
	Absorbed Dose (Gy/proton)	Exp. Error (%)	Absorbed Dose (Gy/proton)	Exp. Error (%)		
1.0	4.59E-17	2.1	4.46E-17	2.0	2.9	16
2.0	4.84E-17	2.1	4.68E-17	2.0	3.3	16
3.0	4.82E-17	2.1	4.64E-17	2.0	3.9	16
4.0	4.71E-17	2.1	4.51E-17	2.0	4.3	16
4.5	4.65E-17	2.1	4.45E-17	2.0	4.5	16
5.0	4.57E-17	2.1	4.37E-17	2.0	4.6	16
5.5	4.50E-17	2.1	4.30E-17	2.0	4.7	16
6.0	4.42E-17	2.1	4.22E-17	2.0	4.8	16
7.0	4.26E-17	2.1	4.06E-17	2.0	4.7	16
8.5	4.00E-17	2.1	3.82E-17	2.0	4.6	16
10.0	3.75E-17	2.1	3.59E-17	2.0	4.3	16
15.0	2.95E-17	2.1	2.85E-17	2.0	3.5	16
25.0	1.78E-17	2.1	1.74E-17	2.0	2.6	16

Table 16: The depth-dose measurements of the 55.3-cm diameter standard therapy beam using the borated and non-borated chambers. The borated chamber response and the percent dose enhancement have been normalized to 100-ppm ^{10}B .

Depth (cm)	Borated Chamber		Non-Borated Chamber		PDE (%)	PDE Error (%)
	Absorbed Dose (Gy/proton)	Exp. Error (%)	Absorbed Dose (Gy/proton)	Exp. Error (%)		
1.0	6.29E-17	2.2	5.87E-17	2.0	7.2	16
2.0	6.67E-17	2.4	6.07E-17	2.0	9.9	16
3.0	6.78E-17	2.6	6.05E-17	2.0	12.0	16
4.0	6.76E-17	2.7	5.96E-17	2.0	13.4	16
4.5	6.73E-17	2.7	5.90E-17	2.0	14.1	16
5.0	6.69E-17	2.8	5.85E-17	2.0	14.4	16
5.5	6.63E-17	2.8	5.78E-17	2.0	14.8	16
6.0	6.55E-17	2.8	5.71E-17	2.0	14.8	16
7.0	6.40E-17	2.8	5.57E-17	2.0	14.8	16
8.5	6.12E-17	2.8	5.35E-17	2.0	14.4	16
10.0	5.82E-17	2.7	5.12E-17	2.0	13.8	16
15.0	4.87E-17	2.5	4.38E-17	2.0	11.2	16
25.0	3.41E-17	2.3	3.14E-17	2.0	8.4	16

Table 17: Measurements used to optimize iron filter thickness for the 20-cm diameter BNCEFNT beam. All data given here is for 5-cm deep in the water phantom. The measurements have been normalized to 100-ppm ^{10}B .

Filter		PDE (%)	Error (%)	Total		(n+ γ)	
Thickness (cm)	Dose Ratio			Dose Ratio	Error (%)	Dose Ratio	Error (%)
0.0	8.5	16	0.95	2.4	1.03	2.0	
15.24	13.3	16	13.0	2.7	14.8	2.0	
17.04	15.3	16	16.8	2.9	19.3	2.0	
18.30	16.3	16	19.7	3.0	22.9	2.0	
19.03	17.2	16	21.6	3.1	25.4	2.0	

Table 18: The depth-dose measurements of the BNCEFNT beam filtered with 18.3-cm of iron and collimated with iron to a diameter of 20 cm at the isocenter using the borated and non-borated chambers. The results have been normalized to 100-ppm ^{10}B .

Depth (cm)	Borated Chamber		Non-Borated Chamber		PDE (%)	PDE Error (%)
	Absorbed Dose (Gy/proton)	Exp. Error (%)	Absorbed Dose (Gy/proton)	Exp. Error (%)		
1.0	2.50E-18	2.5	2.26E-18	2.0	10.6	16
1.6	2.61E-18	2.6	2.32E-18	2.0	12.4	16
2.0	2.65E-18	2.7	2.34E-18	2.0	13.4	16
3.0	2.67E-18	2.8	2.31E-18	2.0	15.3	16
4.0	2.65E-18	2.9	2.28E-18	2.0	16.1	16
5.0	2.58E-18	2.9	2.22E-18	2.0	16.3	16
5.5	2.55E-18	2.9	2.20E-18	2.0	16.0	16
6.0	2.50E-18	2.9	2.16E-18	2.0	15.7	16
7.0	2.40E-18	2.8	2.09E-18	2.0	14.7	16
8.5	2.28E-18	2.6	2.02E-18	2.0	12.9	16
10.0	2.14E-18	2.5	1.93E-18	2.0	11.1	16
15.0	1.73E-18	2.2	1.62E-18	2.0	6.8	16
25.0	1.18E-18	2.1	1.13E-18	2.0	4.3	16

Table 19: The depth-dose measurements of the BNCEFNT beam filtered with 18.3-cm of iron and collimated with iron to a diameter of 10 cm at the isocenter using the borated and non-borated chambers. The results have been normalized to 100-ppm ^{10}B .

Depth (cm)	Borated Chamber		Non-Borated Chamber		PDE (%)	PDE Error (%)
	Absorbed Dose (Gy/proton)	Exp. Error (%)	Absorbed Dose (Gy/proton)	Exp. Error (%)		
1.0	1.67E-18	2.2	1.57E-18	2.0	6.6	16
2.0	1.75E-18	2.3	1.61E-18	2.0	8.3	16
3.0	1.75E-18	2.4	1.60E-18	2.0	9.4	16
4.0	1.71E-18	2.4	1.55E-18	2.0	10.0	16
5.0	1.65E-18	2.4	1.50E-18	2.0	10.0	16
5.5	1.62E-18	2.4	1.48E-18	2.0	9.7	16
6.0	1.59E-18	2.4	1.45E-18	2.0	9.6	16
7.0	1.53E-18	2.3	1.41E-18	2.0	8.9	16
8.5	1.42E-18	2.3	1.32E-18	2.0	7.6	16
10.0	1.32E-18	2.2	1.24E-18	2.0	6.7	16
15.0	1.04E-18	2.1	1.00E-18	2.0	3.9	16
25.0	6.50E-19	2.1	6.34E-19	2.0	2.6	16

B.2 Calculated Results

Table 20: MCNPX depth-dose calculation of the $20 \times 20 \text{ cm}^2$ standard treatment beam. The borated chamber response and the percent dose enhancement were normalized to 100-ppm ^{10}B .

Depth (cm)	Borated Chamber		Non-Borated Chamber		PDE (%)	PDE Error (%)
	Absorbed Dose (Gy/proton)	Exp. Error (%)	Absorbed Dose (Gy/proton)	Exp. Error (%)		
1.0	2.06e-17	2.2	1.99e-17	2.3	3.5	3.8
2.0	2.10e-17	2.3	1.98e-17	2.4	5.6	3.5
3.0	2.11e-17	2.3	1.97e-17	2.5	7.4	3.3
4.0	2.11e-17	2.3	1.94e-17	2.5	8.8	3.3
4.5	2.11e-17	2.3	1.93e-17	2.6	9.5	3.3
5.0	2.11e-17	2.4	1.91e-17	2.6	10.0	3.3
5.5	2.10e-17	2.5	1.90e-17	2.8	10.1	3.4
6.0	2.03e-17	2.4	1.84e-17	2.7	10.4	3.3
7.0	1.98e-17	2.5	1.79e-17	2.7	10.7	3.3
8.5	1.89e-17	2.5	1.71e-17	2.8	10.6	3.4
10.0	1.78e-17	2.6	1.61e-17	2.9	10.5	3.5
15.0	1.52e-17	3.2	1.40e-17	3.5	8.5	4.2
25.0	8.83e-18	4.3	8.25e-18	4.5	7.0	5.7

Table 21: MCNPX depth-dose calculation of the $10 \times 10 \text{ cm}^2$ standard treatment beam. The borated chamber response and the percent dose enhancement were normalized to 100-ppm ^{10}B .

Depth (cm)	Borated Chamber		Non-Borated Chamber		PDE (%)	PDE Error (%)
	Absorbed Dose (Gy/proton)	Exp. Error (%)	Absorbed Dose (Gy/proton)	Exp. Error (%)		
1.0	1.64e-17	2.6	1.62e-17	2.6	1.6	5.8
2.0	1.66e-17	2.6	1.61e-17	2.7	2.6	5.0
3.0	1.62e-17	2.6	1.57e-17	2.7	3.5	4.6
4.0	1.59e-17	2.7	1.53e-17	2.8	4.0	4.6
4.5	1.58e-17	2.7	1.51e-17	2.9	4.5	4.5
5.0	1.56e-17	2.8	1.50e-17	2.9	4.3	4.5
5.5	1.55e-17	3.0	1.49e-17	3.1	4.6	4.6
6.0	1.50e-17	2.9	1.43e-17	3.0	4.8	4.6
7.0	1.46e-17	3.1	1.40e-17	3.3	4.9	4.7
8.5	1.37e-17	3.3	1.31e-17	3.4	4.7	4.9
10.0	1.27e-17	3.5	1.22e-17	3.7	4.5	5.2
15.0	9.86e-18	4.2	9.50e-18	4.4	3.7	6.2
25.0	5.31e-18	6.5	5.14e-18	6.8	3.3	9.3

Table 22: MCNPX depth-dose calculation of the 55.3-cm diameter standard treatment beam. The borated chamber response and the percent dose enhancement were normalized to 100-ppm ^{10}B .

Depth (cm)	Borated Chamber		Non-Borated Chamber		PDE (%)	PDE Error (%)
	Absorbed Dose (Gy/proton)	Exp. Error (%)	Absorbed Dose (Gy/proton)	Exp. Error (%)		
1.0	2.32e-17	2.2	2.20e-17	2.3	5.4	3.2
2.0	2.41e-17	2.0	2.23e-17	2.2	8.4	2.9
3.0	2.45e-17	2.0	2.21e-17	2.2	11.2	2.8
4.0	2.48e-17	2.0	2.20e-17	2.3	12.7	2.7
4.5	2.48e-17	2.0	2.18e-17	2.3	13.6	2.7
5.0	2.48e-17	2.0	2.17e-17	2.3	14.4	2.7
5.5	2.47e-17	2.0	2.16e-17	2.3	14.6	2.7
6.0	2.39e-17	1.9	2.07e-17	2.2	15.1	2.6
7.0	2.36e-17	1.9	2.03e-17	2.2	16.0	2.6
8.5	2.24e-17	2.0	1.94e-17	2.2	15.8	2.7
10.0	2.17e-17	2.1	1.88e-17	2.4	15.5	2.8
15.0	1.86e-17	2.4	1.64e-17	2.7	13.1	3.2
25.0	1.20e-17	2.9	1.09e-17	3.2	10.8	3.9

Table 23: MCNPX depth-dose calculation of the 20-cm BNCEFNT beam. The borated chamber response and the percent dose enhancement were normalized to 100-ppm ^{10}B .

Depth (cm)	Borated Chamber		Non-Borated Chamber		PDE (%)	PDE Error (%)
	Absorbed Dose (Gy/proton)	Exp. Error (%)	Absorbed Dose (Gy/proton)	Exp. Error (%)		
1.0	9.12e-19	4.3	8.48e-19	4.6	7.6	5.2
2.0	8.79e-19	4.1	7.83e-19	4.6	12.4	5.0
3.0	9.13e-19	3.8	7.90e-19	4.4	15.6	4.8
4.0	9.27e-19	3.7	7.93e-19	4.3	17.0	4.7
4.5	8.87e-19	3.7	7.49e-19	4.4	18.4	4.7
5.0	8.77e-19	3.5	7.35e-19	4.1	19.2	4.5
5.5	8.74e-19	3.6	7.42e-19	4.3	17.8	4.6
6.0	8.95e-19	3.9	7.59e-19	4.5	17.8	4.9
7.0	8.21e-19	3.4	6.93e-19	4.0	18.5	4.4
8.5	7.53e-19	3.7	6.43e-19	4.4	17.0	4.7
10.0	6.97e-19	3.3	6.05e-19	3.8	15.3	4.3
15.0	5.58e-19	3.5	5.11e-19	3.8	9.2	4.6
25.0	3.81e-19	5.5	3.61e-19	5.8	5.5	7.0

Table 24: MCNPX depth-dose calculation of the 10-cm BNCEFNT beam. The borated chamber response and the percent dose enhancement were normalized to 100-ppm ^{10}B .

Depth (cm)	Borated Chamber		Non-Borated Chamber		PDE (%)	PDE Error (%)
	Absorbed Dose (Gy/proton)	Exp. Error (%)	Absorbed Dose (Gy/proton)	Exp. Error (%)		
1.0	6.29e-19	5.6	5.96e-19	5.9	5.6	6.8
2.0	6.00e-19	5.3	5.54e-19	5.8	8.3	6.5
3.0	6.13e-19	5.1	5.54e-19	5.6	10.6	6.3
4.0	5.98e-19	4.9	5.36e-19	5.5	11.7	6.2
4.5	5.78e-19	5.2	5.18e-19	5.8	11.6	6.4
5.0	5.73e-19	4.8	5.11e-19	5.4	12.1	6.0
5.5	5.66e-19	5.2	5.06e-19	5.8	11.8	6.4
6.0	5.55e-19	5.0	4.94e-19	5.6	12.3	6.2
7.0	5.18e-19	4.7	4.64e-19	5.2	11.7	5.9
8.5	4.91e-19	5.4	4.45e-19	5.9	10.4	6.6
10.0	4.86e-19	5.2	4.50e-19	5.6	8.1	6.4
15.0	3.35e-19	5.1	3.19e-19	5.3	5.0	6.9
25.0	2.14e-19	7.5	2.07e-19	7.8	3.6	10.4

APPENDIX C

RAW MEASUREMENT DATA

C.1 $20 \times 20 \text{ cm}^2$ Standard Treatment Beam

Table 25: Borated detector measurement data of the $20 \times 20 \text{ cm}^2$ standard therapy beam. Measurements made Jan. 2001.

Cint/X1=		2.784e+14 protons/X1				Voltage = +400V				
Depth (cm)	Off Axis (cm)	Charge (nC)	Monitor Units (MU)	X1	X1 TPCX	Pressure (mB)	Temp (C)	Beam Time (min)	Dose (Gy/proton)	Notes
1.0	0	0.009	0.000	0.00	0.000	999.5	19.8	5.00	9.790E-03	Background
1.0	0	9.781	0.351	39.25	1.021	998.8	18.4	1.19	6.445E-17	
1.0	0	13.962	0.500	55.97	1.021	998.8	18.4	1.71	6.451E-17	
1.0	0	13.952	0.501	55.93	1.021	998.8	18.4	1.71	6.451E-17	
1.0	0	13.942	0.501	55.91	1.021	998.8	18.4	1.71	6.449E-17	
2.0	0	15.235	0.501	55.94	1.020	998.8	18.4	1.70	7.051E-17	
3.0	0	15.733	0.500	55.93	1.020	998.8	18.4	1.69	7.282E-17	
4.0	0	15.929	0.501	55.94	1.020	998.8	18.4	1.71	7.372E-17	
4.4	0	15.975	0.502	56.08	1.020	998.8	18.4	1.16	7.375E-17	
5.0	0	15.929	0.502	56.11	1.021	998.8	18.4	1.16	7.343E-17	
5.0	0	15.924	0.502	56.08	1.020	998.8	18.2	1.16	7.346E-17	
5.0	0	15.889	0.501	55.95	1.021	998.8	18.2	1.16	7.340E-17	
5.5	0	18.888	0.600	67.02	1.021	998.8	18.2	1.38	7.284E-17	
6.0	0	18.734	0.600	67.03	1.021	998.8	18.2	1.39	7.224E-17	
7.0	0	18.216	0.601	67.07	1.021	998.8	18.2	1.39	7.020E-17	
7.0	0	0.000	1.202	134.24	1.021	998.8	18.2	2.79	-9.717E-21	
8.5	0	17.267	0.601	67.07	1.022	998.8	18.2	1.40	6.648E-17	
10.0	0	18.901	0.701	78.29	1.022	998.8	18.2	1.63	6.234E-17	
15.0	0	15.957	0.753	84.00	1.022	998.8	18.2	1.75	4.905E-17	
25.0	0	13.168	1.003	111.87	1.022	998.8	18.2	2.32	3.039E-17	
25.0	0	13.188	1.004	112.01	1.022	998.8	18.2	2.32	3.040E-17	
25.0	0	13.156	1.001	111.63	1.023	998.8	18.2	2.31	3.040E-17	
1.0	0	13.370	0.500	55.28	1.032	986.7	17.9	1.16	6.254E-17	
1.0	0	13.407	0.501	55.38	1.032	986.7	17.9	1.16	6.260E-17	
1.0	0	13.443	0.502	55.49	1.032	986.0	17.9	1.16	6.269E-17	
1.0	0	18.762	0.701	77.47	1.032	986.0	17.9	1.62	6.267E-17	
1.0	0	18.767	0.701	77.49	1.032	986.0	17.9	1.62	6.267E-17	
2.0	0	17.824	0.601	66.37	1.033	986.0	17.9	1.39	6.943E-17	
3.0	0	18.657	0.601	66.29	1.033	986.0	17.9	1.39	7.276E-17	
4.0	0	19.019	0.601	66.33	1.033	985.4	17.9	1.39	7.417E-17	
4.5	0	19.110	0.603	66.51	1.034	985.4	17.9	1.40	7.425E-17	
4.5	0	19.008	0.600	66.16	1.034	985.4	17.9	1.39	7.425E-17	
4.5	0	19.058	0.601	66.30	1.034	985.4	17.9	1.39	7.428E-17	
5.0	0	18.986	0.600	66.14	1.034	985.4	17.9	1.39	7.418E-17	
5.5	0	18.937	0.602	66.37	1.034	985.4	17.9	1.39	7.373E-17	
6.0	0	18.764	0.601	66.28	1.034	985.4	17.9	1.39	7.316E-17	
7.0	0	19.801	0.651	71.74	1.035	984.8	17.9	1.51	7.130E-17	
7.0	0	19.790	0.650	71.63	1.036	984.8	17.9	1.51	7.130E-17	
1.0	0	18.702	0.702	77.26	1.036	984.7	17.9	1.63	6.248E-17	
8.5	0	18.764	0.650	71.51	1.037	984.4	17.9	1.51	6.768E-17	
10.0	0	18.986	0.701	77.07	1.037	984.4	17.9	1.60	6.354E-17	
15.0	0	14.953	0.701	77.08	1.037	984.4	17.9	1.62	5.003E-17	
25.0	0	10.573	0.803	88.22	1.037	984.4	17.9	1.85	3.091E-17	
25.0	0	13.199	1.002	110.09	1.038	984.4	17.9	2.32	3.089E-17	

Table 26: Borated detector measurement data of the $20 \times 20 \text{ cm}^2$ standard therapy beam. Measurements made Dec. 2001.

Cint/X1=		2.767e+14 protons/X1				Voltage = +400V				
Depth (cm)	Off Axis (cm)	Charge (nC)	Monitor Units (MU)	X1	TPCX	Pressure (mB)	Temp (C)	Beam Time (min)	Dose (Gy/proton)	Notes
1.0	0	0.001	0.000	0.00	0.000	985.4	22.7	5.00	1.114E-03	Background
1.0	0	9.428	0.351	38.85	1.037	985.4	22.7	1.00	6.397E-17	
1.0	0	9.476	0.352	39.01	1.037	985.4	22.6	1.01	6.401E-17	
1.0	0	9.425	0.351	38.80	1.037	985.4	22.6	0.99	6.401E-17	
1.0	0	9.438	0.351	38.85	1.037	985.4	22.6	1.00	6.401E-17	
1.6	0	10.016	0.350	38.77	1.037	985.4	22.6	0.98	6.807E-17	
2.0	0	10.283	0.351	38.80	1.037	985.4	22.5	0.99	6.981E-17	
2.0	0	10.310	0.352	38.90	1.037	985.4	22.5	1.00	6.981E-17	
2.0	0	10.292	0.351	38.81	1.037	985.4	22.5	1.02	6.985E-17	
3.0	0	10.719	0.353	39.00	1.037	985.4	22.4	1.03	7.237E-17	
4.0	0	10.857	0.352	38.96	1.038	985.4	22.4	1.02	7.331E-17	
5.0	0	10.807	0.351	38.85	1.037	985.6	22.4	1.02	7.323E-17	
5.0	0	10.794	0.351	38.85	1.038	985.8	22.4	1.02	7.306E-17	
5.0	0	10.817	0.352	38.94	1.037	985.6	22.4	1.02	7.313E-17	
5.5	0	10.704	0.351	38.82	1.037	986.0	22.4	1.00	7.256E-17	
6.0	0	10.634	0.352	38.90	1.037	986.0	22.4	1.02	7.194E-17	
7.0	0	10.346	0.352	38.91	1.037	986.0	22.3	1.01	6.995E-17	
8.5	0	9.796	0.351	38.77	1.038	986.0	22.3	1.02	6.641E-17	
10.0	0	9.198	0.351	38.80	1.038	985.8	22.3	1.02	6.232E-17	
15.0	0	7.277	0.351	38.80	1.038	985.7	22.2	1.01	4.929E-17	
25.0	0	4.552	0.351	39.01	1.038	985.8	22.2	1.02	3.066E-17	

Table 27: Non-borated detector measurement data of the $20 \times 20 \text{ cm}^2$ standard therapy beam. Measurements made Jan. 2001.

Cint/X1=		2.784e+14 protons/X1				Voltage = +400V				
Depth (cm)	Off Axis (cm)	Charge (nC)	Monitor Units (MU)	X1	TPCX	Pressure (mB)	Temp (C)	Beam Time (min)	Dose (Gy/proton)	Notes
1.0	0	0.009	0.000	0.00	0.000	999.5	19.8	5.00	9.790E-03	Background
25.0	0	11.062	1.002	111.66	1.023	998.8	18.2	2.29	2.430E-17	
25.0	0	11.046	1.002	111.61	1.023	998.8	18.2	2.31	2.427E-17	
25.0	0	11.030	1.000	111.44	1.024	998.2	18.2	2.31	2.427E-17	
15.0	0	16.468	1.000	111.41	1.024	998.2	18.2	2.32	3.624E-17	
10.0	0	14.867	0.752	83.71	1.024	998.2	18.2	1.75	4.355E-17	
8.5	0	15.663	0.752	83.73	1.024	998.2	18.2	1.74	4.587E-17	
7.0	0	16.419	0.751	83.66	1.024	998.2	18.2	1.74	4.812E-17	
6.0	0	16.887	0.751	83.64	1.024	998.2	18.2	1.74	4.951E-17	
5.5	0	17.131	0.752	83.70	1.025	998.2	18.2	1.74	5.014E-17	
5.0	0	17.306	0.751	83.52	1.025	998.2	18.2	1.74	5.076E-17	
5.0	0	17.354	0.752	83.69	1.025	998.2	18.2	1.74	5.080E-17	
5.0	0	17.320	0.751	83.57	1.025	998.2	18.2	2.00	5.077E-17	
4.5	0	16.374	0.701	78.01	1.025	998.2	18.2	1.91	5.142E-17	
4.0	0	16.555	0.701	77.92	1.026	998.2	18.2	1.91	5.199E-17	
3.0	0	16.908	0.702	78.05	1.026	998.2	18.2	1.91	5.301E-17	
2.0	0	17.020	0.701	77.90	1.026	998.2	18.2	1.91	5.347E-17	
1.0	0	16.386	0.700	77.83	1.026	998.2	18.2	1.90	5.152E-17	
1.0	0	16.405	0.702	77.95	1.026	998.2	18.2	1.90	5.150E-17	
1.0	0	16.402	0.702	77.94	1.027	998.2	18.2	1.90	5.145E-17	
1.0	0	15.852	0.702	77.70	1.030	986.7	17.9	1.63	5.026E-17	
1.0	0	15.839	0.701	77.64	1.030	986.7	17.9	1.63	5.026E-17	
1.0	0	15.835	0.702	77.63	1.031	986.7	17.9	1.63	5.020E-17	
3.0	0	16.792	0.701	76.98	1.038	983.6	17.9	1.62	5.350E-17	

Table 28: Non-borated detector measurement data of the $20 \times 20 \text{ cm}^2$ standard therapy beam. Measurements made Dec. 2001.

Cint/X1=		2.767e+14 protons/X1				Voltage = +400V				
Depth (cm)	Off Axis (cm)	Charge (nC)	Monitor Units (MU)	X1	X1 TPCX	Pressure (mB)	Temp (C)	Beam Time (min)	Dose (Gy/proton)	Notes
1.0	-5	0.004	0.000	0.00	0.000	985.4	22.7	5.00	4.457E-03	Background
25.0	0	3.800	0.352	38.93	1.038	985.7	22.1	1.01	2.438E-17	
15.0	0	5.655	0.351	38.85	1.038	985.8	22.1	1.02	3.636E-17	
10.0	0	6.789	0.351	38.84	1.038	985.8	22.1	1.02	4.366E-17	
8.5	0	7.140	0.352	38.88	1.038	986.0	22.1	1.02	4.586E-17	
7.0	0	7.491	0.351	38.84	1.038	986.0	22.1	1.02	4.817E-17	
6.0	0	7.722	0.352	38.90	1.038	986.0	22.1	1.02	4.958E-17	
5.5	0	7.792	0.350	38.76	1.037	986.0	22.1	1.02	5.025E-17	
5.0	0	7.929	0.352	38.92	1.038	986.0	22.1	1.04	5.088E-17	
5.0	0	7.924	0.352	38.88	1.038	986.0	22.1	1.02	5.090E-17	
5.0	0	7.940	0.353	38.98	1.038	986.0	22.0	1.03	5.085E-17	
4.0	0	8.147	0.353	39.00	1.038	986.0	22.0	1.02	5.215E-17	
3.0	0	8.274	0.352	38.87	1.038	986.0	22.0	1.02	5.314E-17	
2.0	0	8.348	0.352	38.96	1.038	986.0	22.0	1.03	5.349E-17	
1.6	0	8.251	0.351	38.78	1.038	986.0	22.0	1.02	5.312E-17	
1.0	0	8.031	0.352	38.88	1.038	986.0	22.0	1.02	5.157E-17	
1.0	0	7.973	0.349	38.63	1.038	986.0	22.0	1.01	5.153E-17	

C.2 $10 \times 10 \text{ cm}^2$ Standard Treatment Beam

Table 29: Borated detector measurement data of the $10 \times 10 \text{ cm}^2$ standard therapy beam. Measurements made Jan. 2001.

Cint/X1=		2.784e+14 protons/X1				Voltage = +400V				
Depth (cm)	Off Axis (cm)	Charge (nC)	Monitor Units (MU)	X1	X1 TPCX	Pressure (mB)	Temp (C)	Beam Time (min)	Dose (Gy/proton)	Notes
1.0	0	0.009	0.000	0.00	0.000	999.5	19.8	5.00	9.790E-03	Background
25.0	0	6.689	0.802	87.56	1.044	981.2	17.9	1.86	1.963E-17	
25.0	0	8.337	1.001	109.27	1.044	981.1	17.9	2.31	1.961E-17	
25.0	0	8.362	1.003	109.50	1.045	981.1	17.9	2.32	1.961E-17	
15.0	0	14.274	1.002	109.35	1.045	981.1	17.9	2.32	3.352E-17	
10.0	0	16.753	0.903	98.51	1.045	981.1	17.9	2.09	4.367E-17	
8.5	0	18.060	0.903	98.51	1.046	980.9	17.9	2.09	4.704E-17	
7.0	0	17.121	0.801	87.31	1.046	980.7	17.9	1.85	5.033E-17	
6.0	0	17.830	0.802	87.44	1.046	980.5	17.9	1.85	5.235E-17	
5.5	0	18.097	0.801	87.33	1.046	980.5	17.9	1.85	5.320E-17	
5.0	0	18.359	0.802	87.41	1.047	980.1	17.9	1.85	5.389E-17	
5.0	0	18.347	0.802	87.31	1.047	980.1	17.9	1.84	5.392E-17	
5.0	0	18.330	0.801	87.25	1.047	980.0	17.9	1.84	5.391E-17	
4.5	0	18.560	0.802	87.28	1.047	980.0	17.9	1.84	5.457E-17	
4.0	0	18.731	0.801	87.22	1.048	980.0	17.9	1.85	5.506E-17	
3.0	0	18.916	0.803	87.39	1.048	979.9	17.9	1.85	5.550E-17	
2.0	0	18.603	0.801	87.18	1.048	979.9	17.9	1.85	5.471E-17	
1.0	0	17.379	0.801	87.14	1.048	979.8	17.9	1.85	5.114E-17	
1.0	0	17.390	0.802	87.22	1.048	979.8	17.9	1.85	5.112E-17	
1.0	0	17.369	0.802	87.16	1.049	979.6	17.9	1.84	5.106E-17	

Table 30: Non-borated detector measurement data of the $10 \times 10 \text{ cm}^2$ standard therapy beam. Measurements made Jan. 2001.

Cint/X1=		2.784e+14 protons/X1				Voltage = +400V				
Depth (cm)	Off Axis (cm)	Charge (nC)	Monitor Units (MU)	X1	TPCX	Pressure (mB)	Temp (C)	Beam Time (min)	Dose (Gy/proton)	Notes
1.0	0	0.009	0.000	0.00	0.000	999.5	19.8	5.00	9.790E-03	Background
1.0	0	16.017	0.802	88.08	1.039	982.9	17.9	1.84	4.458E-17	
1.0	0	15.990	0.801	87.94	1.039	982.9	17.9	1.85	4.458E-17	
1.0	0	16.007	0.802	88.01	1.040	982.7	17.9	1.85	4.456E-17	
2.0	0	16.817	0.802	87.97	1.040	982.3	17.9	1.86	4.685E-17	
3.0	0	16.620	0.801	87.81	1.040	982.3	17.9	1.85	4.639E-17	
4.0	0	16.198	0.802	87.94	1.040	982.4	17.9	1.86	4.514E-17	
4.5	0	15.950	0.802	87.92	1.040	982.4	17.9	1.86	4.446E-17	
5.0	0	15.672	0.801	87.75	1.041	982.4	17.9	1.86	4.372E-17	
5.0	0	15.673	0.801	87.73	1.041	982.4	17.9	1.86	4.374E-17	
5.0	0	15.657	0.801	87.66	1.042	982.4	17.9	1.86	4.369E-17	
5.5	0	15.367	0.800	87.55	1.042	981.2	17.9	1.85	4.298E-17	
6.0	0	15.099	0.800	87.53	1.043	981.3	17.9	1.85	4.220E-17	
7.0	0	14.564	0.802	87.67	1.043	981.2	17.9	1.86	4.064E-17	
8.5	0	15.390	0.901	98.45	1.043	981.2	17.9	2.09	3.824E-17	
10.0	0	14.480	0.902	98.60	1.043	981.2	17.9	2.09	3.593E-17	
15.0	0	12.753	1.001	109.35	1.043	981.2	17.9	2.31	2.853E-17	
25.0	0	7.777	1.002	109.50	1.044	981.2	17.9	2.31	1.735E-17	
25.0	0	7.768	1.001	109.29	1.044	981.2	17.9	2.31	1.737E-17	
25.0	0	7.770	1.001	109.32	1.044	981.2	17.9	2.31	1.737E-17	

C.3 55.3-cm Diameter Standard Treatment Beam

Table 31: Borated detector measurement data of the 55.3-cm diameter standard therapy beam. Measurements made Jan. 2001.

Cint/X1=		2.784e+14 protons/X1				Voltage = +400V				
Depth (cm)	Off Axis (cm)	Charge (nC)	Monitor Units (MU)	X1	X1 TPCX	Pressure (mB)	Temp (C)	Beam Time (min)	Dose (Gy/proton)	Notes
1.0	0	0.009	0.000	0.00	0.000	999.5	19.8	5.00	9.790E-03	Background
1.0	0	17.123	0.501	55.94	1.021	999.5	19.8	1.72	7.948E-17	
1.0	0	17.136	0.501	55.95	1.021	999.5	19.8	1.72	7.953E-17	
1.0	0	8.592	0.250	28.04	1.021	999.5	19.8	0.86	7.957E-17	
1.0	0	8.558	0.250	27.91	1.021	999.5	19.8	0.86	7.962E-17	
1.0	0	8.600	0.250	28.04	1.021	999.6	19.8	0.86	7.963E-17	
4.0	0	10.843	0.250	28.05	1.021	1000.0	19.7	0.86	1.003E-16	
5.5	0	10.843	0.250	27.99	1.021	1000.0	19.7	0.86	1.005E-16	
7.0	0	10.474	0.250	27.88	1.021	1000.1	19.7	0.86	9.746E-17	
8.5	0	9.963	0.250	27.97	1.021	1000.1	19.7	0.86	9.242E-17	
10.0	0	9.385	0.250	28.09	1.020	1000.2	19.7	0.87	8.676E-17	
15.0	0	10.370	0.350	39.18	1.021	1000.4	19.7	1.21	6.865E-17	
25.0	0	9.682	0.500	56.02	1.021	1000.3	19.7	1.72	4.483E-17	
25.0	0	9.673	0.500	55.95	1.021	1000.2	19.7	1.72	4.484E-17	
25.0	0	9.674	0.500	55.94	1.021	1000.2	19.7	1.73	4.486E-17	
1.0	0	8.857	0.250	28.16	1.020	1000.7	19.7	0.87	8.163E-17	
2.0	0	9.854	0.251	28.05	1.020	1000.7	19.5	0.86	9.112E-17	
3.0	0	10.536	0.251	28.08	1.020	1000.7	19.5	0.87	9.732E-17	
4.0	0	10.871	0.252	28.16	1.020	1000.7	19.5	0.87	1.001E-16	
5.0	0	10.917	0.251	28.10	1.020	1000.7	19.5	0.86	1.008E-16	
6.0	0	10.777	0.251	28.05	1.020	1000.7	19.5	0.86	9.966E-17	
4.5	0	10.929	0.251	28.11	1.020	1000.7	19.5	0.87	1.008E-16	
4.5	0	10.944	0.252	28.18	1.020	1000.7	19.5	0.87	1.007E-16	
4.5	0	10.944	0.252	28.17	1.020	1000.7	19.5	0.87	1.008E-16	

Table 32: Non-borated detector measurement data of the 55.3-cm diameter standard therapy beam. Measurements made Jan. 2001.

Cint/X1=		2.784e+14 protons/X1				Voltage = +400V				
Depth (cm)	Off Axis (cm)	Charge (nC)	Monitor Units (MU)	X1	X1 TPCX	Pressure (mB)	Temp (C)	Beam Time (min)	Dose (Gy/proton)	Notes
1.0	10	-0.009	0.000	0.00	0.000	999.5	19.8	5.00	-9.790E-03	Background
1.0	0	6.671	0.251	28.06	1.020	1000.5	19.4	0.86	5.865E-17	
1.0	0	6.680	0.251	28.08	1.020	1000.5	19.4	0.87	5.869E-17	
1.0	0	6.679	0.251	28.06	1.020	1000.5	19.4	0.86	5.872E-17	
2.0	0	6.894	0.251	28.02	1.020	1000.5	19.4	0.87	6.070E-17	
3.0	0	6.905	0.252	28.15	1.020	1000.7	19.4	0.87	6.051E-17	
4.0	0	6.796	0.252	28.15	1.020	1000.7	19.4	0.87	5.955E-17	
4.5	0	6.726	0.251	28.10	1.020	1000.7	19.4	0.87	5.904E-17	
5.0	0	6.671	0.252	28.15	1.020	1000.7	19.4	0.87	5.846E-17	
5.5	0	6.568	0.251	28.03	1.020	1000.7	19.4	0.86	5.780E-17	
6.0	0	6.491	0.251	28.04	1.020	1000.7	19.4	0.86	5.710E-17	
7.0	0	6.333	0.251	28.03	1.020	1000.7	19.4	0.86	5.573E-17	
8.5	0	6.104	0.252	28.14	1.020	1000.7	19.4	0.86	5.351E-17	
10.0	0	8.134	0.350	39.17	1.020	1000.8	19.4	1.20	5.122E-17	
15.0	0	6.963	0.351	39.20	1.020	1000.8	19.4	1.20	4.381E-17	
25.0	0	7.127	0.500	55.90	1.020	1000.8	19.4	1.72	3.145E-17	
25.0	0	7.128	0.500	55.93	1.020	1000.8	19.4	1.72	3.144E-17	
25.0	0	7.125	0.500	55.88	1.020	1000.8	19.4	1.72	3.145E-17	
1.0	0	9.352	0.350	39.23	1.020	999.5	18.4	1.21	5.868E-17	
4.5	0	9.399	0.351	39.21	1.020	999.5	18.4	1.21	5.901E-17	
7.0	0	8.887	0.351	39.27	1.020	999.5	18.4	1.21	5.571E-17	
15.0	0	6.953	0.350	39.14	1.020	999.5	18.4	1.20	4.373E-17	

C.4 20-cm Diameter BNCEFNT Beam

Table 33: Borated detector measurement data of the 20-cm diameter iron collimated and iron filtered BNCEFNT beam.

Cint/X1=		2.767e+14 protons/X1				Voltage = +400V				
Depth (cm)	Off Axis (cm)	Charge (nC)	Monitor Units (MU)	X1	TPCX	Pressure (mB)	Temp (C)	Beam Time (min)	Dose (Gy/proton)	Notes
3.0	0	0.003	0.000	0.00	0.000	996.4	19.4	5.00	3.269E-03	Background
3.0	0	10.629	0.352	39.25	1.023	996.4	19.4	0.93	7.076E-17	no filter
3.0	0	10.618	0.350	39.31	1.023	996.4	19.4	0.93	7.058E-17	no filter
5.0	0	10.659	0.351	39.34	1.023	996.7	19.4	0.87	7.077E-17	no filter
7.0	0	10.201	0.352	39.50	1.023	996.4	19.4	0.87	6.748E-17	no filter
9.0	0	9.383	0.352	39.50	1.023	996.4	19.4	0.87	6.207E-17	no filter
8.5	0	4.162	2.003	224.46	1.024	997.0	19.4	4.92	4.834E-18	15.24 cm iron filter
7.0	0	3.435	1.501	168.16	1.024	997.0	19.4	3.70	5.326E-18	15.24 cm iron filter
5.0	0	3.715	1.502	168.08	1.026	997.0	19.4	4.59	5.751E-18	15.24 cm iron filter
3.0	0	3.742	1.501	167.82	1.026	997.0	19.4	4.56	5.802E-18	15.24 cm iron filter
6.0	0	3.596	1.502	167.90	1.027	997.6	19.4	4.61	5.564E-18	15.24 cm iron filter
7.0	0	3.426	1.502	167.82	1.027	997.5	19.4	4.56	5.304E-18	15.24 cm iron filter
7.0	0	3.219	1.752	195.57	1.028	997.6	19.3	6.03	4.269E-18	17.04 cm iron filter
5.0	0	3.511	1.750	195.29	1.029	997.6	19.3	6.01	4.658E-18	17.04 cm iron filter
3.0	0	3.549	1.752	195.30	1.030	997.6	19.3	6.01	4.704E-18	17.04 cm iron filter
3.0	0	2.858	1.751	195.17	1.030	997.6	19.3	5.97	3.790E-18	19.03 cm iron filter
5.0	0	2.825	1.752	195.16	1.030	997.7	19.3	5.96	3.746E-18	19.03 cm iron filter
7.0	0	2.559	1.751	195.03	1.030	998.0	19.3	5.96	3.394E-18	19.03 cm iron filter
5.0	0	3.053	1.751	195.17	1.030	998.2	19.2	5.83	4.045E-18	18.3 cm iron filter
5.0	0	3.054	1.752	195.25	1.030	998.3	19.2	5.81	4.044E-18	18.3 cm iron filter
5.0	0	3.056	1.751	195.05	1.030	998.2	19.2	5.77	4.052E-18	18.3 cm iron filter
3.0	0	3.097	1.751	194.98	1.030	998.2	19.2	5.77	4.107E-18	18.3 cm iron filter
7.0	0	2.753	1.752	195.01	1.031	998.8	19.2	5.84	3.644E-18	18.3 cm iron filter
6.0	0	2.930	1.753	195.05	1.031	998.7	19.2	5.76	3.879E-18	18.3 cm iron filter
5.5	0	3.003	1.754	194.95	1.032	998.2	19.2	5.80	3.975E-18	18.3 cm iron filter
4.0	0	3.124	1.751	194.73	1.032	998.3	19.2	5.80	4.140E-18	18.3 cm iron filter
2.0	0	2.962	1.752	194.70	1.033	998.8	19.2	5.81	3.920E-18	18.3 cm iron filter
1.0	0	2.640	1.750	194.52	1.033	998.8	19.2	5.69	3.497E-18	18.3 cm iron filter
1.0	0	2.620	1.753	196.73	1.022	998.6	18.8	6.07	3.464E-18	18.3 cm iron filter
1.0	0	2.616	1.751	196.55	1.023	998.2	18.8	5.14	3.460E-18	18.3 cm iron filter
1.6	0	2.857	1.753	196.59	1.023	998.2	18.8	5.13	3.779E-18	18.3 cm iron filter
8.5	0	2.522	1.752	196.11	1.025	997.6	18.8	5.14	3.339E-18	18.3 cm iron filter
10.0	0	2.273	1.751	195.91	1.026	997.5	18.8	5.13	3.009E-18	18.3 cm iron filter
15.0	0	1.643	1.751	195.51	1.028	997.0	18.8	5.17	2.175E-18	18.3 cm iron filter
25.0	0	1.044	1.753	195.57	1.028	997.0	18.8	5.16	1.380E-18	18.3 cm iron filter
4.0	5	3.021	1.753	195.38	1.030	996.5	18.8	5.16	4.000E-18	18.3 cm iron filter
4.0	0	3.585	2.001	222.88	1.030	996.4	18.8	5.93	4.162E-18	18.3 cm iron filter
4.0	-5	3.382	2.002	222.89	1.031	996.4	18.8	5.95	3.922E-18	18.3 cm iron filter
4.0	-10	2.426	2.001	222.66	1.031	996.4	18.8	5.94	2.815E-18	18.3 cm iron filter
4.0	-10	2.437	2.002	222.70	1.032	996.3	18.8	5.95	2.825E-18	18.3 cm iron filter
4.0	-15	1.388	2.504	278.24	1.033	995.8	18.8	6.52	1.285E-18	18.3 cm iron filter
4.0	-11	2.116	2.200	244.40	1.033	995.8	18.8	5.70	2.234E-18	18.3 cm iron filter
4.0	-9	3.222	2.202	244.53	1.033	995.8	18.8	5.71	3.401E-18	18.3 cm iron filter
4.0	10	2.845	2.003	222.34	1.034	995.8	18.8	5.20	3.300E-18	18.3 cm iron filter
4.0	14	1.315	2.001	222.05	1.034	995.8	18.8	5.80	1.525E-18	18.3 cm iron filter
4.0	16	1.087	2.204	244.29	1.035	995.8	18.8	6.32	1.144E-18	18.3 cm iron filter
4.0	20	0.658	2.502	277.36	1.036	995.2	18.8	7.10	6.077E-19	18.3 cm iron filter

Table 34: Non-borated detector measurement data of the 20-cm diameter iron collimated and iron filtered BNCEFNT beam.

Cint/X1=		2.767e+14 protons/X1				Voltage = +400V				
Depth (cm)	Off Axis (cm)	Charge (nC)	Monitor Units (MU)	X1	X1 TPCX	Pressure (mB)	Temp (C)	Beam Time (min)	Dose (Gy/proton)	Notes
3.0	-5	0.001	0.000	0.00	0.000	996.4	19.4	5.00	1.090E-03	Background
3.0	0	8.246	0.352	39.50	1.023	996.4	19.4	0.93	5.187E-17	no filter
5.0	0	7.854	0.352	39.43	1.023	996.4	19.4	0.87	4.950E-17	no filter
7.0	0	7.378	0.351	39.34	1.023	996.4	19.4	0.87	4.660E-17	no filter
9.0	0	6.908	0.352	39.49	1.024	996.5	19.4	0.87	4.342E-17	no filter
8.5	0	2.803	2.000	224.26	1.023	996.7	19.4	5.23	3.104E-18	15.24 cm Fe Filter
7.0	0	2.210	1.501	168.09	1.025	997.0	19.4	3.70	3.258E-18	15.24 cm Fe Filter
5.0	0	2.334	1.501	168.02	1.025	997.0	19.4	3.68	3.442E-18	15.24 cm Fe Filter
3.0	0	2.420	1.502	167.94	1.027	997.1	19.4	4.61	3.563E-18	15.24 cm Fe Filter
6.0	0	2.270	1.500	167.67	1.027	997.2	19.4	4.58	3.347E-18	15.24 cm Fe Filter
7.0	0	2.207	1.503	167.81	1.027	997.5	19.4	4.60	3.250E-18	15.24 cm Fe Filter
7.0	0	1.992	1.752	195.57	1.028	997.6	19.4	5.67	2.514E-18	17.04 cm Fe Filter
5.0	0	2.086	1.751	195.31	1.029	997.6	19.3	5.99	2.633E-18	17.04 cm Fe Filter
3.0	0	2.184	1.752	195.34	1.029	997.7	19.3	5.98	2.756E-18	17.04 cm Fe Filter
3.0	0	1.656	1.751	195.12	1.030	997.6	19.3	5.98	2.090E-18	19.03 cm Fe Filter
5.0	0	1.589	1.752	195.09	1.030	997.7	19.3	5.97	2.005E-18	19.03 cm Fe Filter
7.0	0	1.505	1.751	195.03	1.030	998.2	19.2	5.97	1.898E-18	19.03 cm Fe Filter
5.0	0	1.762	1.751	195.25	1.029	998.2	19.2	5.79	2.222E-18	18.3 cm Fe Filter
5.0	0	1.759	1.751	195.26	1.029	998.2	19.2	5.83	2.218E-18	18.3 cm Fe Filter
5.0	0	1.761	1.751	195.22	1.029	998.2	19.2	5.83	2.221E-18	18.3 cm Fe Filter
3.0	0	1.836	1.751	194.97	1.031	998.3	19.2	6.11	2.314E-18	18.3 cm Fe Filter
7.0	0	1.660	1.751	194.95	1.031	998.6	19.2	5.80	2.092E-18	18.3 cm Fe Filter
6.0	0	1.717	1.751	194.78	1.032	998.7	19.2	5.78	2.163E-18	18.3 cm Fe Filter
5.5	0	1.744	1.752	194.84	1.032	998.3	19.2	5.79	2.198E-18	18.3 cm Fe Filter
4.0	0	1.811	1.752	194.81	1.032	998.7	19.2	5.80	2.282E-18	18.3 cm Fe Filter
2.0	0	1.854	1.751	194.65	1.032	998.8	19.2	5.81	2.337E-18	18.3 cm Fe Filter
1.0	0	1.798	1.752	194.62	1.033	998.8	19.2	5.69	2.265E-18	18.3 cm Fe Filter
1.0	0	1.793	1.752	196.86	1.021	999.1	18.8	5.15	2.256E-18	18.3 cm Fe Filter
1.6	0	1.843	1.752	196.37	1.024	998.2	18.8	5.15	2.320E-18	18.3 cm Fe Filter
8.5	0	1.605	1.752	196.17	1.025	998.0	18.8	5.14	2.020E-18	18.3 cm Fe Filter
10.0	0	1.533	1.752	195.87	1.027	997.6	18.8	5.18	1.930E-18	18.3 cm Fe Filter
15.0	0	1.285	1.753	195.80	1.028	997.4	18.8	5.20	1.617E-18	18.3 cm Fe Filter
25.0	0	1.132	2.202	245.62	1.029	996.9	18.8	6.53	1.134E-18	18.3 cm Fe Filter
4.0	0	1.831	1.753	195.38	1.030	996.5	18.8	5.16	2.307E-18	18.3 cm Fe Filter
4.0	-5	2.004	2.001	222.88	1.030	996.4	18.8	5.93	2.213E-18	18.3 cm Fe Filter
4.0	-10	1.433	2.002	222.89	1.031	996.4	18.8	5.95	1.581E-18	18.3 cm Fe Filter
4.0	-15	0.000	2.001	222.66	1.031	996.4	18.8	5.94	-1.316E-21	18.3 cm Fe Filter
4.0	-15	0.484	2.002	222.70	1.032	996.3	18.8	5.95	5.330E-19	18.3 cm Fe Filter
4.0	-20	0.300	2.504	278.24	1.033	995.8	18.8	6.52	2.638E-19	18.3 cm Fe Filter
4.0	-16	0.459	2.200	244.40	1.033	995.8	18.8	5.70	4.603E-19	18.3 cm Fe Filter
4.0	-14	0.646	2.202	244.53	1.033	995.8	18.8	5.71	6.480E-19	18.3 cm Fe Filter
4.0	5	2.048	2.003	222.34	1.034	995.8	18.8	5.20	2.260E-18	18.3 cm Fe Filter
4.0	9	2.078	2.001	222.05	1.034	995.8	18.8	5.80	2.296E-18	18.3 cm Fe Filter
4.0	11	1.102	2.204	244.29	1.035	995.8	18.8	6.32	1.105E-18	18.3 cm Fe Filter
4.0	15	0.604	2.502	277.36	1.036	995.2	18.8	7.10	5.326E-19	18.3 cm Fe Filter

C.5 10-cm Diameter BNCEFNT Beam

Table 35: Borated detector measurement data of the 10-cm diameter iron collimated and iron filtered BNCEFNT beam.

Cint/X1=		2.767e+14 protons/X1				Voltage = +400V				
Depth (cm)	Off Axis (cm)	Charge (nC)	Monitor Units (MU)	X1	TPCX	Pressure (mB)	Temp (C)	Beam Time (min)	Dose (Gy/proton)	Notes
3.0	0	0.003	0.000	0.00	0.000	996.4	19.4	5.00	3.269E-03	Background
5.0	0	1.712	1.750	194.34	1.034	995.2	18.8	4.99	2.272E-18	18.3 cm Fe filter
5.0	0	1.704	1.751	194.24	1.034	995.1	18.8	5.01	2.262E-18	18.3 cm Fe filter
5.0	0	1.705	1.751	194.27	1.035	995.0	18.8	5.03	2.261E-18	18.3 cm Fe filter
4.0	0	1.760	1.751	193.94	1.036	994.6	18.7	5.01	2.336E-18	18.3 cm Fe filter
3.0	0	1.771	1.751	193.94	1.036	994.6	18.7	4.98	2.351E-18	18.3 cm Fe filter
2.0	0	1.726	1.751	193.70	1.037	994.2	18.8	5.68	2.293E-18	18.3 cm Fe filter
1.0	0	1.576	1.752	193.80	1.037	994.6	18.8	5.67	2.091E-18	18.3 cm Fe filter
5.5	0	1.897	2.002	221.32	1.038	994.0	18.7	6.50	2.203E-18	18.3 cm Fe filter
6.0	0	1.848	2.002	221.25	1.038	994.0	18.7	6.48	2.147E-18	18.3 cm Fe filter
7.0	0	1.754	2.002	221.07	1.039	994.0	18.7	5.89	2.037E-18	18.3 cm Fe filter
8.5	0	1.737	2.203	243.25	1.040	994.0	18.7	6.45	1.831E-18	18.3 cm Fe filter
10.0	0	1.572	2.203	243.06	1.040	994.0	18.7	6.34	1.658E-18	18.3 cm Fe filter
15.0	0	1.290	2.504	276.23	1.040	994.0	18.7	7.18	1.196E-18	18.3 cm Fe filter
25.0	0	0.850	2.751	303.34	1.041	994.0	18.7	7.90	7.155E-19	18.3 cm Fe filter
4.0	0	2.008	2.003	220.73	1.041	993.4	18.8	5.77	2.334E-18	18.3 cm Fe filter
4.0	2	1.956	2.001	220.48	1.041	993.4	18.8	6.87	2.275E-18	18.3 cm Fe filter
4.0	4	1.826	2.000	220.38	1.041	993.4	18.8	5.71	2.126E-18	18.3 cm Fe filter
4.0	6	1.021	2.002	220.57	1.041	993.3	18.8	5.74	1.186E-18	18.3 cm Fe filter
4.0	9	0.667	2.002	220.52	1.042	993.1	18.8	5.79	7.729E-19	18.3 cm Fe filter
4.0	11	0.652	2.500	275.30	1.042	992.8	18.8	7.20	6.045E-19	18.3 cm Fe filter
4.0	-4	2.244	2.501	275.41	1.042	993.0	18.8	7.21	2.089E-18	18.3 cm Fe filter
4.0	-10	0.769	2.752	302.78	1.043	992.3	18.8	7.96	6.482E-19	18.3 cm Fe filter
4.0	-15	0.506	2.752	302.80	1.043	992.3	18.8	8.60	4.248E-19	18.3 cm Fe filter
4.0	20	0.350	2.750	302.83	1.042	992.1	18.8	7.94	2.931E-19	18.3 cm Fe filter

Table 36: Non-borated detector measurement data of the 10-cm diameter iron collimated and iron filtered BNCEFNT beam.

Cint/X1=		2.767e+14 protons/X1				Voltage = +400V				
Depth (cm)	Off Axis (cm)	Charge (nC)	Monitor Units (MU)	X1	X1 TPCX	Pressure (mB)	Temp (C)	Beam Time (min)	Dose (Gy/proton)	Notes
3.0	-5	0.001	0.000	0.00	0.000	996.4	19.4	5.00	1.090E-03	Background
5.0	0	1.191	1.751	194.14	1.035	995.0	18.8	5.03	1.504E-18	18.3 cm Fe filter
5.0	0	1.188	1.752	194.11	1.036	994.6	18.8	5.02	1.500E-18	18.3 cm Fe filter
4.0	0	1.228	1.751	194.00	1.036	994.6	18.8	4.99	1.552E-18	18.3 cm Fe filter
3.0	0	1.264	1.752	193.96	1.037	994.6	18.8	5.01	1.596E-18	18.3 cm Fe filter
2.0	0	1.276	1.752	193.77	1.037	994.1	18.7	5.01	1.613E-18	18.3 cm Fe filter
1.0	0	1.242	1.752	193.79	1.038	994.4	18.8	6.40	1.568E-18	18.3 cm Fe filter
5.5	0	1.339	2.003	221.46	1.038	994.0	18.8	6.44	1.480E-18	18.3 cm Fe filter
6.0	0	1.309	2.003	221.36	1.038	994.0	18.7	6.50	1.447E-18	18.3 cm Fe filter
7.0	0	1.273	2.002	221.09	1.039	994.0	18.7	5.90	1.407E-18	18.3 cm Fe filter
8.5	0	1.313	2.200	242.96	1.039	994.0	18.7	6.47	1.321E-18	18.3 cm Fe filter
10.0	0	1.234	2.200	242.90	1.040	994.0	18.7	6.28	1.241E-18	18.3 cm Fe filter
15.0	0	1.133	2.502	276.08	1.041	994.0	18.7	7.20	1.001E-18	18.3 cm Fe filter
25.0	0	0.789	2.751	303.44	1.041	994.0	18.7	7.90	6.337E-19	18.3 cm Fe filter
4.0	-5	0.917	2.003	220.73	1.041	993.4	18.8	5.77	1.014E-18	18.3 cm Fe filter
4.0	-3	1.344	2.001	220.48	1.041	993.4	18.8	6.87	1.488E-18	18.3 cm Fe filter
4.0	-1	1.390	2.000	220.38	1.041	993.4	18.8	5.71	1.540E-18	18.3 cm Fe filter
4.0	1	1.394	2.002	220.57	1.041	993.3	18.8	5.74	1.544E-18	18.3 cm Fe filter
4.0	4	1.300	2.002	220.52	1.042	993.1	18.8	5.79	1.439E-18	18.3 cm Fe filter
4.0	6	0.640	2.500	275.30	1.042	992.8	18.8	7.20	5.668E-19	18.3 cm Fe filter
4.0	-9	0.359	2.501	275.41	1.042	993.0	18.8	7.21	3.172E-19	18.3 cm Fe filter
4.0	-15	0.230	2.752	302.78	1.043	992.3	18.8	7.96	1.842E-19	18.3 cm Fe filter
4.0	-20	0.189	2.752	302.80	1.043	992.3	18.8	8.60	1.511E-19	18.3 cm Fe filter
4.0	15	0.241	2.750	302.83	1.042	992.1	18.8	7.94	1.933E-19	18.3 cm Fe filter

APPENDIX D

MCNPX INPUT FILES

D.1 Neutron source calculation model

```

Fermi Neutron Therapy Target Model - Calculation of source neutron spectrum
c Be Target; Bertini INC
1 1 -1.802 8 -9 -22 $Be Target
2 2 -19.32 9 -10 -22 $Gold Disk
c
3 3 -2.7 (7 42 -11 -26 22):(-22 10 -11):(6 -7 23 -26):(41 -6 23 -24):
(1 -41 23 -25) $Target Housing
4 4 -4.5 (21 -22 6 -8):(6 -7 22 -23) $Clamp
5 5 -16.6 20 -23 4 -6 $Proton Collimator
6 6 -1 -42 $Water Cooling Channel
7 7 -7.87 5 -12 27 -28 $Target Housing collar
8 8 -7.87 12 -13 40 -28 $Primary Collimator
c
9 3 -2.7 (104 -105 -107):(-104 -107 106 100):(100 -103 107 -108):
(101 -102 -106) $Transmission Chamber Housing
10 3 -2.7 (110 -111 -116):(112 -113 -116):(114 -115 -116) $High Voltage Plates
11 11 -2.7 (117 -118 -116):(119 -120 -116):(121 -122 -116):
(123 -124 -116):(125 -126 -116):(127 -128 -116) $Signal Plates
12 7 -7.87 130 -131 132 -133 $Neutron Entrance Port
c
c Area's of Vacuum or Air that are inside of a part
100 0 (1 -4 -23):(4 -6 -20):(6 -8 -21) $Vacuum Chamber Before Target
108 100 -0.001293 (-22 11 -12):(12 -13 -40):(100 -101 -106) $Air in Primary Collimator
109 100 -0.001293 102 -104 -106 #10 #11
112 100 -0.001293 (105 -130 -132) $Air in Neutron Entrance Port
113 100 -0.001293 (130 -131 -132) $Air in Neutron Entrance Port
c
c Area's of Vacuum or Air that are outside of a part
203 100 -0.001293 (11 -12 22 -27):(-27 26 -11 6):(-6 -27 24 3):
(-3 24 41 -25):(25 -3 1 -27):(1 -5 27 -28) $Air Around Target Housing
212 100 -0.001293 (132 -130 105 -133):(-105 103 107 -133):
(-103 100 108 -133):(-100 1 28 -133) $Air outside of Target Assembly
c
1000 0 -1:131:133

1 pz -3.9243 $Target Housing Flange Upsteam Face (3)
2 pz -3.3655 $Target Housing slope point (not used)
3 pz -3.1115 $Target Housing slope point (not used)
4 pz -2.16408 $Proton Collimator Front Face (5)
5 pz -1.82118 $Target Housing Collimator Front Face (7)
6 pz -1.7018 $Target Housing Front Face (3)
7 pz -1.3843 $Clamp (4) Downstream Face (4)
8 pz -1.1049 $Target Upstream Face (1)
9 pz 1.1049 $Target Downstream Face (1)
10 pz 1.1557 $Gold Disk (2) Downstream Face (2)
11 pz 1.4732 $Target Housing (3) Downstream Face

```

```

12 pz 1.67132 $Primary Collimator (8) Upstream Face
13 pz 14.37132 $Primary Collimator (8) Downstream Face
20 cz 0.79375 $Proton Collimator (5) Inter-Radius
21 cz 1.1938 $Clamp (4) inter-radius
22 cz 1.27 $Clamp (4) Collar outer-radius/ Target Radius
23 cz 2.225 $Proton Collimator (5) & (4) outer-radius
24 cz 2.54 $Target Housing (3) Intermediate Radius
25 cz 3.302 $Target Housing (3) Flange outerradius
26 cz 4.7625 $Target Housing (3) Outer Radius
27 cz 5.08 $Target Housing Collar (7) Inter Radius
28 cz 10.16 $Primary Collimator (8) & (7) outerradius
40 kz -0.027312 0.0262993 1 $Primary Collimator Opening (8)
41 z -3.3655 3.302 -3.1115 2.54
42 tz 0.2032 0 0 2.54 0.3175 0.3175 $Outside of Water cooling channel (6)
c
c Aluminium Transmission Chamber (9)
100 pz 14.37132 $ Chamber Flange Upstream Face
101 pz 14.51864 $ Chamber Upsteam Face Outside wall
102 pz 14.59484 $ Chamber Upsteam Face Inside Wall
103 pz 15.48384 $ Chamber Flange Downstream Face
104 pz 17.78 $ Chamber Downstream Face Inside Wall
105 pz 17.78762 $ Chamber Downstream Face Outside Wall
106 cz 7.3025 $ Chamber Inside Surface
107 cz 7.62 $ Chamber Outside Surface
108 cz 8.89 $ Chamber Flange Outside Surface
c
c Aluminium Transmission Chamber High Voltage Plates (10)
110 pz 14.87678
111 pz 14.95552
112 pz 15.79626
113 pz 15.875
114 pz 16.96974
115 pz 17.04848
116 cz 5.715
c
c Aluminium Transmission Chamber Signal Plates (11)
117 pz 14.95806
118 pz 14.98346
119 pz 15.23492
120 pz 15.26032
121 pz 15.51686
122 pz 15.54226
123 pz 16.129
124 pz 16.1544
125 pz 16.4084
126 pz 16.4338
127 pz 16.6878
128 pz 16.7132
c
c Starting Collimation
c First Neutron Entrance Port (12)
130 pz 24.3205 $Neutron Entrance Port Upstream Wall (12)
131 pz 31.3055 $Neutron Entrance Port Downstream Wall (12)
132 z 24.3205 4.24688 31.3055 5.1689 $Inside of Neutron Entrance Port (12)
133 cz 15.24 $Outside Radius of Neutron Entrance Port (12)
c
c Tally Surface segments in degrees as seen from center of target @ 31.3055 cm
9000 cz 0.54644 $1 deg
9001 cz 1.09321 $2 deg
9002 cz 1.64065 $3 deg
9003 cz 2.18909 $4 deg
9004 cz 2.73888 $5 deg
9005 cz 3.290 $6 deg
9006 cz 3.844 $7 deg
9007 cz 4.400 $8 deg
9008 cz 5.1689 $9.3756 deg
9009 cz 5.520 $10
c
c *****IMPORTANCE REGIONS*****
c 1 2 3 4 5 6 7 8 9
c 10 11 12
c 100 108 109
c 112 113

```



```
c *****TALLY ENERGY STRUCTURE*****
c EO 1e-5 1e-4 1e-3 1e-2 8i 1e-1 8i 1 8i 10 8i 100
c *****TALLIES*****
c F1:n 130
c FC1 Neutron tally as function of energy on surface 131
c
c F11:n 130
c FS11 -9000 -9001 -9002 -9003 -9004 -9005 -9006 -9007 -9008 -9009
c E11 1e-5 100
c C11 0 .5 .866 1
c FT11 FRV 0 0 1
c FC11 Neutron tally as function of radius.
c *****
c
lca j j 1
SSW 130 (113) PTY=N
phys:n 71 j 20
cut:n j 1e-9
prdmp j j j 2
ctme 20000
```

D.2 20 × 20 cm² Standard therapy beam model

```

Fermilab NTF Collimator w 20x20 standard inserts.
c
c CELLS
12 1 -7.87 200 -202 400 -302
13 1 -7.87 202 401 300 -301
14 1 -7.87 (-203 202 301 -304):(302 -304 200 -202)
15 2 -1.37 (203 402 -304 301):(-402 303 -304 -208)
19 3 -2.699 -304 303 208 -209
20 3 -2.699 304 -305 207 -209
21 1 -7.87 306 -309 205 -206
22 1 -7.87 304 -306 200 -206
24 1 -7.87 200 -201 306 -309
25 5 -3.53 306 -307 201 -205
26 5 -3.53 308 -309 201 -204
27 4 -2.35 308 -309 204 -205
28 1 -7.87 201 -205 307 -308
c
100 7 -1.0 -310 210 -211 u=3 $Tally Cell
101 7 -1.0 320 -321 210 -211 u=3 $Tally Cell
102 7 -1.0 322 -323 210 -211 u=3 $Tally Cell
115 7 -1.0 -210:211:(310 -320):(321 -322):323 u=3 $Remaining Phantom
c
116 0 -311 227 -228 fill=3 $Phantom
c
117 6 -.001293 (209 -227 -309):(207 -209 305 -309):(206 -207 304 -309):
(227 -228 311 -309):(228 -226 -309) $ Air
c
200 0 230 -200 -309 $Source Region
c
300 0 (200 -202 -400):(202 -203 -301 #13):(203 -209 -303 #15) fill=1 $Filter
301 2 -1.37 (604 -605 610):(605 -606 601):(606 -607 611):(607 -608 602):
(608 -609 612) u=1 $Benelox Removable Liner
302 8 -1.50 ((604 -605 -610):(605 -606 -601):(606 -607 -611):(607 -608 -602):
(608 -609 -612)) 603 u=1 $Concrete/Poly Removable Liner
303 6 -0.001293 (604 -609 -603):(613 -202) u=1
c
1000 0 -230:226:309 $Outside universe
c
c SURFACES
c
200 pz 24.3205
201 pz 25.5905
202 pz 31.3055
203 pz 60.198
204 pz 97.028
205 pz 103.378
206 pz 104.648
207 pz 107.188
208 pz 109.093
209 pz 109.728
c
210 pz 189
211 pz 191
c
226 pz 230
c
c ***CHANGE to move phantom
227 pz 185
228 pz 221.6
c
230 pz -1
c
300 cz 7.62
301 cz 12.7
302 cz 15.24
303 cz 15.875
304 cz 22.225
305 cz 24.13
306 cz 25.4
307 cz 31.59125
308 cz 34.29
309 cz 76.2
310 cz 1
311 cz 22.88
c

```

```

320 cz 4.75
321 cz 5.25
322 cz 9.75
323 cz 10.25
c
400 z 24.3205 4.24688 31.3055 5.1689
401 z 43.7134 7.62 48.768 12.7
402 z 75.438 12.7 79.248 15.875
c
601 z 52.578 4.445 56.388 5.715
602 z 75.438 5.715 79.248 6.985
603 z 31.3055 1.86 109.728 6.52
604 pz 31.3055
605 pz 52.578
606 pz 53.388
607 pz 75.438
608 pz 79.248
609 pz 109.8
610 cz 4.445
611 cz 5.715
612 cz 6.985
613 pz 0
c
c tr1 0 0 24.3205
c *****IMPORTANCES*****
c      12 13 14 15 19 20 21 22 24 25
c      26 27 28
c      100 101 102
c      115 116 117
c      200
c      300 301 302 303
c      1000
imp:n  1 1 1 1 1 1 1 1 1 1
      1 1 1
      1 1 1
      1 1 1
      1
      1 1 1 1
      0
imp:p  1 1 1 1 1 1 1 1 1 1
      1 1 1
      1 1 1
      1 1 1
      1
      1 1 1 1
      0
imp:h  1 1 1 1 1 1 1 1 1 1
      1 1 1
      1 1 1
      1 1 1
      1
      1 1 1 1
      0
imp:e  0 0 0 0 0 0 0 0 0 0
      0 0 0
      1 1 1
      1 1 1
      0
      0 0 0 0
      0
c *****
mode n p h e d t s a
c *****SOURCE DEF*****
SSR OLD 130 NEW 200
c sdef erg=d2 dir=d3 vec=0 0 1 pos=0 0 0 par=1
c si2 1.00000e-05 1.00000e-04 1.00000e-03 1.00000e-02 2.00000e-02 3.00000e-02
c      4.00000e-02 5.00000e-02 6.00000e-02 7.00000e-02 8.00000e-02 9.00000e-02
c      1.00000e-01 2.00000e-01 3.00000e-01 4.00000e-01 5.00000e-01 6.00000e-01
c      7.00000e-01 8.00000e-01 9.00000e-01 1.00000e+00 2.00000e+00 3.00000e+00
c      4.00000e+00 5.00000e+00 6.00000e+00 7.00000e+00 8.00000e+00 9.00000e+00
c      1.00000e+01 2.00000e+01 3.00000e+01 4.00000e+01 5.00000e+01 6.00000e+01
c      7.00000e+01
c sp2 0.00000e+00 1.15826e-07 9.56867e-07 8.15276e-06 6.54268e-06 2.91185e-05
c      3.59253e-06 7.84624e-06 7.55651e-06 1.61060e-05 1.28825e-05 1.48511e-05
c      5.70329e-06 1.55085e-04 1.48989e-04 2.13710e-04 1.14516e-04 1.38239e-04
c      2.00873e-04 1.08475e-04 9.69866e-05 1.07365e-04 5.23179e-04 1.98955e-04
c      1.05525e-04 6.76163e-05 5.34447e-05 4.83748e-05 3.89503e-05 4.02425e-05

```

```

c      4.04447e-05 3.07750e-04 3.44128e-04 2.34320e-04 1.54216e-04 7.21327e-05
c      1.09715e-05
c si3  -1 .984808 .996195 .997564 .998630 .999391 .999848
c      1
c sp3  0 0      2.97998E-3 1.68559e-2 1.74814e-2 1.93356e-2 1.31190e-2
c      1.90276e-2
c *****MATERIALS*****
m1      $ 1010-1020 Steel den=
      26054.24c 0.0581
      26056.24c 0.9175
      26057.24c 0.0215
m2      $ Benelex
      6000.24c 6
      1001.24c 9.998443 1002.24c .001557 $ C
      8016.24c 5 $ H
m3      $Aluminum
      13027.24c 1
m4      $ Ord. Concrete den=2.35 see Chilton p.374
      1001.24c -1.2998e-2 1002.24c -2.0241e-6
      8016.24c -1.165
      13027.24c -0.153
      14028.24c -6.7973e-1 14029.24c -3.4416e-2 14030.24c -2.2854e-2
      20000.24c -.194
      26054.24c -5.81e-2 26056.24c -2.6608e-2 26057.24c -6.235e-4
m5      $ Magnetite Concrete
      1001.24c -1.0998e-2 1002.24c -1.7127e-6
      8016.24c -1.168
      13027.24c -0.116
      14028.24c -8.854e-2 14029.24c -4.483e-3 14030.24c -2.9769e-3
      20000.24c -.251
      24050.24c -9.0815e-3 24052.24c -1.7512e-1 24053.24c -1.9856e-2
      24054.24c -4.9422e-3
      26054.24c -9.7782e-2 26056.24c -1.5442 26057.24c -3.6185e-2
c
m6      7014.24c .7843 8016.24c .2109
      6000.24c .0001 $ Air @ STP
c
m7      $ Water
      1001.24c 2 $ H
      8016.24c 1 $ O
mt7     lwtr.01t
c
m8      $ Concrete w/ Poly den=1.5 see Chilton p.374 and Fermilab
      1001.24c -0.21697 1002.24c -3.3787e-5
      6000.24c -1.2241
      8016.24c -1.165
      13027.24c -0.153
      14028.24c -6.7973e-1 14029.24c -3.4416e-2 14030.24c -2.2854e-2
      20000.24c -.194
      26054.24c -5.81e-2 26056.24c -2.6608e-2 26057.24c -6.235e-4
mt8     poly.01t
c
m999   5010.50c 1 $ B-10
c *****
c *****TALLIES*****
f14:n 100 101 102
FM14  1.4064e-7 999 207 $Convert to MeV/g for B-10 neutron capture
c Per ppm Boron. Using 2.34 MeV per capture.
c
+6 100 101 102
c *****
phys:n 71 j 71
prtmp j j j 3

```

D.3 Conceptual design with W collimator and full C moderation

```

5cm diameter, 10cm thick W collimator near the head
c 1.5cm thick W filter in front of collimator
c full graphite reflection
c Collimator not used. SSR file used to simulate
c 20x20 standard treatment beam.
c
c CELLS
12 1 -7.87 200 -202 400 -302
13 1 -7.87 202 401 300 -301
14 1 -7.87 (-203 202 301 -304):(302 -304 200 -202)
15 2 -1.37 (203 402 -304 301):(-402 303 -304 -208)
19 3 -2.699 -304 303 208 -209
20 3 -2.699 304 -305 207 -209
21 1 -7.87 306 -309 205 -206
22 1 -7.87 304 -306 200 -206
24 1 -7.87 200 -201 306 -309
25 5 -3.53 306 -307 201 -205
26 5 -3.53 308 -309 201 -204
27 4 -2.35 308 -309 204 -205
28 1 -7.87 201 -205 307 -308
c
c
200 0 230 -200 -309
c
299 2 -1.37 (-401 300 -301 -1):(1 -2 3 -301):(2 -4 8 -301):
      (4 -5 8 -402):(5 -6 7 -303):(6 -209 9 -303) $ benelex
300 0 (200 -202 -400):(202 -1 -300):(1 -2 -3):(2 -5 -8):(5 -6 -7):
      (6 -229 -9) fill=2
301 0 610 -601 u=2 fill=3 trcl=1
c
305 6 -0.001293 (605 -611):(611 -640 -641) u=3 $ Air
c
319 1 -7.87 (611 -740 -629 621):(611 -640 641 -621) u=3 $ Inner Filter Holder
320 1 -7.87 740 -741 -629 u=3 $ Filter
321 1 -7.87 741 -742 -629 u=3 $ Filter
322 1 -7.87 742 -743 -629 u=3 $ Filter
323 1 -7.87 743 -744 -629 u=3 $ Filter
324 1 -7.87 744 -745 -629 u=3 $ Filter
325 1 -7.87 745 -746 -629 u=3 $ Filter
326 1 -7.87 746 -747 -629 u=3 $ Filter
327 1 -7.87 747 -748 -629 u=3 $ Filter
328 1 -7.87 748 -749 -629 u=3 $ Filter
329 1 -7.87 749 -612 -629 u=3 $ Filter
c
330 1 -7.87 (612 -642 621 -624):(642 -613 645 -624) u=3 $ Inner Filter Holder
c
331 1 -7.87 612 -613 624 -629 u=3 $ Outer Filter Holder
332 6 -0.001293 (611 -613 629) u=3 $ Air
c
406 1 -7.87 613 -614 622 -623 u=3 $ 3" Sch. 80 Pipe
407 1 -7.87 613 -615 623 -625 u=3 $ 3-1/2" Sch. 40 Pipe
408 1 -7.87 613 -617 625 -627 u=3 $ 5" Sch. XXH Pipe
409 1 -7.87 617 -620 626 -627 u=3 $ 5" Sch. 80 Pipe
410 1 -7.87 613 -620 628 -630 u=3 $ 6" Sch. 80 Pipe
411 6 -0.001293 613 -620 627 -628 u=3 $ Air
412 8 -0.95 616 -619 630 u=3 $ Poly
413 6 -0.001293 613 -616 630 u=3 $ Air
c
414 6 -0.001293 (612 -613 -621):(613 -614 -622):(642 -613 -645 -624) u=3 $ Air
415 6 -0.001293 (614 -615 -623):(615 -617 -625) u=3 $ Air
416 6 -0.001293 (751 -620 -772):(617 -751 -626):(619 -620 630) u=3 $ Air
c
420 6 -0.001293 751 -752 772 -626 u=3 $ Beam Shaper
421 6 -0.001293 752 -753 772 -626 u=3 $ Beam Shaper
422 6 -0.001293 753 -754 772 -626 u=3 $ Beam Shaper
423 6 -0.001293 754 -755 772 -626 u=3 $ Beam Shaper
424 6 -0.001293 755 -756 772 -626 u=3 $ Beam Shaper
425 6 -0.001293 756 -757 772 -626 u=3 $ Beam Shaper
426 6 -0.001293 757 -758 772 -626 u=3 $ Beam Shaper
427 6 -0.001293 758 -759 772 -626 u=3 $ Beam Shaper
428 6 -0.001293 759 -760 772 -626 u=3 $ Beam Shaper
429 6 -0.001293 760 -620 772 -626 u=3 $ Beam Shaper
c

```

```

450 13 -19.3 773 -775 772 -778 $head collimator
c
c
500 7 -1.04 -310 210 -211 -705
501 7 -1.04 -310 211 -212
502 7 -1.04 -310 212 -213
503 7 -1.04 -310 213 -214
504 7 -1.04 -310 214 -215
505 7 -1.04 -310 215 -216
506 7 -1.04 -310 216 -217
507 7 -1.04 -310 217 -218
508 7 -1.04 -310 218 -219
509 7 -1.04 -310 219 -220 -705
c
520 7 -1.04 (-704 701):(-701 -705 702 310):(-702 -706 703): $head
      (-701 -705 702 -310 -210):
      (-701 -705 702 -310 220)
c
530 6 -.001293 (206 -207 304 -309):(207 -209 305 -309):(209 -229 9 -309)
531 6 -.001293 (229 -773 -309):(773 -212 311 -309 705 707):(775 707 -772 -211)
532 6 -.001293 (224 705 -800 -309 -707 -708):(212 -800 311 -309 705):
      (705 -707 -701 708 -311):(705 -707 311 -309)
533 6 -.001293 (-705 704 701 -309 -708):(-705 704 311 -309 701):
      (-705 -702 703 706):(-705 -703 -309) $ Air around head
535 6 -.001293 (707 800 -225 -309 311):(802 -225 -309) $ Air around beamstop
542 12 -1.60 (707 -311 804 -802 772):(707 -311 219 -802 -772):
      (-707 701 708 -311) $ reflector
543 13 -19.3 (773 -775 778 -311) $reflector/radiator
544 13 -19.3 (707 -311 775 -804 772 -778) $headrest
545 12 -1.60 (707 -311 775 -804 772 778) $adjacent to headrest
c
550 13 -19.3 773 -777 -772 $ 1st beam target
551 6 -0.001293 777 -776 -772
552 6 -0.001293 776 -775 -772 $ 2nd beam target
c
1000 0 -230:225:309
c SURFACES
c
1 pz 52.578
2 pz 56.388
3 z 52.578 7.62 56.388 8.89
4 pz 75.438
5 pz 79.248
6 pz 83.058
7 z 79.248 8.89 83.058 10.795
8 cz 8.89
9 cz 10.798
c
200 pz 24.3205
201 pz 25.5905
202 pz 31.3055
203 pz 60.198
204 pz 97.028
205 pz 103.378
206 pz 104.648
207 pz 107.188
208 pz 109.093
209 pz 109.727
c
210 pz 180
211 pz 182
212 pz 184
213 pz 186
214 pz 188
215 pz 190
216 pz 192
217 pz 194
218 pz 196
219 pz 198
220 pz 200
224 pz 179.5
225 pz 250
c
229 pz 109.728
c
230 pz -1
c

```

```

300 cz 7.62
301 cz 12.7
302 cz 15.24
303 cz 15.875
304 cz 22.225
305 cz 24.13
306 cz 25.4
307 cz 31.59125
308 cz 34.29
309 cz 76.2
310 cz 1
311 cz 30
312 cz 11.28
313 cz 6
314 cz 7
c
400 z 24.3205 4.24688 31.3055 5.1689
401 z 43.7134 7.62 48.768 12.7
402 z 75.438 12.7 79.248 15.875
c
600 pz -.01
601 pz 100
602 z 6.985 2.2225 85.4075 6.51
603 pz 6.985
604 pz 40
605 pz -.011
606 pz 85.42
607 pz 60
608 z 6.985 4.2225 85.4075 8.51
c
610 pz 0
c
611 pz 6.985
612 pz 25.91
613 pz 32.0675
614 pz 39.6875
615 pz 57.4675
616 pz 58.75
617 pz 72.7075
618 pz 83.897
619 pz 85.42
620 pz 110
c
621 cz 3.175
622 cz 3.683
623 cz 4.506
624 cz 6.35
625 cz 5.159
626 cz 6.111875
627 cz 7.065
628 cz 7.316
629 cz 7.619
630 cz 8.414
c
640 pz 7.62
641 cz 2.54
642 pz 29.1465
645 z 29.1465 3.175 32.0675 3.683
c
c new head phantom lines
c sq A B C D E F G x y z
c 701 px 6.525 $ Top of head
c 702 px -6.525 $ Bottom of head/top of neck
c 703 px -14.925 $ Bottom of neck
c 704 sq 0.019560858 0.015625 0.01 0 0 0 -1 6.525 0 190 $ Top of head surface
701 px 2.525 $ Top of head
702 px -10.525 $ Bottom of head/top of neck
703 px -18.925 $ Bottom of neck
704 sq 0.019560858 0.015625 0.01 0 0 0 -1 2.525 0 190 $ Top of head surface
705 sq 0 0.015625 0.01 0 0 0 -1 0 0 190 $ Main head surface
706 c/x 0 190 5.4 $ neck surface
c 707 sq 0 0.013841 0.0090703 0 0 0 -1 0 0 190 $ reflector surface
707 c/x 0 190 10.5 $ reflector surface
708 sq 0.0170875 0.0090703 0.0090703 0 0 0 -1 2.525 0 190 $ reflector surface
c
740 pz 7.62

```



```

1.00m 1.00m
1.00m 1.00m 1.00m 1.00m 1.00m 1.00m 1.00m 1.00m 1.00m 1.00m 1.00m 1.00m
1.00m 1.00m 1.00m 1.00m 1.00m 1.00m 1.00m 1.00m 1.00m 1.00m 1.00m 1.00m
0
imp:e 0.00 1.00m 1.00m 1.00m 1.00m 1.00m 1.00m 1.00m 1.00m 1.00m 1.00m
1.00m 1.00m 1.00m
0.00 1.00m
1.00m 1.00m 1.00m
1.00m 1.00m 1.00m 1.00m 1.00m 1.00m 1.00m 1.00m 1.00m 1.00m 1.00m
1.00m 1.00m 1.00m 1.00m 1.00m 1.00m 1.00m 1.00m 1.00m 1.00m 1.00m
1.00m 1.00m 1.00m
1.00m 1.00m 1.00m 1.00m 1.00m 1.00m 1.00m 1.00m 1.00m 1.00m 0.00
1.00 1.00m 1.00m
0 0 1 1 0 1 0 0 0 0 0 0
0
imp:d 0.00 1.00m 1.00m 1.00m 1.00m 1.00m 1.00m 1.00m 1.00m 1.00m 1.00m
1.00m 1.00m 1.00m
0.00 1.00m
1.00m 1.00m 1.00m
1.00m 1.00m 1.00m 1.00m 1.00m 1.00m 1.00m 1.00m 1.00m 1.00m 1.00m
1.00m 1.00m 1.00m 1.00m 1.00m 1.00m 1.00m 1.00m 1.00m 1.00m 1.00m
1.00m 1.00m 1.00m
1.00m 1.00m 1.00m 1.00m 1.00m 1.00m 1.00m 1.00m 1.00m 1.00m 0.00
1.00 1.00m 1.00m
0 0 1 1 0 1 0 0 0 0 0 0
0
imp:t 0.00 1.00m 1.00m 1.00m 1.00m 1.00m 1.00m 1.00m 1.00m 1.00m 1.00m
1.00m 1.00m 1.00m
0.00 1.00m
1.00m 1.00m 1.00m
1.00m 1.00m 1.00m 1.00m 1.00m 1.00m 1.00m 1.00m 1.00m 1.00m 1.00m
1.00m 1.00m 1.00m 1.00m 1.00m 1.00m 1.00m 1.00m 1.00m 1.00m 1.00m
1.00m 1.00m 1.00m
1.00m 1.00m 1.00m 1.00m 1.00m 1.00m 1.00m 1.00m 1.00m 1.00m 0.00
1.00 1.00m 1.00m
0 0 1 1 0 1 0 0 0 0 0 0
0
imp:s 0.00 1.00m 1.00m 1.00m 1.00m 1.00m 1.00m 1.00m 1.00m 1.00m 1.00m
1.00m 1.00m 1.00m
0.00 1.00m
1.00m 1.00m 1.00m
1.00m 1.00m 1.00m 1.00m 1.00m 1.00m 1.00m 1.00m 1.00m 1.00m 1.00m
1.00m 1.00m 1.00m 1.00m 1.00m 1.00m 1.00m 1.00m 1.00m 1.00m 1.00m
1.00m 1.00m 1.00m
1.00m 1.00m 1.00m 1.00m 1.00m 1.00m 1.00m 1.00m 1.00m 1.00m 0.00
1.00 1.00m 1.00m
0 0 1 1 0 1 0 0 0 0 0 0
0
imp:a 0.00 1.00m 1.00m 1.00m 1.00m 1.00m 1.00m 1.00m 1.00m 1.00m 1.00m
1.00m 1.00m 1.00m
0.00 1.00m
1.00m 1.00m 1.00m
1.00m 1.00m 1.00m 1.00m 1.00m 1.00m 1.00m 1.00m 1.00m 1.00m 1.00m
1.00m 1.00m 1.00m 1.00m 1.00m 1.00m 1.00m 1.00m 1.00m 1.00m 1.00m
1.00m 1.00m 1.00m
1.00m 1.00m 1.00m 1.00m 1.00m 1.00m 1.00m 1.00m 1.00m 1.00m 0.00
1.00 1.00m 1.00m
0 0 1 1 0 1 0 0 0 0 0 0
0

```

```

c *****
mode n p h e d t s a
c *****SOURCE DEF*****
SSR OLD 209 NEW 229
c *****MATERIALS*****
m1 26054.24c -5.52e-2 $Fe
    26056.24c -9.04e-1
    26057.24c -2.16e-2
    6000.24c -2.98e-3 $C
    24052.24c -1.80e-3 $Cr
    24053.24c -2.08e-4
c m1 $ low alloy steel NIST 1269 "Line Pipe Steel" - Rev. B min. isotopes
c 26054.24c -5.52e-2 $Fe
c 26056.24c -9.04e-1
c 26057.24c -2.16e-2
c 6000.24c -2.98e-3 $C
c 25055.60c -1.35e-2 $Mn
c 24052.24c -1.80e-3 $Cr
c 24053.24c -2.08e-4

```

```

c      5010.60c  -1.84e-7  $B-10
c      5011.60c  -8.16e-7  $B-11
c      72000.60c -2.00e-5  $Hf
c      79197.60c -2.00e-6  $Au
c      47107.60c -1.03e-6  $Ag
c      47109.60c -9.72e-7
c      27059.60c -1.40e-4  $Co
c      73181.60c -8.00e-5  $Ta
c      74182.24c -2.61e-6  $W
c      74183.24c -1.42e-6
c      74184.24c -3.07e-6
c      74186.24c -2.90e-6
m2    $ Benelex
      6000.24c  6
      1001.24c  9.998443 1002.24c .001557
      8016.24c  5
m3    $Aluminum
      13027.24c 1
m4    $ Ord. Concrete den=2.35 see Chilton p.374
      1001.24c -1.2998e-2 1002.24c -2.0241e-6
      8016.24c -1.165
      13027.24c -0.153
      14028.24c -6.7973e-1 14029.24c -3.4416e-2 14030.24c -2.2854e-2
      20000.24c -.194
      26054.24c -5.81e-2 26056.24c -2.6608e-2 26057.24c -6.235e-4
m5    $ Magnetite Concrete
      1001.24c -1.0998e-2 1002.24c -1.7127e-6
      8016.24c -1.168
      13027.24c -0.116
      14028.24c -8.854e-2 14029.24c -4.483e-3 14030.24c -2.9769e-3
      20000.24c -.251
      24050.24c -9.0815e-3 24052.24c -1.7512e-1 24053.24c -1.9856e-2
      24054.24c -4.9422e-3
      26054.24c -9.7782e-2 26056.24c -1.5442 26057.24c -3.6185e-2
c
m6    7014.24c .7843 8016.24c .2109
      6000.24c .0001 $ Air @ STP
c
m7    $ Brain tissue, icru 44
      1001.24c -0.107 $ H-1
      6000.24c -0.145
      7014.24c -0.022
      8016.24c -0.712 $ 0
      15031.24c -0.004
mt7   lwtr.01t
m8    $ POLYETHYLENE Polyethylene: CH2 , 0.92 g/cc
      1001.24c 0.9998443 1002.24c 0.0001557
      6000.24c 0.5
mt8   poly.01t
m12   6000.24c 1
mt12  grph.01t
c m13 $ lead -11.35
c      82206.24c .241447
c      82207.24c .220827
c      82208.24c .523481
c m13 $ Bi -9.747
c      83209.24c 1
m13   $ W -19.3
      74182.24c .2631
      74183.24c .1428
      74184.24c .3064
      74186.24c .2864
c
m999  5010.50c  1 $ B-10
c *****
c
c *****TALLIES*****
c
+f6 500 501 502 503 504 505 506 507 508 509
sd6 6.28319 r r r r r r r r r r
c
f14:n 500 501 502 503 504 505 506 507 508 509
FM14 1.4064e-7 999 207
sd14 6.28319 r r r r r r r r r r
c Per ppm Boron. Using 2.34 MeV per capture.
c
c *****

```

```
phys:n 71 j 71
prdmp j j j 3
tmesh
rmesh3 total
cora3 -1 1
corb3 -15 -13 -11 -9 -7 -5 -4 -3 -2 -1 0 1 2 3 4 5 7 9 11 13 15
corc3 177.5 178.5 179.5 180 181 182 183 184 185 186 187 188
      190 191 192 193 194 195 196 197 198 200
endmd
```

D.4 Conceptual design with W collimator and Partial C moderation

```

5cm diameter, 10cm thick W collimator near head
c 1.5cm thick W filter in front of collimator
c partial graphite reflection
c Collimator not used. SSR file used to simulate
c 20x20 standard treatment beam.
c
c CELLS
12 1 -7.87 200 -202 400 -302
13 1 -7.87 202 401 300 -301
14 1 -7.87 (-203 202 301 -304):(302 -304 200 -202)
15 2 -1.37 (203 402 -304 301):(-402 303 -304 -208)
19 3 -2.699 -304 303 208 -209
20 3 -2.699 304 -305 207 -209
21 1 -7.87 306 -309 205 -206
22 1 -7.87 304 -306 200 -206
24 1 -7.87 200 -201 306 -309
25 5 -3.53 306 -307 201 -205
26 5 -3.53 308 -309 201 -204
27 4 -2.35 308 -309 204 -205
28 1 -7.87 201 -205 307 -308
c
c
200 0 230 -200 -309
c
299 2 -1.37 (-401 300 -301 -1):(1 -2 3 -301):(2 -4 8 -301):
      (4 -5 8 -402):(5 -6 7 -303):(6 -209 9 -303) $ benelex
300 0 (200 -202 -400):(202 -1 -300):(1 -2 -3):(2 -5 -8):(5 -6 -7):
      (6 -229 -9) fill=2
301 0 610 -601 u=2 fill=3 trcl=1
c
305 6 -0.001293 (605 -611):(611 -640 -641) u=3 $ Air
c
319 1 -7.87 (611 -740 -629 621):(611 -640 641 -621) u=3 $ Inner Filter Holder
320 1 -7.87 740 -741 -629 u=3 $ Filter
321 1 -7.87 741 -742 -629 u=3 $ Filter
322 1 -7.87 742 -743 -629 u=3 $ Filter
323 1 -7.87 743 -744 -629 u=3 $ Filter
324 1 -7.87 744 -745 -629 u=3 $ Filter
325 1 -7.87 745 -746 -629 u=3 $ Filter
326 1 -7.87 746 -747 -629 u=3 $ Filter
327 1 -7.87 747 -748 -629 u=3 $ Filter
328 1 -7.87 748 -749 -629 u=3 $ Filter
329 1 -7.87 749 -612 -629 u=3 $ Filter
c
330 1 -7.87 (612 -642 621 -624):(642 -613 645 -624) u=3 $ Inner Filter Holder
c
331 1 -7.87 612 -613 624 -629 u=3 $ Outer Filter Holder
332 6 -0.001293 (611 -613 629) u=3 $ Air
c
406 1 -7.87 613 -614 622 -623 u=3 $ 3" Sch. 80 Pipe
407 1 -7.87 613 -615 623 -625 u=3 $ 3-1/2" Sch. 40 Pipe
408 1 -7.87 613 -617 625 -627 u=3 $ 5" Sch. XXH Pipe
409 1 -7.87 617 -620 626 -627 u=3 $ 5" Sch. 80 Pipe
410 1 -7.87 613 -620 628 -630 u=3 $ 6" Sch. 80 Pipe
411 6 -0.001293 613 -620 627 -628 u=3 $ Air
412 8 -0.95 616 -619 630 u=3 $ Poly
413 6 -0.001293 613 -616 630 u=3 $ Air
c
414 6 -0.001293 (612 -613 -621):(613 -614 -622):(642 -613 -645 -624) u=3 $ Air
415 6 -0.001293 (614 -615 -623):(615 -617 -625) u=3 $ Air
416 6 -0.001293 (751 -620 -772):(617 -751 -626):(619 -620 630) u=3 $ Air
c
420 6 -0.001293 751 -752 772 -626 u=3 $ Beam Shaper
421 6 -0.001293 752 -753 772 -626 u=3 $ Beam Shaper
422 6 -0.001293 753 -754 772 -626 u=3 $ Beam Shaper
423 6 -0.001293 754 -755 772 -626 u=3 $ Beam Shaper
424 6 -0.001293 755 -756 772 -626 u=3 $ Beam Shaper
425 6 -0.001293 756 -757 772 -626 u=3 $ Beam Shaper
426 6 -0.001293 757 -758 772 -626 u=3 $ Beam Shaper
427 6 -0.001293 758 -759 772 -626 u=3 $ Beam Shaper
428 6 -0.001293 759 -760 772 -626 u=3 $ Beam Shaper
429 6 -0.001293 760 -620 772 -626 u=3 $ Beam Shaper
c

```

```

450 13 -19.3 773 -775 772 -778 $head collimator
c
c
500 7 -1.04 -310 210 -211 -705
501 7 -1.04 -310 211 -212
502 7 -1.04 -310 212 -213
503 7 -1.04 -310 213 -214
504 7 -1.04 -310 214 -215
505 7 -1.04 -310 215 -216
506 7 -1.04 -310 216 -217
507 7 -1.04 -310 217 -218
508 7 -1.04 -310 218 -219
509 7 -1.04 -310 219 -220 -705
c
520 7 -1.04 (-704 701):(-701 -705 702 310):(-702 -706 703): $head
      (-701 -705 702 -310 -210):
      (-701 -705 702 -310 220)
c
530 6 -.001293 (206 -207 304 -309):(207 -209 305 -309):(209 -229 9 -309)
531 6 -.001293 (229 -773 -309):(773 -212 311 -309 705 707):(775 707 -772 -211)
532 6 -.001293 (224 705 -800 -309 -707 -708):(212 -800 311 -309 705):
      (705 -707 -701 708 -311):(705 -707 311 -309)
533 6 -.001293 (-705 704 701 -309 -708):(-705 704 311 -309 701):
      (-705 -702 703 706):(-705 -703 -309) $ Air around head
535 6 -.001293 (707 800 -225 -309 311):(802 -225 -309) $ Air around beamstop
542 6 -.001293 (707 -311 804 -802 772):(707 -311 219 -802 -772):
      (-707 701 804 708 -311) $ reflector
543 13 -19.3 (773 -775 778 -311) $reflector/radiator
544 13 -19.3 (707 -311 775 -804 772 -778) $headrest
545 12 -1.60 (707 -311 775 -804 772 778):
      (-707 701 -804 708 -311) $adjacent to headrest
c
550 13 -19.3 773 -777 -772 $ 1st beam target
551 6 -0.001293 777 -776 -772
552 6 -0.001293 776 -775 -772 $ 2nd beam target
c
1000 0 -230:225:309
c SURFACES
c
1 pz 52.578
2 pz 56.388
3 z 52.578 7.62 56.388 8.89
4 pz 75.438
5 pz 79.248
6 pz 83.058
7 z 79.248 8.89 83.058 10.795
8 cz 8.89
9 cz 10.798
c
200 pz 24.3205
201 pz 25.5905
202 pz 31.3055
203 pz 60.198
204 pz 97.028
205 pz 103.378
206 pz 104.648
207 pz 107.188
208 pz 109.093
209 pz 109.727
c
210 pz 180
211 pz 182
212 pz 184
213 pz 186
214 pz 188
215 pz 190
216 pz 192
217 pz 194
218 pz 196
219 pz 198
220 pz 200
224 pz 179.5
225 pz 250
c
229 pz 109.728
c
230 pz -1

```

```

c
300 cz 7.62
301 cz 12.7
302 cz 15.24
303 cz 15.875
304 cz 22.225
305 cz 24.13
306 cz 25.4
307 cz 31.59125
308 cz 34.29
309 cz 76.2
310 cz 1
311 cz 30
312 cz 11.28
313 cz 6
314 cz 7
c
400 z 24.3205 4.24688 31.3055 5.1689
401 z 43.7134 7.62 48.768 12.7
402 z 75.438 12.7 79.248 15.875
c
600 pz -.01
601 pz 100
602 z 6.985 2.2225 85.4075 6.51
603 pz 6.985
604 pz 40
605 pz -.011
606 pz 85.42
607 pz 60
608 z 6.985 4.2225 85.4075 8.51
c
610 pz 0
c
611 pz 6.985
612 pz 25.91
613 pz 32.0675
614 pz 39.6875
615 pz 57.4675
616 pz 58.75
617 pz 72.7075
618 pz 83.897
619 pz 85.42
620 pz 110
c
621 cz 3.175
622 cz 3.683
623 cz 4.506
624 cz 6.35
625 cz 5.159
626 cz 6.111875
627 cz 7.065
628 cz 7.316
629 cz 7.619
630 cz 8.414
c
640 pz 7.62
641 cz 2.54
642 pz 29.1465
645 z 29.1465 3.175 32.0675 3.683
c
c new head phantom lines
c sq A B C D E F G x y z
c 701 px 6.525 $ Top of head
c 702 px -6.525 $ Bottom of head/top of neck
c 703 px -14.925 $ Bottom of neck
c 704 sq 0.019560858 0.015625 0.01 0 0 0 -1 6.525 0 190 $ Top of head surface
701 px 2.525 $ Top of head
702 px -10.525 $ Bottom of head/top of neck
703 px -18.925 $ Bottom of neck
704 sq 0.019560858 0.015625 0.01 0 0 0 -1 2.525 0 190 $ Top of head surface
705 sq 0 0.015625 0.01 0 0 0 -1 0 0 190 $ Main head surface
706 c/x 0 190 5.4 $ neck surface
c 707 sq 0 0.013841 0.0090703 0 0 0 -1 0 0 190 $ reflector surface
707 c/x 0 190 10.5 $ reflector surface
708 sq 0.0170875 0.0090703 0.0090703 0 0 0 -1 2.525 0 190 $ reflector surface
c

```



```

1.00m 1.00m 1.00m
1.00m 1.00m 1.00m 1.00m 1.00m 1.00m 1.00m 1.00m 1.00m 1.00m 1.00m
1.00m 1.00m 1.00m 1.00m 1.00m 1.00m 1.00m 1.00m 1.00m 1.00m 1.00m
1.00m 1.00m 1.00m 1.00m 1.00m 1.00m 1.00m 1.00m 1.00m 1.00m 1.00m 1.00m
0
imp:e 0.00 1.00m 1.00m 1.00m 1.00m 1.00m 1.00m 1.00m 1.00m 1.00m
1.00m 1.00m 1.00m
0.00 1.00m
1.00m 1.00m 1.00m
1.00m 1.00m 1.00m 1.00m 1.00m 1.00m 1.00m 1.00m 1.00m 1.00m 1.00m
1.00m 1.00m 1.00m 1.00m 1.00m 1.00m 1.00m 1.00m 1.00m 1.00m
1.00m 1.00m 1.00m
1.00m 1.00m 1.00m 1.00m 1.00m 1.00m 1.00m 1.00m 1.00m 1.00m 0.00
1.00 1.00m 1.00m
0 0 1 1 0 1 0 0 0 0 0 0
0
imp:d 0.00 1.00m 1.00m 1.00m 1.00m 1.00m 1.00m 1.00m 1.00m 1.00m
1.00m 1.00m 1.00m
0.00 1.00m
1.00m 1.00m 1.00m
1.00m 1.00m 1.00m 1.00m 1.00m 1.00m 1.00m 1.00m 1.00m 1.00m
1.00m 1.00m 1.00m 1.00m 1.00m 1.00m 1.00m 1.00m 1.00m
1.00m 1.00m 1.00m
1.00m 1.00m 1.00m 1.00m 1.00m 1.00m 1.00m 1.00m 1.00m 1.00m 0.00
1.00 1.00m 1.00m
0 0 1 1 0 1 0 0 0 0 0 0
0
imp:t 0.00 1.00m 1.00m 1.00m 1.00m 1.00m 1.00m 1.00m 1.00m 1.00m
1.00m 1.00m 1.00m
0.00 1.00m
1.00m 1.00m 1.00m
1.00m 1.00m 1.00m 1.00m 1.00m 1.00m 1.00m 1.00m 1.00m 1.00m
1.00m 1.00m 1.00m 1.00m 1.00m 1.00m 1.00m 1.00m 1.00m
1.00m 1.00m 1.00m
1.00m 1.00m 1.00m 1.00m 1.00m 1.00m 1.00m 1.00m 1.00m 1.00m 0.00
1.00 1.00m 1.00m
0 0 1 1 0 1 0 0 0 0 0 0
0
imp:s 0.00 1.00m 1.00m 1.00m 1.00m 1.00m 1.00m 1.00m 1.00m 1.00m
1.00m 1.00m 1.00m
0.00 1.00m
1.00m 1.00m 1.00m
1.00m 1.00m 1.00m 1.00m 1.00m 1.00m 1.00m 1.00m 1.00m 1.00m
1.00m 1.00m 1.00m 1.00m 1.00m 1.00m 1.00m 1.00m 1.00m
1.00m 1.00m 1.00m
1.00m 1.00m 1.00m 1.00m 1.00m 1.00m 1.00m 1.00m 1.00m 1.00m 0.00
1.00 1.00m 1.00m
0 0 1 1 0 1 0 0 0 0 0 0
0
imp:a 0.00 1.00m 1.00m 1.00m 1.00m 1.00m 1.00m 1.00m 1.00m 1.00m
1.00m 1.00m 1.00m
0.00 1.00m
1.00m 1.00m 1.00m
1.00m 1.00m 1.00m 1.00m 1.00m 1.00m 1.00m 1.00m 1.00m 1.00m
1.00m 1.00m 1.00m 1.00m 1.00m 1.00m 1.00m 1.00m 1.00m
1.00m 1.00m 1.00m
1.00m 1.00m 1.00m 1.00m 1.00m 1.00m 1.00m 1.00m 1.00m 1.00m 0.00
1.00 1.00m 1.00m
0 0 1 1 0 1 0 0 0 0 0 0

```

```

c *****
mode n p h e d t s a
c *****SOURCE DEF*****
SSR OLD 209 NEW 229
c *****MATERIALS*****
m1 26054.24c -5.52e-2 $Fe
    26056.24c -9.04e-1
    26057.24c -2.16e-2
    6000.24c -2.98e-3 $C
    24052.24c -1.80e-3 $Cr
    24053.24c -2.08e-4
c m1 $ low alloy steel NIST 1269 "Line Pipe Steel" - Rev. B min. isotopes
c 26054.24c -5.52e-2 $Fe
c 26056.24c -9.04e-1
c 26057.24c -2.16e-2
c 6000.24c -2.98e-3 $C
c 25055.60c -1.35e-2 $Mn
c 24052.24c -1.80e-3 $Cr

```

```

c      24053.24c  -2.08e-4
c      5010.60c  -1.84e-7  $B-10
c      5011.60c  -8.16e-7  $B-11
c      72000.60c -2.00e-5  $Hf
c      79197.60c -2.00e-6  $Au
c      47107.60c -1.03e-6  $Ag
c      47109.60c -9.72e-7
c      27059.60c -1.40e-4  $Co
c      73181.60c -8.00e-5  $Ta
c      74182.24c -2.61e-6  $W
c      74183.24c -1.42e-6
c      74184.24c -3.07e-6
c      74186.24c -2.90e-6
m2     $ Benelex
      6000.24c  6
      1001.24c  9.998443 1002.24c .001557
      8016.24c  5
m3     $Aluminum
      13027.24c 1
m4     $ Ord. Concrete den=2.35 see Chilton p.374
      1001.24c -1.2998e-2 1002.24c -2.0241e-6
      8016.24c -1.165
      13027.24c -0.153
      14028.24c -6.7973e-1 14029.24c -3.4416e-2 14030.24c -2.2854e-2
      20000.24c -.194
      26054.24c -5.81e-2 26056.24c -2.6608e-2 26057.24c -6.235e-4
m5     $ Magnetite Concrete
      1001.24c -1.0998e-2 1002.24c -1.7127e-6
      8016.24c -1.168
      13027.24c -0.116
      14028.24c -8.854e-2 14029.24c -4.483e-3 14030.24c -2.9769e-3
      20000.24c -.251
      24050.24c -9.0815e-3 24052.24c -1.7512e-1 24053.24c -1.9856e-2
      24054.24c -4.9422e-3
      26054.24c -9.7782e-2 26056.24c -1.5442 26057.24c -3.6185e-2
c
m6     7014.24c .7843 8016.24c .2109
      6000.24c .0001 $ Air @ STP
c
m7     $ Brain tissue, icru 44
      1001.24c -0.107 $ H-1
      6000.24c -0.145
      7014.24c -0.022
      8016.24c -0.712 $ 0
      15031.24c -0.004
mt7    lwtr.01t
m8     $ POLYETHYLENE Polyethylene: CH2 , 0.92 g/cc
      1001.24c 0.9998443 1002.24c 0.0001557
      6000.24c 0.5
mt8    poly.01t
m12    6000.24c 1
mt12   grph.01t
c m13  $ lead -11.35
c      82206.24c .241447
c      82207.24c .220827
c      82208.24c .523481
c m13  $ Bi -9.747
c      83209.24c 1
m13    $ W -19.3
      74182.24c .2631
      74183.24c .1428
      74184.24c .3064
      74186.24c .2864
c
m999   5010.50c 1 $ B-10
c *****
c
c *****TALLIES*****
c
+f6 500 501 502 503 504 505 506 507 508 509
sd6 6.28319 r r r r r r r r r r
c
f14:n 500 501 502 503 504 505 506 507 508 509
FM14 1.4064e-7 999 207
sd14 6.28319 r r r r r r r r r r
c Per ppm Boron. Using 2.34 MeV per capture.
c
c

```

```
c *****
phys:n 71 j 71
prcmp j j j 3
tmesh
rmesh3 total
cora3 -1 1
corb3 -15 -13 -11 -9 -7 -5 -4 -3 -2 -1 0 1 2 3 4 5 7 9 11 13 15
corc3 177.5 178.5 179.5 180 181 182 183 184 185 186 187 188
      190 191 192 193 194 195 196 197 198 200
endmd
```

REFERENCES

- [1] Cancer facts and figures 2002. Technical report, American Cancer Society, Inc., Atlanta, GA, 2002.
- [2] K.K. Herfarth, S. Gutwein, and Debus J. Postoperative radiotherapy of astrocytomas. *Seminars in Surgical Oncology*, 20:13–23, 2001.
- [3] M. Catterall, H.J.G. Bloom, D.V. Ash, L. Walsh, A. Richardson, D. Uttley, N. Gowing, P. Lewis, and B. Chaucer. Fast neutrons compared with megavoltage X-rays in the treatment of patients with supratentorial glioblastoma: A controlled pilot study. *Int. J. Radiation Oncology Biol. Phys.*, 6:261–266, 1980.
- [4] F.M. Waterman, F.T. Kuchnir, L.S. Skaggs, D.K. Bewley, B.C. Page, and F.H. Attix. The use of ^{10}B to enhance the tumour dose in fast-neutron therapy. *Phys. Med. Biol.*, 23(4):592–602, 1978.
- [5] J. Chadwick. Possible existence of a neutron. *Nature*, 129:312, 1932.
- [6] J.H. Lawrence and E.O. Lawrence. The biological action of neutron rays. *Proc. Natl. Acad. Sci. USA*, 22(2):124–133, 1936.
- [7] R.E. Zirkle and P.C. Aegersold. Relative effectiveness of x-rays and fast neutrons in retarding growth. *Proc. Natl. Acad. Sci. USA*, 22(2):134–138, 1936.
- [8] J.H. Lawrence, P.C. Abersold, and E.O. Lawrence. Comparative effects of x-rays and neutrons on normal and tumor tissue. *Proc. Natl. Acad. Sci. USA*, 22(9):543–557, 1936.
- [9] R.S. Stone. The treatment of cancer with fast neutrons. *Radiology*, 39:608–620, 1942.
- [10] R.S. Stone. Neutron therapy and specific ionization. *Am. J. Roentgenol*, 59:771–785, 1948.
- [11] L.H. Gray, A.D. Conger, M. Ebert, S. Hornsey, and O.C.A. Scott. The concentration of oxygen dissolved in tissues at the time of irradiation as a factor in radiotherapy. *Br. J. Radiol.*, 26:638–648, 1953.
- [12] M. Catterall, I. Sutherland, and D.K. Bewley. First results of a randomized clinical trial of fast neutrons compared to X and gamma rays in treatment of advanced tumours of the head and neck. *Br. Med. J.*, 2:653–656, June 1975.

- [13] M. Catterall, D.K. Bewley, and I. Sutherland. Second report on results of a randomized clinical trial of fast neutrons compared to x or gamma rays in treatment of advanced tumours of head and neck. *Br. Med. J.*, page 642, June 1977.
- [14] Nuclear data for neutron therapy: Status and future needs. Technical Report IAEA-TECDOC-992, International Atomic Energy Agency (IAEA), Vienna, Austria, December 1997.
- [15] G.L. Locher. Biological effects and therapeutic possibilities of neutrons. *Am. J. Roentgenol.*, 36:1–13, 1936.
- [16] Hans Svensson and Torsten Landberg. Neutron therapy - the historical background. *Acta Oncologica*, 33(3):227–231, 1994.
- [17] W.H. Sweet. The use of nuclear disintegrations in the diagnosis and treatment of brain tumor. *N. Engl. J. Med.*, 245:875–878, 1951.
- [18] J.T. Godwin, L.E. Farr, W.H Sweet, and J.S. Robertson. Pathological study of eight patients with glioblastoma multiforme treated by neutron capture therapy using boron 10. *Cancer*, 8:601–615, 1955.
- [19] H. Hatanaka, M. Moritani, and M. Camillo. Possible alteration of the blood-brain barrier by boron-neutron capture therapy. *Acta Oncologica*, 30(3), 1991.
- [20] Arlene J. Lennox. Proton linacs for boron neutron capture therapy. In *Proceedings of the 15th Biennial Particle Accelerator Conference*, volume 3, pages 1756–1758, Washington, DC USA, May 17-20, 1993. IEEE.
- [21] K.R. Saroja, JoAnne Mansell, F.R. Hendrickson, Lionel Cohen, and Arlene Lennox. Failure of accelerated neutron therapy to control high grade astrocytomas. *Int. J. Radiat. Oncol. Biol. Phys.*, 17:1295–1297, 1989.
- [22] J.J. Battermann. Fast neutron therapy for advanced brain tumors. *J. Radiation Oncology Biol. Phys.*, 6:333–335, 1980.
- [23] Philippe Paquis. Boron neutron capture enhancement (BNCE) of fast neutron irradiation for glioblastoma: Increase of thermal neutron flux with heavy material collimation, a theoretical evaluation. *Journal of Neuro-Oncology*, 41(1):21–30, 1999.
- [24] David W. Nigg, Charles A. Wemple, Ruedi Risler, John K. Hartwell, Yale D. Harker, and George E. Laramore. Modification of the University of Washington Neutron Radiotherapy Facility for optimization of neutron capture enhanced fast-neutron therapy. *Medical Physics*, 27(2):359–367, 2000.
- [25] J. Burmeister, C. Kota, M. Yudelev, and R.L. Maughan. Paired Mg and Mg(B) ionization chambers for the measurement of boron neutron capture dose in neutron beams. *Med. Phys.*, 26(11):2482–2487, 1999.

- [26] C. Kota, R.L. Maughan, J. Burmeister, and J.D. Forman. A modified fast neutron therapy beam for boron neutron capture enhanced fast neutron therapy (BNCEFNT). In Borje Larsson, John Crawford, and Regin Weinreich, editors, *Advances in Neutron Capture Therapy*, volume I. Elsevier, New York, 1997.
- [27] R.L. Maughan, C. Kota, and M. Yudelev. A microdosimetric study of the dose enhancement in a fast neutron beam due to boron neutron capture. *Phys. Med. Biol.*, 37:1957–1961, 1992.
- [28] Jean-Philippe Pignol, Pascal Cuendet, Nicole Brassart, Georges Fares, Florence Colomb, Cheikh M’Bake Diop, Roland Sabbattier, Ahmed Hachem, and Gilles Prevot. Combined use of FLUKA and MCNP-4A for the Monte Carlo simulation of the dosimetry of ^{10}B neutron capture enhancement of fast neutron irradiations. *Medical Physics*, 25(6):885–891, June 1998.
- [29] Jean-Philippe Pignol, Philippe Paquis, Pascal Cuendet, David Gibon, Cheikh M’Bake Diop, and Roland Sabbattier. Beam collimation and bolusing material optimizations for ^{10}B boron neutron capture enhancement of fast neutron (BNCEFNT): Definition of the optimum irradiation technique. *Medical Physics*, 43(5):1151–1159, 1999.
- [30] Jean-Philippe Pignol. Personal Communication, April 2002.
- [31] I. Rosenberg and M. Awschalom. Characterization of a p(66)Be(49) neutron therapy beam I: Central axis depth dose and off-axis ratios. *Med. Phys.*, 8:105–107, 1981.
- [32] M. Awschalom, G. M. Lee, M. L. Palmer, and D. E. Young. Fermilab neutron radiotherapy facility. *IEEE Trans Nucl Sci*, NS-24(3):1055–1057, June 1977.
- [33] Trade Name, American Masonite Corporation, Chicago, IL.
- [34] Katja M. Langen. *Microdosimetric Investigations at the Fast Neutron Therapy Facility at Fermilab*. PhD thesis, University of Wisconsin-Madison, 1997.
- [35] Standard Imaging, Inc., 7601 Murphy Drive Middleton, Wisconsin 53562-2532. Phone: 608-831-0025, Fax: 608-831-2202, Internet: www.standardimaging.com.
- [36] J.B. Smathers, V.A. Otte, A.R. Smith, P.R. Almond, F.H. Attix, J.J. Spokas, W.M. Quam, and L.J. Goodman. Composition of A-150 tissue-equivalent plastic. *Med. Phys.*, 4:74, 1977.
- [37] AAPM Report No. 7. Protocol for neutron beam dosimetry. Technical report, American Association of Physicists in Medicine, Madison, WI, 1980.
- [38] L.J. Goodman. Density and composition uniformity of A-150 tissue equivalent plastic. *Phys. Med. Biol.*, 23:753, 1978.
- [39] *Neutron Dosimetry for Biology and Medicine, ICRU Report 26*. International Commission on Radiation Units and Measurements, Bethesda, Maryland, 1977.
- [40] *Radiation Quantities and Units, ICRU Report 33*. International Commission on Radiation Units and Measurements, Bethesda, Maryland, 1980.

- [41] *Physical Aspects of Irradiation, ICRU Report 10b*. International Commission on Radiation Units and Measurements, Bethesda, Maryland, 1964.
- [42] International Commission on Radiological Protection. *Recommendations of the International Commission on Radiological Protection, ICRP Publication 26*. Pergamon Press, New York, 1975. Annals of the ICRP, 1, No. 3.
- [43] *Tissue Substitutes in Radiation Dosimetry and Measurement, ICRU Report 44*. International Commission on Radiation Units and Measurements, Bethesda, Maryland, 1989.
- [44] M. Awschalom, I. Rosenberg, and R.K. Ten Haken. A new look at displacement factor and point of measurement corrections in ionization chamber dosimetry. *Med. Phys.*, 10(3):307–313, 1983.
- [45] M. Awschalom, I. Rosenberg, and A. Mravca. Kermas for various substances averaged over their energy spectra of fast neutron therapy beams: A study in uncertainties. *Med. Phys.*, 10(4):395–409, 1983.
- [46] J.J. Broerse, B.J. Mijnheer, and J.R. Williams. European protocol for neutron dosimetry for external beam therapy. *Br. J. Radiology*, 54:822, 1981.
- [47] P. Shapiro, F.H. Attix, L.S. August, R.B. Theus, and C.C. Rogers. Displacement correction factor for fast-neutron dosimetry in a tissue equivalent phantom. *Med. Phys.*, 3:87, 1976.
- [48] G.M. Hale and P.G. Young. ENDF/B-VI revision 1, material 525 B-10 (neutron), 1991. 5-B-10 LANL EVAL-NOV89.
- [49] ASTM E 262-97 standard test method for determining thermal neutron reaction and fluence rates by radioactive techniques. Technical report, American Society of Testing and Materials, West Conshohocken, PA, 1998.
- [50] Laurie S. Waters, editor. *MCNPX User's Manual, Version 2.1.5*. Los Alamos National Laboratory, 1999. LA-UR-99-6058.
- [51] Judith F. Briesmeister, editor. *MCNP - A General Monte Carlo N-Particle Transport Code: Version 4B*. Los Alamos National Laboratory, March 1997. LA-12625-M.
- [52] R.E. Prael and H. Lichtenstein. *User Guide to LCS: The LAHET Code System*. Los Alamos National Laboratory, 1989. LA-UR-89-3014.
- [53] S.G. Mashnik and A.J. Sierk. Improved cascade-exciton model of nuclear reactions. In T.A. Gabriel, editor, *Proc. Fourth Workshop on Simulating Accelerator Radiation Environments (SARE4)*, pages 29–51, Knoxville, TN, September 14-16, 1998, 1999. ORNL.
- [54] A.J. Sierk and S.G. Mashnik. Modeling fission in the cascade-exciton model. In T.A. Gabriel, editor, *Proc. Fourth Workshop on Simulating Accelerator Radiation Environments (SARE4)*, pages 53–67, Knoxville, TN, September 14-16, 1998, 1999. ORNL.

- [55] M. B. Chadwick, P. G. Young, S. Chiba, S. C. Frankle, G. M. Hale, H. G. Hughes, A. J. Koning, R. C. Little, R. E. MacFarlane, R. E. Prael, and L. S. Waters. Cross section evaluations to 150 MeV for accelerator-driven systems and implementation in MCNPX. *Nucl. Sci. and Eng.*, 131(3):293, March 1999.
- [56] J.E. Sweezy and N.E. Hertel. Benchmarking MCNPX: Comparing measured and calculated total neutron yields for 100-MeV protons on various target materials. In *Proc. of the Fourth International Topical Meeting on Nuclear Applications of Accelerator Technology*, pages 424–430, La Grange Park, IL, 2000. American Nuclear Society. (Washington, DC, November 12-15, 2000).
- [57] J.J Duderstadt and L.J. Hamilton. *Nuclear Reactor Analysis*. John Wiley and Sons, Inc., New York, 1996.
- [58] K.F. Eckerman, M. Cristy, and J.C. Ryman. The ORNL mathematical phantom series. Technical report, Oak Ridge National Lab., Dec. 1996.
- [59] P. G. Young, E. D. Arthur, and other. Transport data libraries for incident proton and neutron energies to 100 Mev. Technical report, Los Alamos National Laboratory, July 1990. Report LA-11753-MS.